UNIVERSITY OF NAPLES FEDERICO II

Department of Civil, Architectural and Environmental Engineering

Ph.D. Course in

CIVIL SYSTEMS ENGINEERING

Cycle XXXV

Thesis Title:

Updating annual rainfall maxima statistics in a data-scarce region: the case study of Southern Italy

Scientific disciplinary sector:
ICAR/02

Tutors:

Prof. Ing. Domenico Pianese
Prof. Ing. Salvatore Manfreda
Prof. Ing. Luigi Cimorelli

Ph.D. Candidate:

Ing. Angelo Avino

***Ph.D. Course Coordinator*:**

Prof. Ing. Andrea Papola

Table of Contents

List of Figures

List of Tables

Abstract

The growing number of extreme hydrological events observed has raised the level of attention toward the impact of climate change on the rainfall process, which is difficult to quantify given its strong spatial and temporal heterogeneity. Therefore, that impact cannot be determined on the individual hydrological series but must be assessed on a regional and/or district scale. With this objective, the present thesis aims at identifying the trends and dynamics of extreme sub-daily rainfall in southern Italy in the period 1970-2020.

The database of annual maxima was assembled using all available rainfall data (provided by the National Hydrographic and Mareographic Service - SIMN, and the Regional Civil Protection). However, due to the frequent changes (location, type of sensor, and managing agencies) experienced by the national monitoring network, the time-series were found to be extremely uneven and fragmented. Since the spatio-temporal discontinuity could invalidate any statistical analysis, gap-filling techniques (deterministic and geostatistical) were applied to reconstruct the missing data.

In particular, the "Spatially-Constrained Ordinary Kriging" (SC-OK) method was used, namely a mixed procedure that adopts the Ordinary Kriging (OK) approach with the spatial constraints of the Inverse Distance Weighting (IDW) technique. The SC-OK procedure allows to reconstruct only missing data for the stations selected by the IDW method (those with a sufficient number of functioning neighbouring rain gauges).

The reconstructed dataset has been used to explore trends and regional patterns in annual maxima, highlighting how rainfall are evolving in the most recent years.

In recent years, the frequency of extreme events triggered by rainfall (e.g., landslides, river and pluvial floods) has markedly increased, commonly with serious consequences for society, natural ecosystems, and productive activities worldwide.

As extensively discussed in the literature (the Fifth and Sixth Assessment Report of the IPCC), the climate crisis is increasingly impacting Europe, with every region of the continent recording fatalities and severe economic losses due to extreme weather events every year. The European Environment Agency (EAA) tried to quantify the losses in terms of human lives and economic damage by analysing data provided by two separate sources (NatCatSERVICE, Munich Re GmbH; and CATDAT, RiskLayer GmbH). Researchers have revealed that, in the period 1980-2020, the total economic losses (Figure 1a) triggered by extreme events amount to around EUR 500 billion, while victims (Figure 1b) range between 86,000 and 142,000. In particular, weather (heavy rainfall) and hydrological (floods) events have caused between 34 and 44% of the total losses.

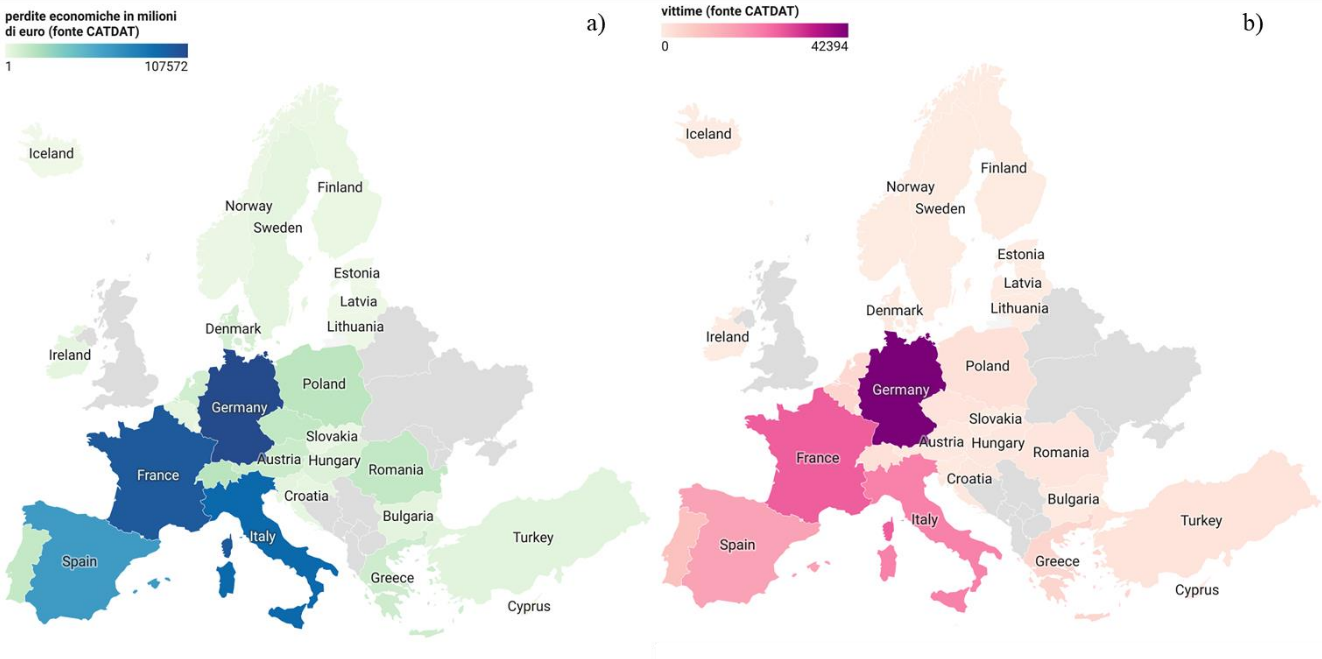

Figure 1 *- a) Total economic losses and b) victims caused by weather (extreme rainfall phenomena) and hydrological (floods) events in Europe in the period 1980-2020. Sources: European Environment Agency (EAA)*

The analyses show that extreme weather phenomena affect all European countries; however, significant differences can be identified between regions. Indeed, Italy is the nation that have experienced the most relevant damage in relation to the extent of its territory, with estimated losses of over 200,000 euros per square kilometre in the analysed period. To better understand, recent studies by the Institute for Environmental Protection and Research (ISPRA) (ReNDiS, 2020) and by Legambiente (Report “CittàClima 2022”, 2022) showed that the total damage caused by flood events that occurred in Italy from 1951 to 2018 presents a significant increase in the period 2001-2018 and that flooding from heavy rainfall is the main cause of economic losses in Italy.

Additionally, Italy is also a country with a high hydrogeological risk due to the increased population density, urbanization, abandonment of mountainous areas, unauthorized buildings, and deforestation. A technical report by the Italian Ministry of Environment quantified that approximately 2.6% of the national territory (an area of 7774 km^2) is classified as having a high hazard of flooding.

Therefore, the analysis of ever more complex and interconnected phenomena, such as the increasing intensity and pattern of extreme rainfall and its consequences on the Italian territory, is one of the crucial points in contrasting climate change. We need to understand the characteristics and entity of extreme events, identify the areas at higher risk, investigate where the phenomena are more frequent and analyse their impacts in order to develop and implement strategies for adaptation and mitigation.

Extreme precipitation phenomena present a strong spatial and temporal heterogeneity and, therefore, it is challenging to quantify the effects of climate change at the local scale. Instead, these impacts should be assessed on a regional and/or district scale. Therefore, this work aims at developing an in-depth statistical analysis of extreme rainfall events of short duration (sub-hourly) in specific areas of the national territory (southern Italy) in order to identify trends and dynamics. A systematic characterisation of these high-intensity extreme phenomena, however, requires a complete and homogeneous dataset over the entire territory of interest, as the main difficulty in understanding the rainfall regime is its great variability in both time and space.

Such an analysis, to be carried out, requires: i) collection and harmonisation of the database of short duration rainfall annual maxima in Southern Italy (Apulia, Basilicata, Calabria, Campania and Molise) over the period 1928-2020; ii) development and implementation of geostatistical techniques for the temporal and spatial reconstruction of missing rainfall data; iii) assessment of rainfall trends.

Thus, the first activity concerns the gathering of the various datasets provided by the National Hydrographic and Mareographic Service (SIMN) for the years 1930-1999 (published in the Hydrological Yearbooks) and by the Functional Centres of the Civil Protection for the period 2000-2020 in order to assemble the extreme rainfall database for southern Italy. However, different regional authorities provided different types of data with different spatial and temporal coverage, resulting in strong inhomogeneities in the constructed dataset. Furthermore, due to the activation/dismissal of rain gauges over the years and the handover of monitoring activities from SIMN to regions, there is often a lack of consistency between the position, name, and altitude of the stations or missing data for one or more years. Therefore, uneven and fragmented series are not suitable for a trend assessment.

The next step aims at reconstructing missing values in order to obtain complete and homogeneous time-series, which are crucial for a correct statistical analysis. The reconstruction can be carried out using several gap-filling procedures, classified into deterministic and geostatistical methods. In this work, a new procedure was developed that combines a spatial reconstruction method (ordinary kriging) with the parameters of a deterministic approach (inverse distance weighting method). Additionally, these parameters were calibrated by means of specific genetic algorithms, aiming at maximising the length of the reconstructed series while minimising the reconstruction error.

The reconstructed rainfall series were analysed by using non-parametric tests for trend detection: i) Mann-Kendall (MK) test and Spearman's rho (SR) correlation test to assess the presence of long-term trends in the rainfall series (at-site trend detection); ii) Regional Kendall (RK) test to investigate general trends in a given area (regional trend detection); iii) Innovative Trend Analysis (ITA) method to identify trend at local and regional scales by means of a graphical approach; iv) Record-Breaking (RB) analysis to detect the presence of trends in terms of the occurrence frequency of extreme rainfall events; v) Pettitt test to analyse change-point, and therefore, trend in the series.

All the branches of the analysis are sequential in order to be useful for the overarching purpose of understanding the spatio-temporal patterns of rainfall extremes in a complex area from both the orographic and the climatic perspectives.

Thesis structure

The thesis is organized as follows:

Chapter 1 reviews the observation-based studies focusing on the detection of trends in extreme rainfall intensities both at global (section 1.1.1) and national (section 1.1.2) scales. The main point of this chapter is the analysis of the reasons of the lack of studies investigating short-duration rainfall extremes.

Chapter 2 provides an overview of the widely used gap-filling procedures existing in the literature, pointing out advantages and limitations.

Chapter 3 describes the study area (section 3.1), which is the southern part of Italy including Apulia, Basilicata, Calabria, Campania and Molise regions, the pluviometric monitoring system (3.2) and the assembled database of annual maximum rainfall depths for sub-daily durations (3.3). Section 3.4, instead, introduces the proposed procedure to estimate missing rainfall data, pointing out the advantages (3.4.1), and describes the implementation (3.4.2) and validation (3.4.3) steps. Finally, a detailed overview of the reconstructed database is provided (3.3.2).

Chapter 4 reports the results of the trend analysis at local and regional scales by means of non-parametric tests, in particular, Mann-Kendall (MK) test (section 4.2), Spearman's rho (SR) correlation test (4.3), Regional Kendall (RK) test (4.4), Innovative Trend Analysis (ITA) test (4.5), Record-Breaking (RB) analysis (4.6) and Pettitt test (4.7).

Chapter 1. Rainfall Extremes

1.1 STATE OF THE ART ON RAINFALL EXTREMES

In the last few decades, the world has experienced a number of natural catastrophes and extreme weather phenomena (heatwaves, droughts, heavy precipitation, floods, and tropical cyclones), which scientists and experts have now largely linked to the ongoing global climate change.

Climate change refers to long-term shifts in meteorological condition patterns in a region over a long period of time. It's the longer-term trend that differentiates climate change from natural variability. These shifts may be natural due to the variations in the solar cycle; however, since the 1800s, human activities have been the main driver of climate change, mainly due to the burning of fossil fuels (coal, oil, and gas), deforestation, intensive agriculture, and extensive land-use changes.

According to NASA, climate change represents "*a broad range of global phenomena created predominantly by burning fossil fuels, which add heat-trapping gases to Earth's atmosphere. These phenomena include the increased temperature trends described by global warming, but also encompass changes such as sea-level rise; ice mass loss in Greenland, Antarctica, the Arctic and mountain glaciers worldwide; shifts in flower/plant blooming; and extreme weather events*."

In recent decades, changes in climate regime, which are driven by increased human emissions of heat-trapping greenhouse gases, are having widespread effects on the social and natural ecosystem worldwide and are happening faster than scientists previously assessed. However, the magnitude of changes beyond the next few decades will depend mainly on the amount of greenhouse gases emitted globally. Global annual averaged temperature increase could be limited to 1.5°C or less with a significant reduction in the emissions of greenhouse gases. Instead, without considerable reductions in these emissions, that increase, relative to preindustrial times, could exceed 1.5°C by the end of this century, resulting in high-impacts of local, regional and global risks to human society and natural environments.

Therefore, climate change, global warming, and the resulting hydrological variations are not only a concern of the scientific community but also arouse keen interest in the political and economic spheres due to the increasing effects they are having and will have on natural and social ecosystems.

In this regard, the Intergovernmental Panel on Climate Change (IPCC) was set up by the World Meteorological Organization (WMO) and United Nations Environment Programme (UNEP) in 1988 to provide an objective source of scientific information concerning to climate change. This working group is in charge of assessing scientific, technical and socio-economic knowledge on the understanding of human-induced climate change, its potential impacts and the possible actions for adaptation and mitigation.

The IPCC's Sixth Assessment Report (IPCC, 2021) provides an overview of the state of knowledge on climate change, emphasizing new results since the publication of the Fifth Assessment Report in 2014. It is based on the reports of the three Working Groups of the IPCC (dealing respectively with physical science; impacts, adaptation and vulnerability; mitigation) as well as on the three Special Reports (related to Global Warming of 1.5°C; Climate Change and Land; Ocean and Cryosphere in a Changing Climate).

These Reports highlighted that the magnitude of recent changes on a global scale, as well as the current status of many components of the climate system, are unprecedented over many centuries or even thousands of years. Human-induced climate change is already affecting climate extremes in every region worldwide, leading to an increase in global warming. Evidence of observed changes in extremes such as heatwaves, heavy precipitation, droughts, floods, and tropical cyclones, and, in particular, their attribution to human influence, has strengthened since the Fifth Assessment Report.

The IPCC's Sixth Assessment Report stated that:

- approximately 3.3 to 3.6 billion people live in contexts that are highly vulnerable to climate change.
- vulnerability of ecosystems and people to climate change differs significantly among and within regions.
- if global warming exceeds 1.5°C in the coming decades or later, then many human and natural systems will deal with additional severe risks, compared to remaining below 1.5°C.

In addition, it found that human emissions of heat-trapping gases have already warmed the climate by nearly 1.1 degrees Celsius since pre-industrial times (starting in 1750). The global average temperature is expected to reach or exceed 1.5 °C within the next few decades. In particular, between 1880 and 2012, an increase in average temperature of 0.85 °C has been observed at the global scale, as shown in the IPCC's report after reviewing the majority of the relevant scientific literature done by climate scientists worldwide. According to the latest observations, the average global temperature has increased more since 2012; in fact, the last decade has seen an increase of around 1 °C, compared to the reference year of 1880.

In Figure 2 is reported a graph (created by NASA) depicting temperature anomalies from 1880 to the present. The zero line is exactly the average of the thirty-year period 1951-1980, the grey circles represent the annual anomaly values, while the solid black line is the 5-year moving mean. It is clear that temperatures have been increasing rapidly, with an alarming upward peak in the last years (in particular, +0.87°C compared to the zero line in 2015).

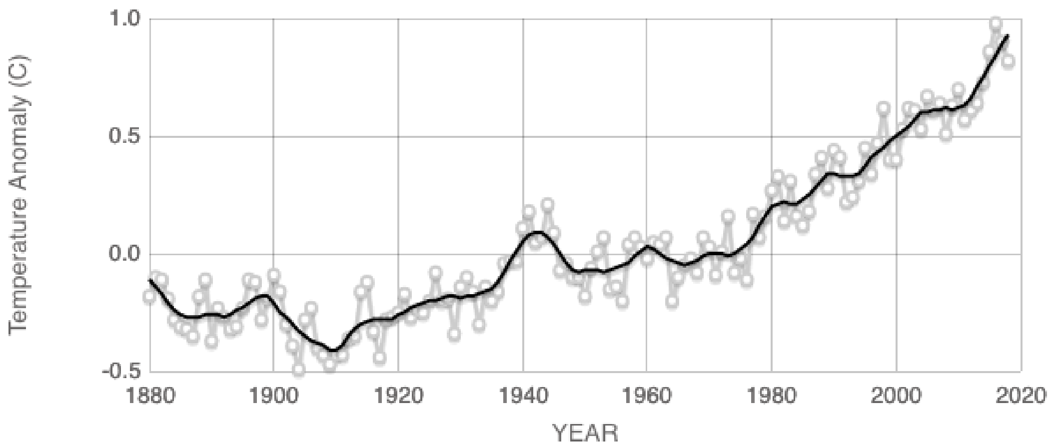

Figure 2 *- Temperature anomalies (°C) in the period 1880-2019. The grey circles represent the annual anomaly values, while the solid black line is the 5-year moving mean. Sources: NASA (climate.nasa.gov)*

Thus, Figure 2 shows very clearly that there are two intervals in the period 1880-2019 when the average temperature of the planet increased significantly: the first between 1920 and 1950 and the second between 1980 and 2019. In this second period, the temperature is increased with the greatest growth rate.

Comparable results were found by the four leading study centres in the world that deal with processing data at the global scale, namely the National Aeronautics and Space Administration (NASA) and the US Atmospheric and Oceanic Agency (NOAA), the Met Office Hadley Centre - British Meteorological Office, and the Japanese Meteorological Agency (JMA). Although these institutes independently analysed the observed data, they came to nearly identical results as highlighted in the following graph (Figure 3), developed by a team of scientists from NASA's Goddard Institute for Space Studies (GISS).

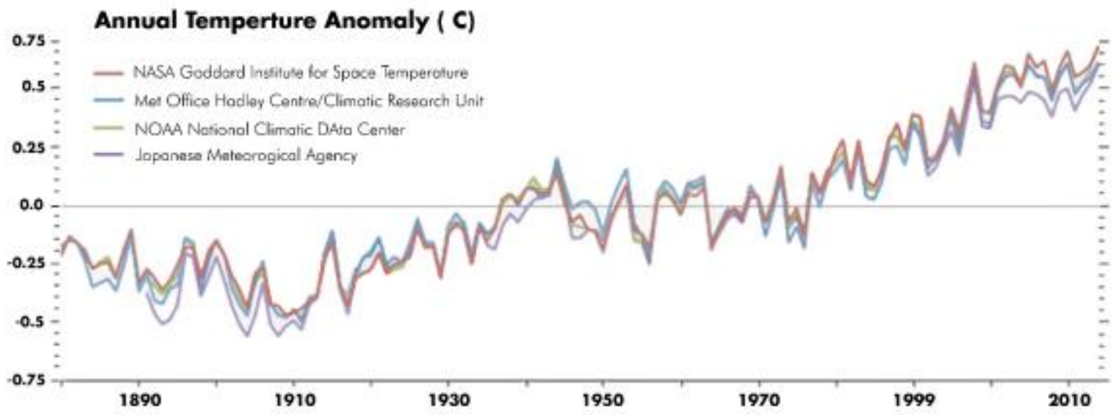

Figure 3 *- Global temperature anomalies over the past centuries assessed by the four leading research centres in the world. Source: NASA's Goddard Institute for Space Studies (GISS 10)*

Figure 3 clarifies that the scientific community worldwide, even if using different methods and approaches, has found similar outcomes, i.e., that the global average temperature has increased by 0.8°C since 1880 and that two-thirds of this increase has occurred since 1975. In addition, NASA experts revealed that only in some areas of the North Atlantic and the United States has the temperature decreased slightly, while in the rest of the world (where continuous measurements are available) the temperature has increased. Additionally, the upward trend has been very marked in central Asia, North and South America, and parts of Africa.

The Global Climate Update Report of the World Meteorological Organisation (WMO) explicitly pointed out that there is a 50% probability that the annual average temperature at the global level will temporarily reach 1.5°C above the pre-industrial level for at least one of the next five years. This possibility has steadily increased since 2015, when it was close to zero. At the same level, the Global Climate Update from Annual to Decadal by the UK Met Office stated that the probability of the 2022-2026 average temperature being higher than the last five years (2017-2021) is 93%.

The average global temperature increase, occurred since 1975 (Figure 3), is also evident in Italy as shown in Figure 4. The blue line represents the 12-month moving average, while the solid red line represents the 10-year moving average.

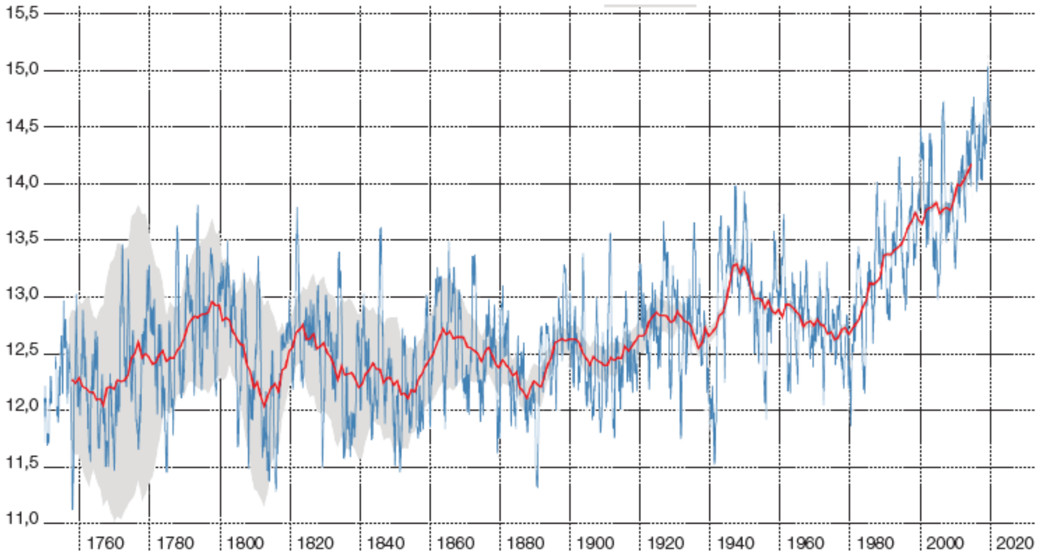

Figure 4 *- Temperature in Italy in the period 1760-2020. The blue line represent the annual temperature values, while the solid red line is the 10-year moving mean. Sources: Berkeley Earth*

The average annual temperature in Italy increased by around 1.2 degrees in the period from 1981 to 2010. To understand the relevance, it is sufficient to consider that previously the national temperature had taken about a century to rise by 1.7 degrees. Since the 1990s, the average temperature has increased at a much higher rate than the world average; in fact, in 1990 the national average temperature increase was about 1.1°C compared to 0.4°C worldwide. Then, in 2000 the world average temperature was at +0.6°C, in Italy was at +1.6°C; the two statistics have changed to +0.7°C and +1.9°C, respectively, in 2010 and to +0.9°C and +2.4°C in 2020.

In light of this, experts agree that global warming, as a consequence of ongoing climate change, is real and is responsible for several environmental disasters worldwide, ranging from melting glaciers to rising sea levels, from increased heat waves to severe flooding. In fact, the climate scenario for the 21st century predicted by the IPCC (IPCC, 2014) are alarming; increased frequency of extreme meteorological events, long drought periods, severe floods, considerable decrease in summer precipitation, and an increase in the intensity of short and intense rainfall events are the expected climatic conditions.

Therefore, the investigation of changes in meteorological phenomena has become more pressing due to the growing awareness of climate change and in view of the evident economic and social impacts that these events have in several significant sectors, such as human health, agriculture, food and water security, water supply, transportation, energy, biodiversity, and ecosystems.

As stated above, climate change could have effects on several environmental variables, such as precipitation, temperature, atmospheric composition, and average sea level (e.g., Kundzewicz, 2019; Wardekker & Lorenz, 2019; Tangney, 2020). However, precipitation represents the most important hydrological variable for water resources management and hydrological hazard mitigation. The response of precipitation extremes to climate change has been the focus of extensive study because, in the scientific community, there is very high confidence that the frequency and intensity of heavy rainfall events are increasing in most regions as global temperature increases.

In this study, we started by analysing the effects of climate change on the temperature variable and then moved on to the analysis of precipitation. This approach was followed because the recent increases in heavy rainfall were suggested to be linked with global warming due to the increased atmospheric water vapour and warmer air (IPPC, 1995). Atmospheric temperature strongly influences the intensity of extreme rainfall, as warmer air can hold more water than cooler air and therefore has the potential to provide more moisture to rainfall events. In view of global warming, it is important to understand the relationship between rainfall intensity and atmospheric temperature. It is well known that the concentrations of water vapour (which provide the water for precipitation) increase according to the Clausius-Clapeyron rate, providing an increase in the water holding capacity of air of approximately 6-7% per degree Celsius rise in temperature. However, according to Allen and Ingram (2002), the global average precipitation is expected to increase at only about 2-3% per °C of warming. The two assertions lead to the conclusion that rainfall increases at the Clausius-Clapeyron rate but falls less often, resulting in more intense precipitation events (Ingram, 2016). Additionally, intense rainfall, instead, are expected to increase with warming at an even higher rate than the Clausius-Clapeyron, as shown by observed precipitation data at shorter time-scales (ranging from minutes to hours).

To sum up, observations show that precipitation extremes intensify in response to a warming climate, even if the sensitivity of precipitation extremes to warming is still uncertain due to the several physical factors that govern the phenomenon (O’Gorman, 2015).

1.1.1 Assessment of observed trends in rainfall extremes at the global scale

The previous section summarises the results of several studies that have demonstrated a strong link between the intensity of extreme rainfall and the atmospheric temperature. Given that there has been approximately 1°C of atmospheric warming during the 20th and early 21st centuries, in this thesis we try to investigate and discuss the evidence that rainfall extremes have intensified at rates previously described by carefully reviewing the scientific literature. Therefore, in order to understand the effects of the ongoing climate change on rainfall patterns and accelerate the development of adaptation and mitigation strategies, long-term changes need to be identified in terms of the frequency and intensity of extreme events. In particular, understanding the rainfall regime is crucial in the design of hydraulic systems and infrastructures for the exploitation of water resources for civil, industrial, and agricultural purposes, for the protection of communities, and the mitigation of hydrogeological risk. Thus, the need to investigate changes in rainfall patterns has been the most important topic in climatic research for water resource managers and the scientific community over the last few decades, and it remains one of the major challenges nowadays.

As reported in the work of Ingram (2016), globally, extreme rainfall is increasing with warming, but regional or local changes are less certain and detectable. With the aim of setting an empirical baseline, in the last few years, significant effort has been devoted by the scientific community to investigating the temporal and spatial variability of extreme rainfall (e.g., Ohba and Sugimoto, 2019; Shortridge, 2019). Therefore, several studies have been published focusing on the detection of trends in extreme rainfall intensities. The majority of the observation-based studies are based on data recorded at annual, seasonal, or, at most, daily time resolution and demonstrate that extreme precipitation events have increased in intensity and/or frequency at global scales. These include recent assessments at large regional (e.g., United States [Groisman et al., 2012]; South America [Skansi et al., 2013]; China [Yang et al., 2012; Gu et al., 2017]; Australia [Nicholls and Lavery, 1992]; Europe [Moberg et al., 2006; Zolina et al., 2009; van den Besselaar et al., 2012]) and global scales (Groismann et al., 1999; Groisman et al., 2005; Alexander et al., 2006; Donat et al., 2013a, 2013b; Westra et al., 2013a).

It is challenging to draw accurate conclusions about extreme rainfall trends because the assessment has been done, over the year, using different datasets for different time periods and geographical areas. However, in this section, we want to present some globally significant conclusions by summarizing the most recent research.

In examining intense precipitation at the daily scale over the United States in the period 1948-2009, Groisman et al. revealed that moderately heavy precipitation (rainfall amount under 25.4 mm in 1 day) has become less frequent compared to daily events with precipitation totals above the aforementioned threshold. In addition, significant upward tendencies were detected in the frequency of very heavy (daily events above 76.2 mm) and extreme precipitation events (above 154.9 mm), with up to 40% increases in their frequency in the period 1979-2009 compared to the 1948-1978 interval.

In South America, instead, Skansi et al. analysed changes in precipitation extremes by using an extended network of daily quality-controlled records covering the years 1950-2010. They demonstrated that the area is becoming wetter as a whole, with Amazonia and the south-eastern portion leading the increase in the total amount of annual precipitation. The most interesting aspect is that the upward trend seems to be more related to the intensification of heavy rainfall than to increases in the duration or frequency of consecutive wet days.

In China, daily rainfall data from 485 stations over the period 1961-2006 were used to examine changes in seasonal extreme rainfall. Yang et al. used the non-parametric Pettitt test to detect change points in the mean and variance of the rainfall distribution as well as the Mann-Kendall test and Sen's slope estimator to assess the presence of monotonic trends and trend magnitude. They found that most of the change points occurred in the 1980s, when China underwent a socioeconomic development. Additionally, a decreasing tendency was pointed out in autumn season, while the opposite in spring and winter. In summer, instead, extreme rainfall exhibited an overall tendency towards increases in the south and decreases in the north.

These findings contradict those presented by Gu et al., that analysed 1-day precipitation data from 728 meteorological stations across China covering a period of 1951-2014. By applying the stepwise regression method and the modified Mann-Kendall test, they provided limited evidence of non-stationarity in both annual and seasonal extreme precipitation, thus not being able to draw conclusions about the presence of a possible climate change signal.

In Australia, Nicholls and Lavery used a set of 191 high-quality rainfall series to examine rainfall trends during the twentieth century. They detected trends in annual, winter, and summer rainfall. In particular, summer rainfall over much of eastern Australia increased abruptly around 1950. Instead, in the south-west part most stations recorded a smoother trend to lower winter precipitation, although there was a small area characterized by a marked increase.

In Europe, Moberg et al. analysed century-long daily precipitation series over the period 1901-2000 using the EMULATE database (Figure 5). The project “European and North Atlantic daily to multidecadal climate variability” (EMULATE) developed a dataset containing daily temperature and precipitation measurements for more than 200 stations over the Europe, thus overcoming the obstacle of the lack of a validated and homogeneous database.

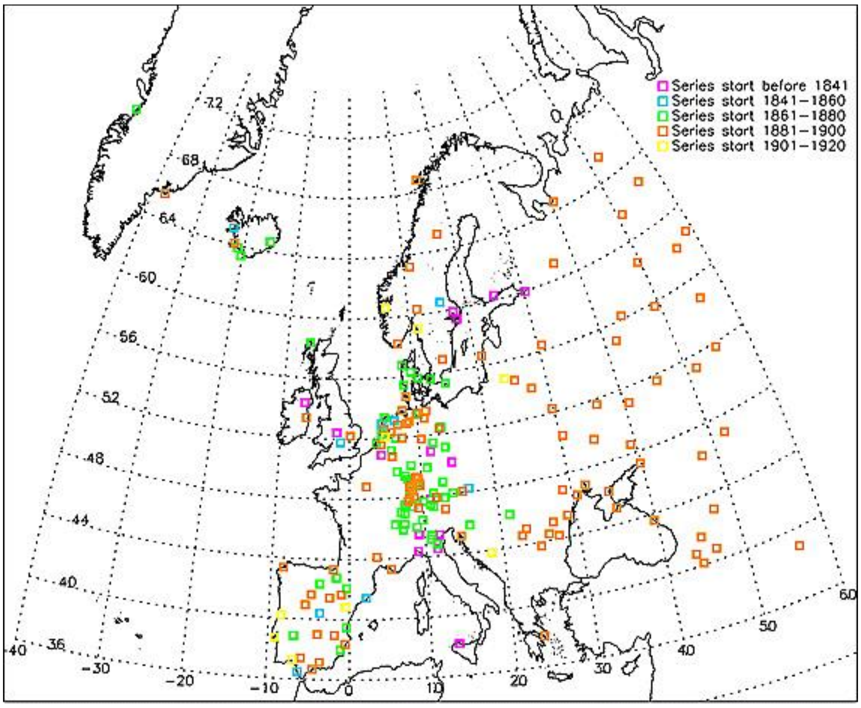

Figure 5 *- Locations of all 195 stations west of 60°E with daily precipitation series in the EMULATE database. The start period for each series is indicated by the colours. Sources: Moberg et al. (2006)*

It is very interesting to point out that the map shows the start period for each series in the database; in particular, in central-eastern Europe and Iberian peninsula all stations started to record in the period 1881-1900, while in central-northern part the majority of rain gauges started working earlier. In addition, it is worth noting that there are no measuring stations in the majority of Italy; the few that exist are concentrated in the northern part, with measurements starting in the period 1861-1880.

By using the EMULATE database, the authors found that winter precipitation totals, averaged over 121 European stations, have increased significantly by around 12% per 100 years. Figure

6 maps the stations that present a significant increasing trend in winter precipitation totals. The majority of stations in central and northern Europe were characterized by a marked upward trend.

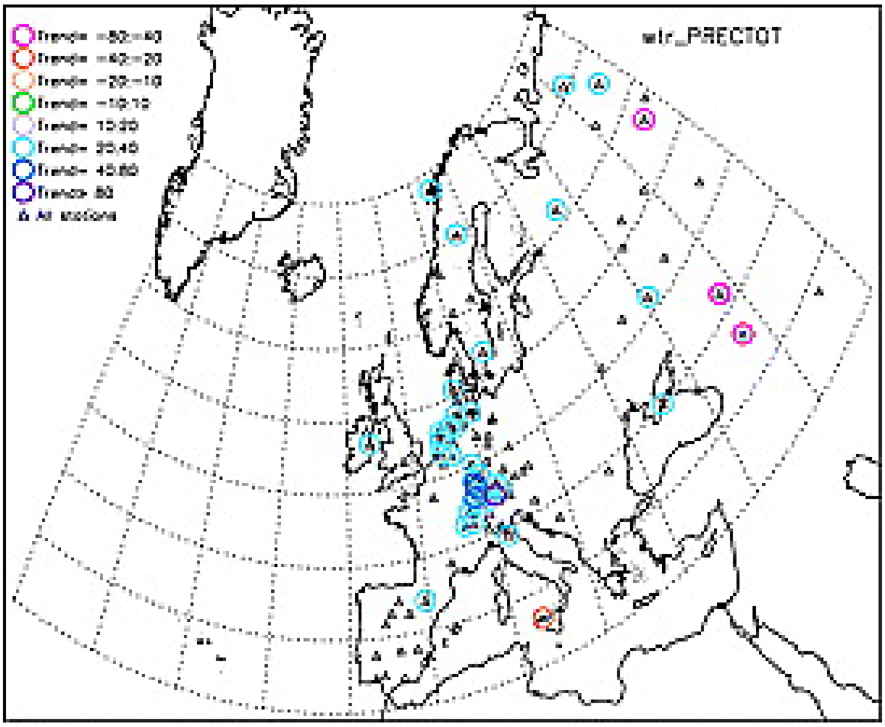

Figure 6 *- Locations of stations with significant (at the 5% level) trends over the period 1901-2000 in precipitation totals for winter. The colours indicate the size of trends (unit is % change with respect to the 1961-1990 average) as identified in the legends. Sources: Moberg et al. (2006)*

Instead, no overall long-term trend occurred in summer precipitation totals, but there was an overall weak (statistically insignificant) tendency for summer precipitation to have become slightly more intense but less common. However, the authors could not draw more robust conclusions at the spatial scale due to data inhomogeneities and the relative sparseness of station density in many parts of Europe.

Again, regarding Europe, van den Besselaar et al. analysed the daily precipitation series from the European Climate Assessment and Dataset (ECA&D, http://www.ecad.eu). For each station, they estimated the linear trend (using ordinary least squares) in the total precipitation amount over the period 1951-2010 for winter (December, January, February) and summer (June, July, August) periods, as shown in Figure 7.

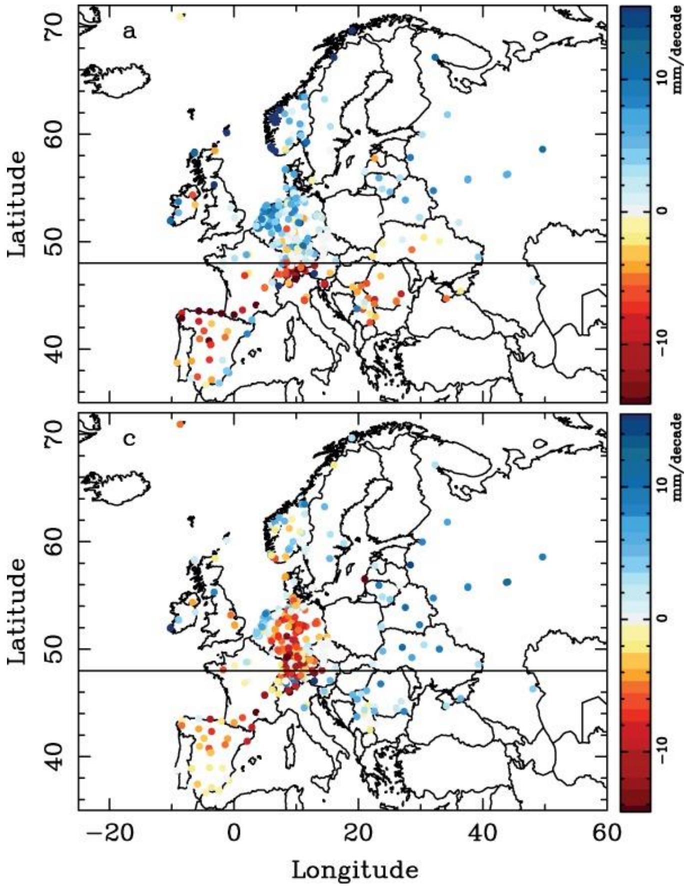

Figure 7 - Trend (estimated using ordinary least squares) in total precipitation amount in winter (December, January, February) in the top and summer (June, July, August) in the bottom over the period 1951-2010. Sources: van den Besselaar et al. (2012)

They demonstrated that Northern Europe presents a wetting trend in winter, while Southern Europe shows a tendency towards drying. In particular, the average trend for Northern Europe in winter, spring and autumn was positive, while the opposite in summer. Instead, in Southern Europe the average trend in winter, spring and summer was negative and positive in autumn.

In addition, the authors tried to investigate if the seasonal maxima of 1-day precipitation and the total annual precipitation over Northern and Southern Europe show similar signs of trend and they found very interesting results. In fact, they pointed out that in Northern Europe, the changes in extreme precipitation were approximately the same as that for the trend in total precipitation amount. Instead, in Southern Europe, the 1-day maximum precipitation with a 20-year return period stays about the same in winter, but becomes slightly wetter in other seasons, although the regional trend in total precipitation amount in winter and summer indicates drying. A further relevant result is the median reduction of about 21% in return period of 1-day maximum rainfall between the first (1951-1970) and last (1991-2010) 20-year periods for all regions and seasons. It is worth noting that an overall decreasing trend in return periods is indicative of increasing precipitation extremes. These outcomes are consistent with those reported by Trenberth et al. (2007), who highlighted that the number of heavy precipitation events (e.g., 95th percentile) has increased within many land regions over Europe, even in regions with a reduction in total precipitation amounts.

These analysed studies highlighted the presence of positive trends in total annual rainfall in the mid- to upper latitude regions of the world. Instead, over the Mediterranean area (mid- to low latitude) several regional studies has shown a dominant decreasing trend. For example, Piervitali et al. (1998) reported that the rainfall regime over the central-western Mediterranean (in particular, Italy and Spain) experienced a reduction of about 20% in the total precipitation in the period 1951-1995. The highest decrease of 26% (around 157 mm) occurred over the southern belt including Tunisia and the southern part of Italy and Spain. The Mediterranean area is a region particularly sensitive to climate and specifically to precipitation changes because it lies in the transition zone between the North Africa climate, very hot and dry, and the central European climate, which is instead temperate and generally very rainy. To this regard, Alpert et al. (2002) showed that in the Mediterranean area the rainfall regime behaves in a paradoxical way, namely extreme daily rainfall increases in spite of the fact that total annual rainfall decreases. In most areas worldwide, the trends in total rainfall, either positive or negative, have been observed to have the same sign as the trends in the amounts of 1-day heavy precipitation events. Only in a few specific regions (e.g., northern Japan, the Asian part of Russia and southern Africa), Groisman et al. (1999) and Easterling et al. (2000) found that a decrease in total rainfall was associated with an increase in the frequency of 1-day heavy precipitation events. Such behaviour has been observed by Alpert et al.; in fact, although a decreases in annual rainfall was found, they detected: an increase in the torrential rainfall (exceeding 128 mm per day) in Italy with a growth factor of 4 and in Spain in the period 1951-1995; no significant trends, instead, in Israel and Cyprus.

Groisman et al. (2005) conducted a global scale analysis of this type. In detail, they analysed changes in very heavy precipitation, i.e., daily rainfall that falls into the upper 0.3% of precipitation events. This threshold corresponds to a return period of approximately 3-5 years for annual and 10-20 years for seasonal precipitation. For the study, the authors used the daily total precipitation datasets assembled at the National Climatic Data Centre (NCDC), reported in Figure 8 and 9 (lightly shaded regions).

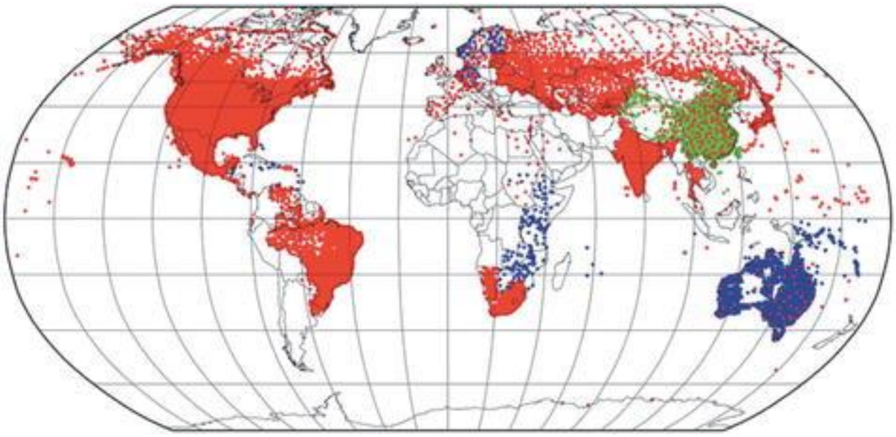

Figure 8 *- Map of stations with daily precipitation available at the U.S. National Climate Data Centre. Sources: Groisman et al. (2005)*

The analysis was carried out for the period 1901-1990 by using the regional averaging technique. The results are reported in Figure 9.

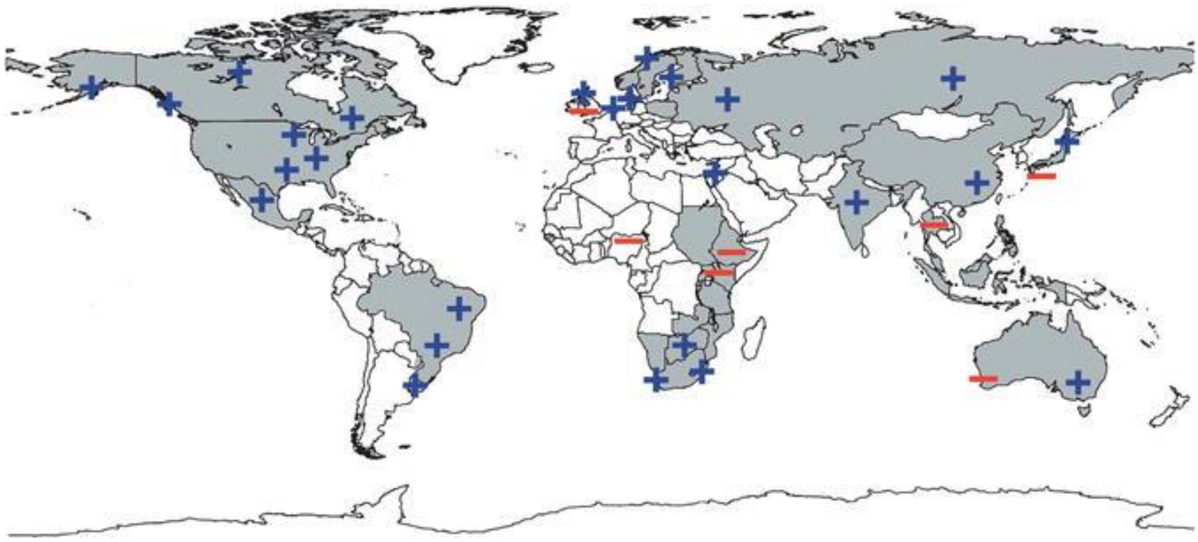

Figure 9 *- Regions where changes in very heavy precipitation during the past decades were documented compared to the change in the annual and/or seasonal precipitation. Sources: Groisman et al. (2005)*

In the Figure 9, positive sign represents changes in very heavy precipitation that are higher than changes in precipitation totals, while negative sign stands for regions where an increase in very heavy precipitation occurred while no change or even a decrease in precipitation totals was observed. Therefore, it is possible to gather that in a large part of the globe (Pacific coast of north-western America, south-eastern Australia, southern Africa, eastern Brazil and Uruguay, central United States, central Mexico and northern Europe) there have been changes of the same sign (increasing or decreasing) in both the totals and the 1-day heavy precipitation events. Instead, in some cases (south-western Australia, northern Japan and south-eastern Africa) there was no increase in the seasonal total but there was still an increase in the frequency of 1-day heavy precipitation events.

However, the majority of published studies on extreme precipitation analysis in recent decades have been carried out on a global scale, although it has been challenging due to the multiplicity of dynamic mechanisms that influence their spatial and temporal regimes.

One of the first relevant works on a global scale is that of Alexander et al. (2006). They developed a global gridded dataset, HadEX, using the three international daily datasets freely available as their data source, in particular 1) the GCOS Surface Network (GSN) database, 2) the European Climate Assessment (ECA) dataset and 3) the daily Global Historical Climatology Network (GHCN-Daily) database. The ECA data were used to cover Europe in this analysis, while GHCN-Daily data for the United States and Brazil. The GSN data were managed to supplement these sources of data, primarily in Africa. Figure 10 shows the locations of the 5948 precipitation stations used in their study. However, in trends detection, they chose only the stations with a completeness of at least 80% in period under consideration (1901-2003) and ended no earlier than 1999. The stations are primarily located in North America, Eurasia and Australia, although a few stations are situated in Brazil and Sri Lanka. The authors used these stations to investigate changes in the context of a century long timescale, examining several Climatic Changes Indices as suggested by the Expert Team on Climate Change Detection and Indices (ETCCDI). In addition, to reduce bias, they decided to grid the indices onto a regular latitude-longitude grid by weighting each station according to its distance and angle from the centre of a search radius.

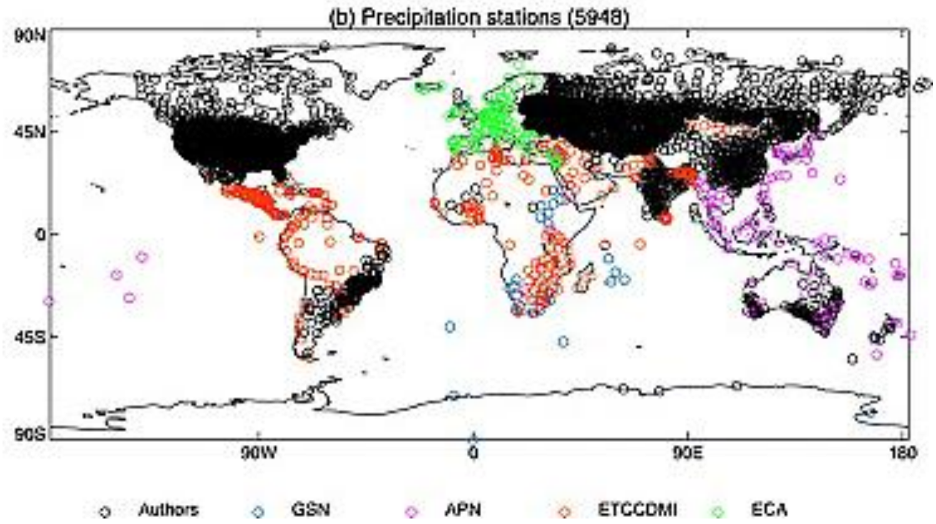

Figure 10 *- Locations of precipitation stations available in the HadEX database. The colours represent the different data sources. Sources Alexander et al. (2006)*

The authors found a general increase in heavy precipitation days and daily intensity, as reported in Figure 11.

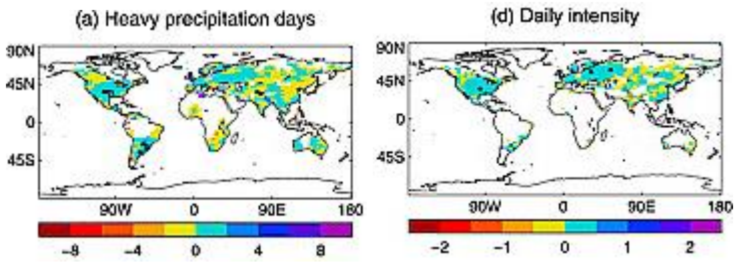

Figure 11 *- Trends for annual series of precipitation indices for 1951–2003 for (a) heavy precipitation days (in days per decade), (d) daily intensity (in mm per decade). Trends were calculated only for the grid boxes with sufficient data (at least 40 years of data during the period and the last year of the series is no earlier than 1999). Sources: Alexander et al. (2006)*

The authors showed that there have been significant increases of up to 2 days per decade in the number of days in a year with heavy precipitation in south-central United States, parts of South America, large portions of Europe and the European area of Russia; while a not significant decrease in parts of Asia. An increase was also observed in simple daily intensity in south-central United States and Europe, in agreement with the results presented by Kiktev et al. (2003).

In addition, they also examined temporal changes and trends for a subset of stations with complete coverage over the period 1901-2003 for some precipitation indices, such as i) max 1-day precipitation, ii) max 5-day precipitation, iii) very wet days (corresponding to 95th

percentile) iv) extremely wet days (corresponding to 99th per centile). These results are highlighted by Alexander et al. in the following Figure 12.

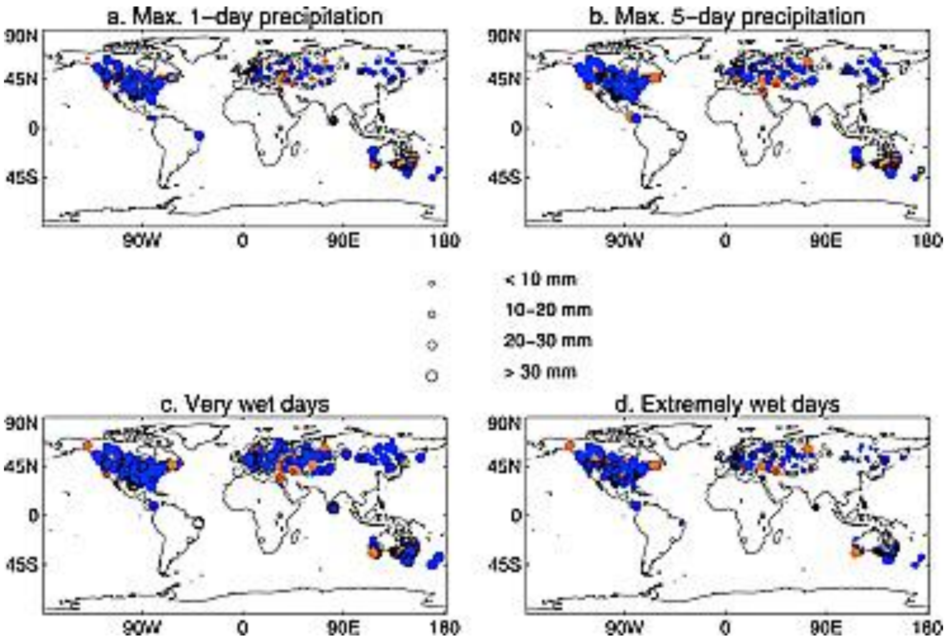

Figure 12 *- The 100-year trends for a selection of precipitation indices [a) max 1-day precipitation; b) max 5-day precipitation; c) very wet days; d) extremely wet days] for the period 1901-2003 for a subset of stations with at least 80% complete data between 1901 and 2003. Black circles indicate a nonsignificant change. Blue (red) solid circles indicate a significant increase (decrease) at the 5% level. Sources: Alexander et al. (2006)*

The analysis of the above-mentioned indices showed that 28%, 25%, 28% and 13% of stations have exhibited significant increases respectively, especially in south-central United States and large portions of Europe and the European area of Russia.

Several studies have observed the increase in extreme precipitation through the analysis of specific rainfall indices. As previously reported, Groisman et al. (2005) found widespread increases in very intense precipitation (defined as the upper 0.3% of daily precipitation events) across the midlatitudes. However, their index is much more severe than any of the indices used in the work of Alexander et al., such as extremely wet days indicator, which corresponds to the upper 1% of daily rainfall. Thus, a direct comparison is not possible between the two studies.

To summarize the findings of these studies, we can state that globally the number of regions that have experienced an increase in extreme daily rainfall events is greater than the number of regions that have experienced a decrease in the period 1900-2003, although these trends are often statistically non-significant and spatially inconsistent. In fact, the majority of precipitation indices showed a tendency toward wetter conditions but not all resulted to be statistically significant.

It is worth pointing out that one of the main successes of work Alexander et al. is to have developed the new database (HadEX), which contains 27 climatic indices (temperature and daily precipitation) recommended by the ETCCDI on a $3.75° \times 2.5°$ longitude-latitude grid from 1951 to 2003.

However, as highlighted by Donat et al., 2013a, it covers a relatively short period (53 years) and contains numerous data gaps both in space and time, especially for the precipitation indices. Therefore, in Donat et al., 2013b, they updated HadEX to develop the HadEX2 dataset. This new version covers a much longer period, 1901 to 2010; the location of the 11588 stations is reported in Figure 13.

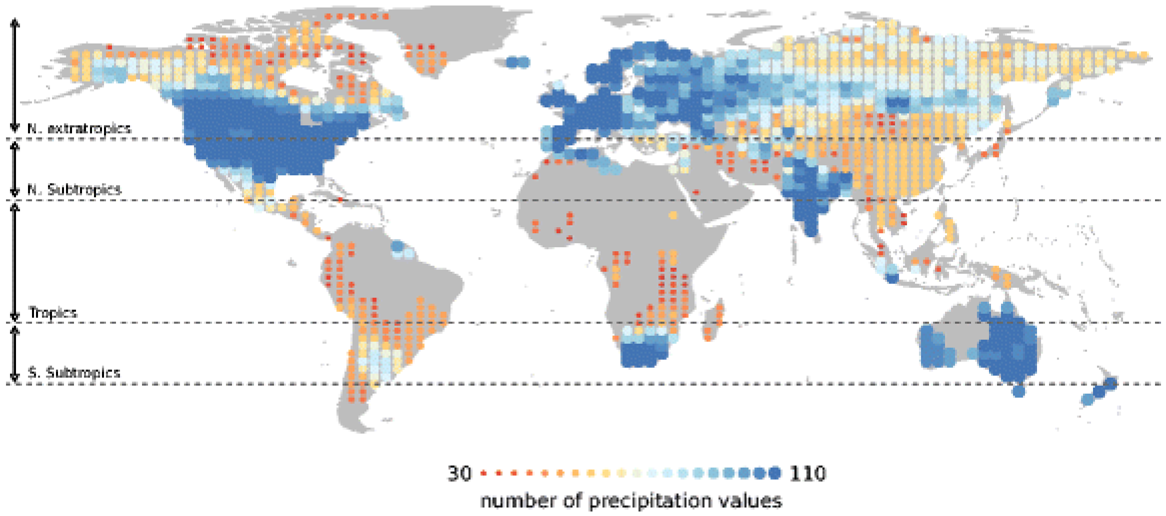

Figure 13 - *Locations of precipitation stations available in the HadEX2 database. The magnitude of the time-series length is represented by the colour and size of the dots Sources: Lehmann et al. (2015)*

Thus, using this database, they analysed different indices over global land areas, carrying out relevant findings which, however, are quite similar to those presented in the work of Alexander et al. In particular, most of the precipitation indices (i.e., number of heavy precipitation days and average intensity of daily precipitation) show changes toward more intense precipitation over the eastern half of North America as well as over large parts of Eastern Europe, Asia, and South America. Areas with trends showing less frequent and intense precipitation are observed in the Mediterranean area, in Southeast Asia, and the north-western part of North America.

Similar results were carried out by Westra et al. (2013) exploiting the annual maximum daily precipitation time series obtained from a global dataset of 8326 high-quality land-based stations with more than 30 years of observations over the period 1900-2009. They found statistically significant positive trend on two-thirds of stations by means of the Mann-Kendall non-parametric trend test.

The aforementioned database (HadEX2) has been further extended (to the period 1901-2018) and updated in the version HadEX3 gridded land surface extreme indices (Dunn et al., 2020). Using this database, Gimeno et al. (2022) detected positive and statistically significant trends in terms of annual daily precipitation in North and central America, Central Amazonia, West Africa, northern Europe, Southeast Asia, and northeast Russia. Negative trends, instead, are less common; however, some downward tendencies have been observed in large part of South America, the eastern portion of the Iberian Peninsula, and part of Southeast Asia.

Thus, we can state that, since 2013, several studies (Asadieh and Krakauer, 2015; Kunkel and Frankson, 2015; Alexander, 2016; and Donat et al., 2016) have provided observational evidence of intensifications of annual maximum daily precipitation in different regions worldwide.

The paper of Fisher and Knutti (2016) moves in that direction. They summarised all prior research on how global warming and climate change affect rainfall regime by using the following graph (Figure 14).

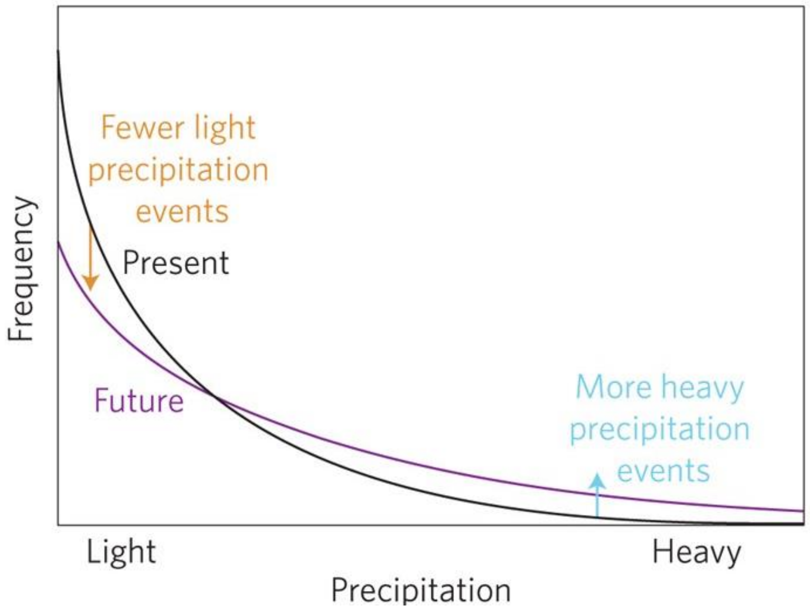

Figure 14 *- Schematic illustrating the change in rainfall distribution. Sources: Fischer and Knutti (2016)*

They stated that "*[…] the response of precipitation to increased greenhouse gas concentrations is complex. […] This behaviour is commonly illustrated with a simple schematic (Figure 14) suggesting that the wettest days become more frequent at the expense of days with light or no precipitation*".

In addition, they compared the frequency of daily precipitation data in the period 1981-2013 to the baseline period 1951-1980 for different all-day percentiles according to the EOBS gridded observation data set, and the ECA (European Climate Assessment) station series. The results are reported in Figure 15. The authors concluded that very heavy rainfall intensification is emerging over Europe (Figure 15a); in particular the number of days with very heavy precipitation has increased of about 45% (years 1981-2013 compared to 1951-1980), whatever the data source used (EOBS or ECA, Figure 15b).

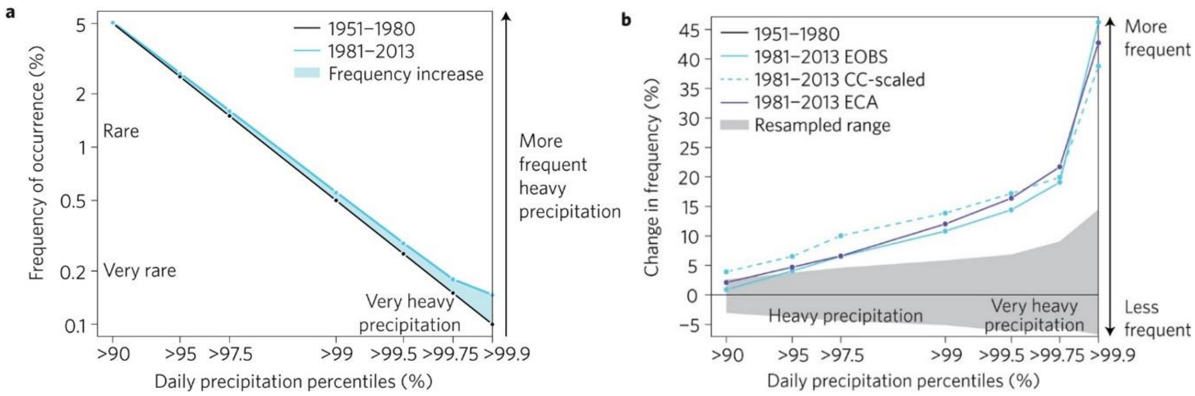

Figure 15 *- a) Observed frequency of occurrence of heavy precipitation in Europe in the periods 1951-1980 (black) and 981-2013 (light blue solid) according to the EOBS gridded observation dataset; b) Ratio of observed daily precipitation frequency in 1981-2013 versus 1951-1980 according to the EOBS gridded observation dataset (light blue solid) and the ECA station series (violet solid). Sources: Fischer and Knutti (2016)*

Pursuing this line of research, Papalexiou and Montanari (2019) tried to explore changes in the frequency and magnitude of rainfall extremes spanning from local to global scales, by using more than 8,730 high-quality daily precipitation records. The focus of the work is on the 1964-2013 period during which global warming was particularly marked with an evident linear increase (towards +0.8°C) in global temperature anomalies, as shown in Figure 16.

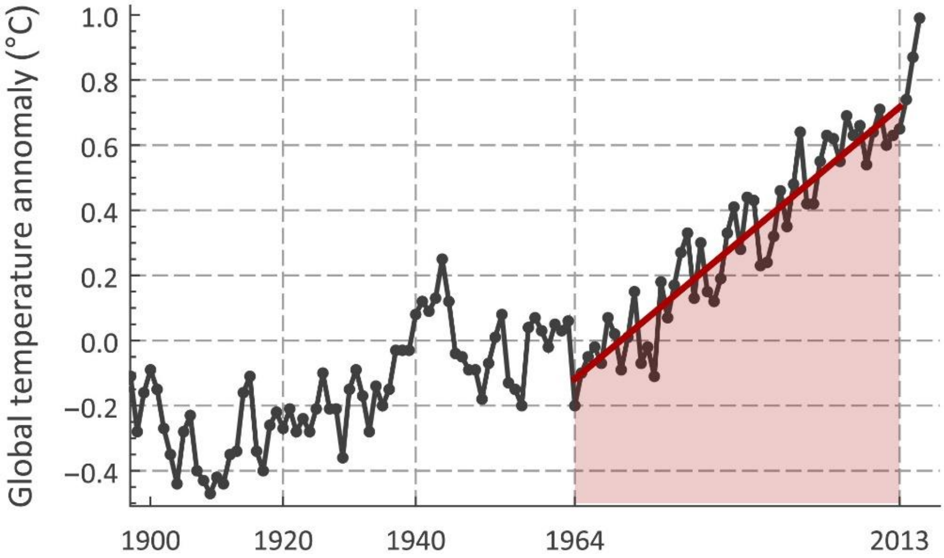

Figure 16 - *Global temperature anomalies in the period 1900-2013. Sources: Papalexiou and Montanari (2019)*

The innovative idea of their study lies in decomposing precipitation into frequency and magnitude. In fact, they developed two correlated databases of extremes (one for frequency and one for magnitude) and assessed trends and changes in both the features independently, as reported in Figure 17. These maps show the percentage of stations with positive and negative trends and the ratios of positive to negative trends both in frequency and magnitude at different spatial scales (i.e., globe scale (GL), North hemisphere (NH), Northwest (NW), Northeast (NE), and Southeast (SE) Earth's quadrants).

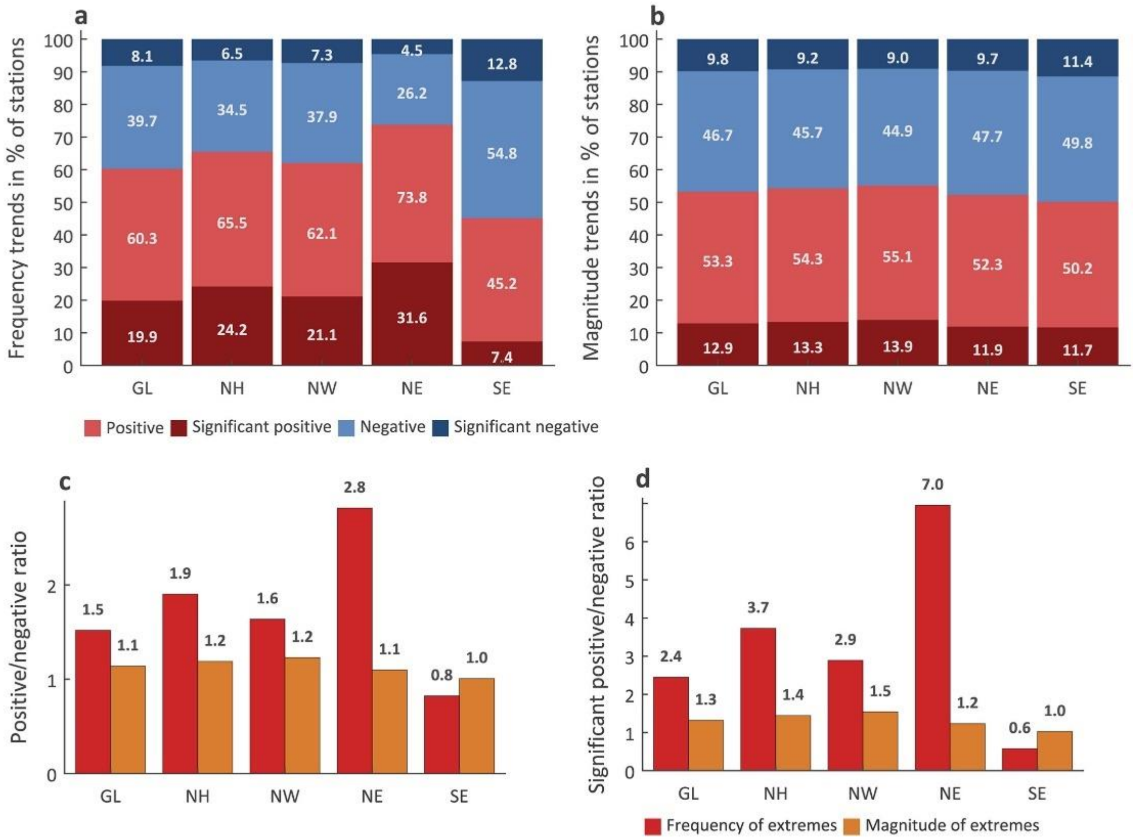

Figure 17 *- The percentage of stations with positive and negative trends in frequency (a) and magnitude (b). The ratios of positive to negative (c) and of significant positive to significant negative (d) trends. Results refer to globe (GL), North hemisphere (NH), Northwest (NW), Northeast (NE), and Southeast (SE) Earth's quadrants. Sources: Papalexiou and Montanari (2019)*

The authors discovered trends in magnitude, though they are less evident than in frequency; for example, at the global scale, approximately 20% of the series exhibits a statistically significant trend in terms of frequency; however, this tendency drops to 13% in terms of magnitude.

In general, this study highlighted an increasing trend in observed daily precipitation extremes with a global value of the ratio of significant-positive to significant-negative trends equal to 2.4 in the frequency and 1.3 in the magnitude. This ratio reaches a maximum value of 7.0 for the NE zone in the frequency and of 1.5 for the NW zone in the magnitude. Therefore, the NE area (where Italy is located) is characterised by a high increase in extreme daily events over the period 1964-2013.

It is also worth analysing the spatial variation of frequency and magnitude of precipitation extremes, that Papalexiou and Montanari investigated by averaging the time series in 5°×5° cells. The results are depicted in the following two maps (Figure 18).

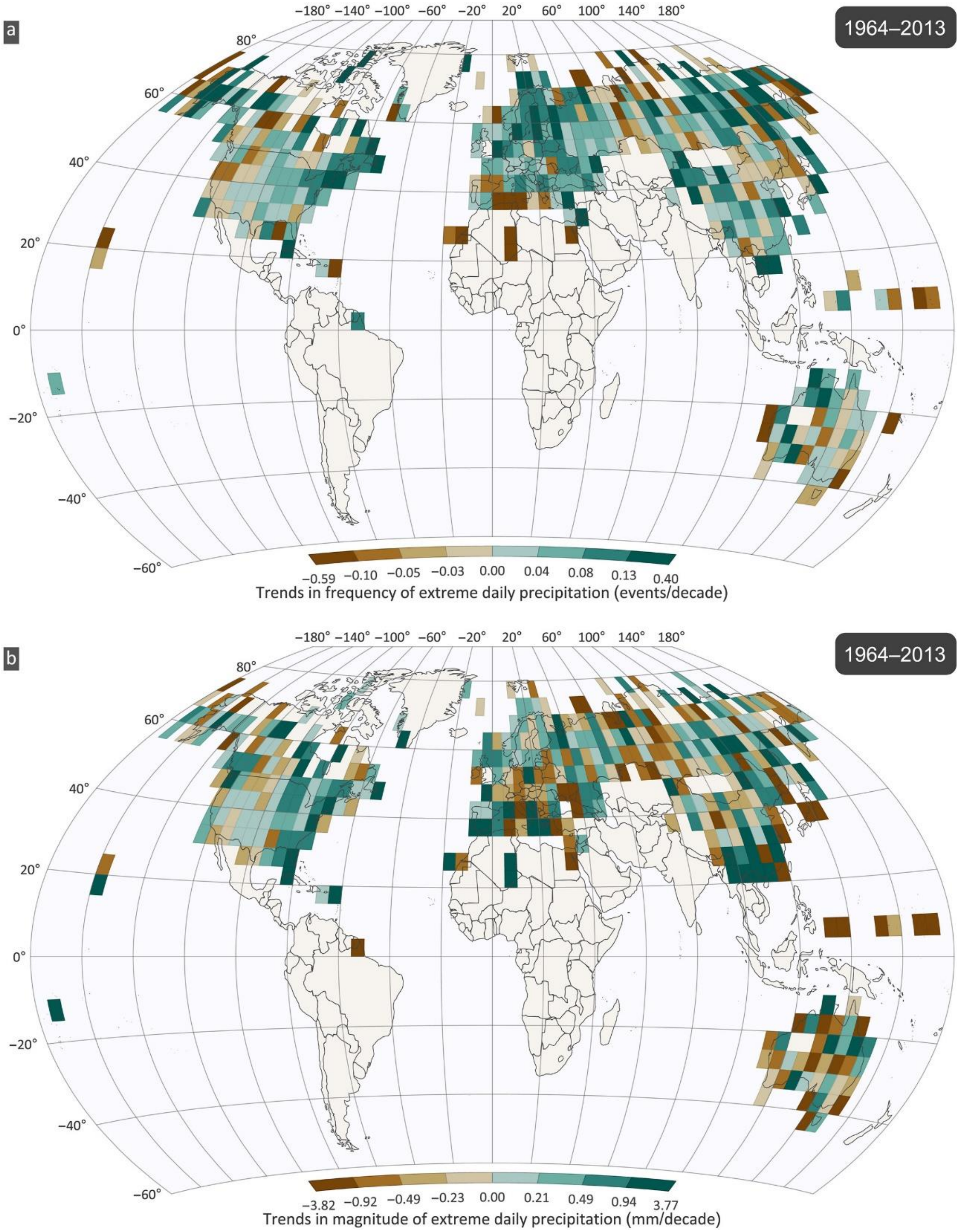

Figure 18 *- a) mean trend values in frequency as number of extreme events per decade and b) mean trend value in magnitude as mm per decade, both in 5°×5° grid cells and over the period 1964-2013. Sources: Papalexiou and Montanari (2019)*

Strongly positive trends in extreme frequency (number of daily extremes per decade) are in Europe, Russia, most of China, excluding a central-north region, norther Australia and the mid-

western part of the Unites States. At the global level, 66.4% of the grid cells studied show positive changes.
Instead, concerning to trends in extreme magnitude, high values of increase (mm per decade) are detected in Eurasia (Vietnam, Cambodia, and Thailand) and in central Russia (north of Mongolia). Regarding Europe, the western part (from Portugal to northern Norway) shows a marked positive trend while in central and eastern portion low-value cells are observed. At the global level, 56.7% of the analysed grid cells show positive changes.

Reviewing the scientific literature, it is evident that the majority of the observation-based studies exploring trends in extreme rainfall intensity are based on data recorded at the daily time scale. Instead, only a few studies investigate sub-daily rainfall extremes as highlighted by Westra et al. (2014) through a review of the most recent published research works. Despite the variability of the outcomes, they underline an increase in the intensity of short-duration events for most of the continental macro-regions.
The shortage of studies on the short-duration extremes is a remarkable issue, considering that it may not be possible to directly downscale conclusions from daily-scale analyses to the sub-daily intervals due to the different generating mechanisms of extreme rainfall at different time scales (Barbero et al., 2017; Guerreiro et al., 2018). In fact, short-duration rainfall are too sensitive to local climatic changes and orography.
Most studies on hourly rainfall extremes have been carried out focusing on local sites or small regions (Hong Kong and the Netherlands [Jakob et al., 2011]; North and Central America [Muschinski and Katz, 2013]; Europe and Mediterranean [Wang et al., 2011]; Asia [Yu and Li, 2012]), instead, far fewer studies deal with large regional- or global scale assessments. These studies, however, point out a general increase in intensity of short-duration events (from minutes to hours).
According to Westra et al., the relative scarcity in literature of large-scale studies investigating trends in hourly rainfall extremes is largely due to the lack of long-term, high-quality observations at sub-daily time scales and, therefore, the absence of an international repositories for data (records are often subjected to restricted access by the national authorities [Page et al., 2004] and, when available, they are often unevenly distributed). Additionally, not many countries across the world systematically record precipitation events due to the instrumental limitations to measure high-intensity rainfall and the inhomogeneities in the equipment

technology used over time. However, when rainfall series are available, they are often interspersed and fragmented (Teegavarapu, 2012).

A preliminary effort to collate a homogeneous database of short-duration rainfall was that of Dunn et al. (2012), that developed the Hadley Centre Integrated Surface Database (HadISD) dataset. However, the length of available records was limited, with the majority of the stations having at least 20 years of data, as shown in Figure 19.

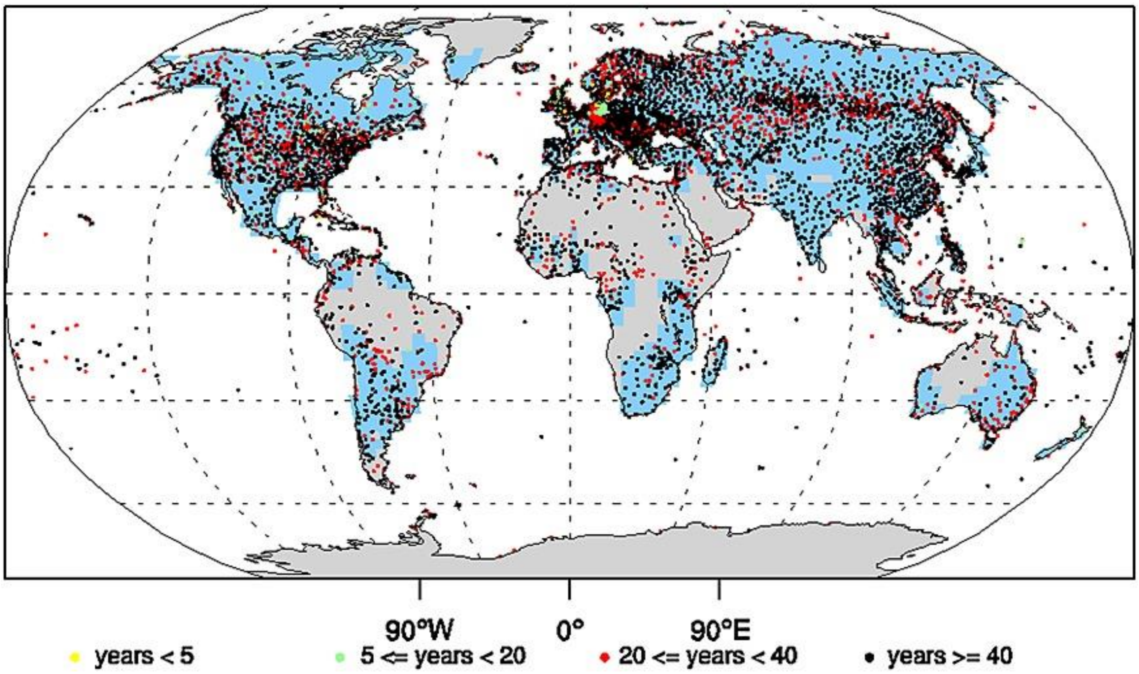

Figure 19 *- Locations of available sub-daily precipitation data from the HadISD dataset (Dunn et al., 2012). Dot colours represent record length for each station. Sources: Westra et al. (2014)*

The overall shortage of sub-daily rainfall measurements and the uneven spatial coverage of rain gauges in different countries across the world was also emphasised by Lewis et al. (2019). They developed a global sub-daily rainfall dataset, the Global Sub-Daily Rainfall Dataset (GSDR), based on gauged observations comprising 23687 stations with an average record length of 13 years.

As shown in Figure 20, the majority of rain gauges contains a large percentage of missing data; in detail, approximately 7% of stations have complete series and less than 17% (mainly located in United States, Japan, and Australia) have length of over 30 years of observations.

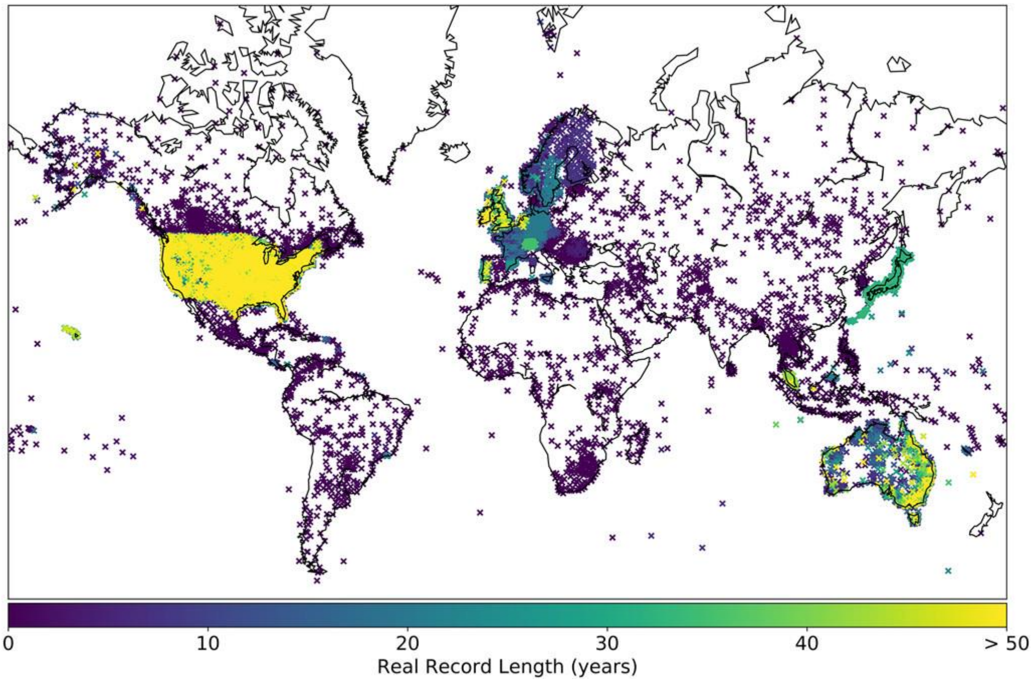

Figure 20 *- Locations and length of available sub-daily precipitation time-series from the GSDR database. Sources: Lewis et al. (2019)*

The lack of literature for many parts of the world might also be attributed partly to the difficulties in assessing changes. In fact, it is expected that sub-daily rainfall trends varies regionally and by duration due local climatic factors. By moving from large-scale analysis to local-scale studies, new trends and distinct behaviours can be identified. In fact, large-scale studies can potentially mask the presence of significant local trends by smoothing out the strong variability of rainfall regimes, as shown in Italy by Libertino et al. (2019).

In view of this, the need for an in-depth analysis of hourly rainfall extremes on a global and/or local scale is becoming increasingly clear as sub-daily extreme rainfall is intensifying more quickly than daily precipitation events (Morrison et al., 2019; Fowler et al., 2021). Additionally, the spatial and temporal variability of hourly rainfall is crucial for water resources management and for the identification and mitigation of their socioeconomic impacts. In fact, extreme short-duration rainfall can result in devastating floods that endanger people, infrastructure, and natural ecosystems. Therefore, it is essential to understand how extreme rainfall events are evolving and how they will change in warmer conditions.

1.1.2 Assessment of observed trends in rainfall extremes at the national scale

In Italy, as in many other countries of the world, studies on precipitation trends have shown discordant results (Brunetti et al., 2000; Brunetti et al., 2001) due to the natural variability of precipitation regime. Therefore, the detection of trends in rainfall extremes time-series has become a topic of particular interest, and to this end, high-intensity and short-duration rainfall time series were collected and statistical analysis techniques were further investigated.

Several studies have analysed rainfall patterns on daily to annual time scales, highlighting a statistically significant decrease in annual precipitation and in the number of rainy days (Buffoni et al., 1999; Brunetti et al., 2004; Brunetti et al., 2006). In particular, climatic conditions at the Italian scale have evolved according to the following patterns:

- the total annual precipitation has reduced by around 47 mm for the north and 104 mm for the south in the last 100 years.
- the number of rainy days has decreased by about 14% and the reduction rate has been much higher in winter than in the other seasons.
- an increasing trend in the intensity and a decreasing trend in rainfall duration has been detected, especially in winter;

The actual state of changes in the Italian precipitation has been draw by Caporali et al. (2020) through a review of the most relevant published studies on the analysis of total annual o seasonal precipitation. This work has been a breakthrough by summarizing the knowledge derived from local studies in a single analysis and highlighting the main patterns of rainfall changes in the last decades. In the review, they analysed 54 studies on the Italian precipitation regime, published in the period 1999-2018 and divided according to three indices: time-series length (short term, long term, centennial trend), macro-area (Italy - IT [13 studies], North - N [28 studies], Centre - C [20 studies], South and Island, - S [25 studies]) and season (winter, spring, summer, autumn, annual). The authors summarized the results in the following Figure 21.

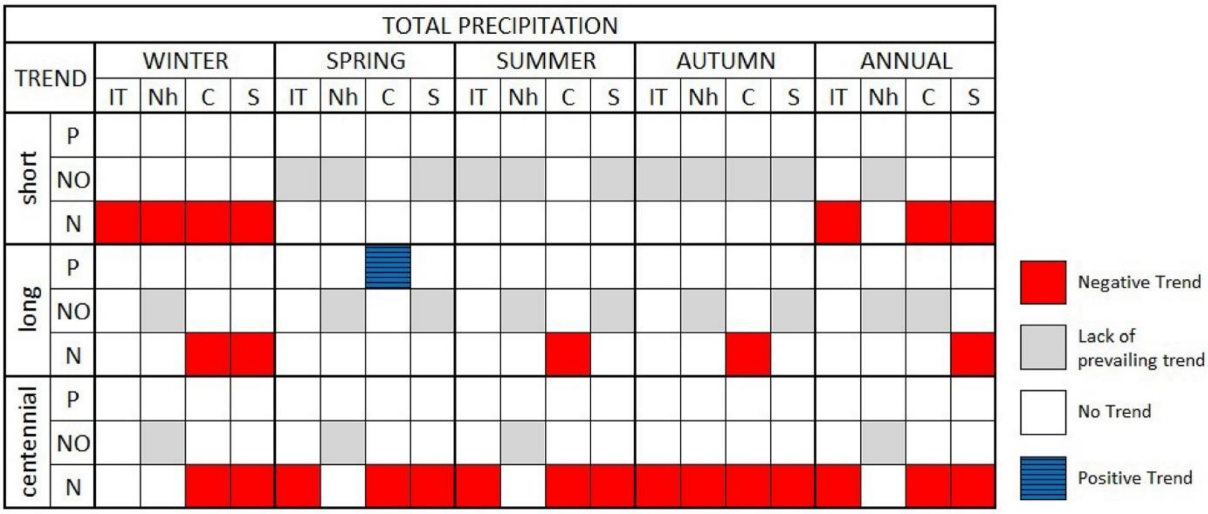

Figure 21 *- Summary of the results on the Total Annual and Seasonal Precipitation index. Each box represents a combination of the three analysed features: time-series length (short term, long term, centennial trend), macro-area (Italy - IT, North - N, Centre - C, South & Island - S) and season (winter, spring, summer, autumn, annual). The filled boxes show the share higher than 50% in the review, red for negative trends, hatched blue for positive trends and grey for lack-of significant trend. Sources: Caporali et al. (2020)*

As highlighted by the authors, the overall results of the review suggest that the majority of the studies agree about a decrease at the annual scale of the total precipitation throughout the Italian territory, except for the Northern Italy, for short and centennial time coverage of the series.

In particular, for short-term precipitation series, a prevalent negative trend was observed on annual basis at the country-level (except for the northern regions), which is mainly led by the negative trends in the winter season all over Italy. No trend evidence was detected for the other seasons in any region.

Additionally, concerning long-term trend analysis, the analysis revealed a generalized no trend prevalence for Northern Italy at the annual and seasonal scales. Instead, Central Italy turned out to be characterized by a negative trend in winter, summer, and autumn, a prevailing positive in spring, and no trend on annual basis. Finally, for Southern Italy a negative trend is clear at the annual and for the winter period, while there are no trends for the other seasons. It is worth noting that none of the considered studies analysed the Italian territory as a whole.

By analysing the centennial trend analysis studies for the entire Italian territory, the authors highlighted a marked decreasing trend at the annual time scale and in spring, summer and autumn, while less significant in winter. In Northern Italy, no clear trend emerges, while Central and Southern Italy show a sharp negative trend at the annual time scale and in the other subperiods.

These results are confirmed by recent published works, not included in the review. In particular, regional studies performed in Italy mainly evidenced a decrease in annual rainfall especially in the southern (Caloiero et al., 2011a; Caloiero et al., 2019) and in the central regions of the country (Scorzini and Leopardi, 2019; Gentilucci et al., 2019), while in its northern part, the decreasing tendencies in the annual values resulted rarely significant.

Focusing more on southern Italy, Caloiero et al. (2018) explored trends of monthly rainfall in Southern Italy. They observed a generalized negative trend of rainfall anomalies at annual scale, while different tendencies at seasonal scale. In particular, a downward trend emerged in winter and autumn, especially in Campania and Sicily, while only Calabria, Basilicata and Apulia showed evident upward trend for spring anomalies. No clear trends were detected in summer period in the whole area.

Furthermore, annual and winter monthly negative precipitation trends were registered for several regions of southern Italy, such as in Apulia (Lionello et al., 2014), Basilicata (Piccarreta et al., 2004; Piccarreta et al., 2006; Piccarreta et al., 2013), Calabria (Caloiero et al., 2011b; Brunetti et al., 2012; Caloiero et al., 2020), Campania (Diodato, 2007; Longobardi and Villani, 2010) and Sicily (Cannarozzo et al., 2006; Liuzzo et al., 2016).

As can be observed, several rainfall trends studies have essentially been conducted at a regional or slightly larger scale due to the lack of a national database. In fact, in Italy, data collection has been independently managed by the single regions since 1998 with the dismissal of the National Agency for Hydro-Meteorological Monitoring (SIMN); therefore, data significantly from differ one region to another with regard to time aggregation, quality and observation period. Recently, in order to overcome the lack of a national database, several global rainfall datasets have been created using different methodologies, such as satellite or reanalysis datasets. The climate global reanalysis produced by the European Center for Medium Weather Forecast (ECMWF), called European Reanalysis (ERA), is among the most well-known and used datasets. ERA-5, the fifth generation of reanalysis database, assimilates a large number of satellite and ground-based data and has been widely used to detect possible trends in Italy. For example, Chiaravellotti et al. (2022), by using rainfall data extracted from the dataset ERA5-Land during the period 1950-2020, detected a few relevant trends at the annual scale, mostly in northern Italy (positive trend). At seasonal scale, the results showed a marked negative trend in winter and positive in the other seasons.

Nevertheless, most of the studies were carried out on an annual, seasonal, or at most daily time scales as shown by Caporali et al. (2020). Additionally, they confirmed the widespread awareness that studies on short-duration rainfall are still scarce in the literature, due to the lack of continuous sub-daily precipitation series. A systematic frequency analysis of these highly intense events would require a complete countrywide dataset, but this kind of information is still lacking for the Italian territory. The few available studies have been conducted on a regional or smaller area scale.

In particular, in the north-western part of Lombardy region, Uboldi and Lussana (2018) discovered that the rainfall annual maxima for 6 to 24-h durations increased significantly from the first half (1950-1977) to the second half (1978-2005) of the analysed period. Instead, a decreasing trend was observed for 1-h duration events.

In Tuscany region, a statistically significant increasing trend during the years 1970-1994 was found in extreme events at different durations (1, 3, 6, 12 and 24 hr) (Crisci et al., 2002). Instead, Fatichi and Caporali (2009), using precipitation time series recorded in the period 1916-2003, highlighted an absence of trends in the intensity of extreme events of 3, 6, 12 hours in almost all the stations over the region.

In Marche region, Soldini and Darvini (2017) analysed annual maximum rainfall for 1, 3, 6, 12 and 24 hours and 15 and 30 minutes in the period 1951-2013, detecting no trend in most of the analysed rain gauges. Some positive trends were observed only for rainfall of 15 and 30 minutes, while for the other durations the percentage of stations with positive and/or negative trends were less than 5%.

In Apulia region, Polemio and Lonigro (2015) analysed rainfall series of short-duration (from 1 h to 5 days) annual maxima in the period 1921-2005 detecting a generalised decreasing trend except for a small number of stations with an increasing trend in series as long as 6h-duration.

An attempt to investigate the tendency of short duration rainfall events in Sicily was proposed by Bonaccorso et al. (2005). They found that precipitation of shorter durations (less than three hours) exhibited generally an increasing trend, while the opposite was observed for events of longer durations. Such a negative trend is confirmed when the process is integrated over even larger temporal window up to the annual scale. Additionally, Arnone et al. (2013) detected in the period 1950-2005 a positive trend for the shortest duration (1 hr) at about 14% of the stations, while for the duration of 3, 6 and 12 hr only at about 6% of the rain gauges. Instead, for the 24 hr duration no trends were identified.

One of the first study on a larger scale was conducted by Libertino et al. (2019). They exploited a new dataset of sub-daily annual maxima named I-RED (i.e., Italian Extreme Rainfall Dataset, Libertino et al., 2018b) considering only time series with at least 30 years in the period 1928-2014 in order to analyse the influence of the spatial scale on observed trends. They underlined an increase in the north-eastern part of the country, while a decreasing trend in the southern extreme of the peninsula (Calabria region). Additionally, a general downward tendency for shorter durations was observed in the northwest of the country, turning to an increasing trend when longer durations are considered. The opposite, instead, was detected in Sicily.

The novelty of the study was to explore different spatial scales when performing extreme rainfall trend analyses (from the country scale to individual regions and to small local areas). They demonstrated that, even if no statistically significant trend can be identified at the country scale, significant regional trends arise when smaller scales are considered due to the effects of the local climatic patterns.

The results of the study by Libertino et al. are not very clear at the southern Italy scale, except in Calabria region, where a general decreasing tendency was detected. Indeed, the small number of stations with continuous series or with a limited number of gaps does not allow to draw conclusions at the local scale (single rain gauges) or in larger- to regional-scale domains.

In view of this, the spatial and temporal analysis of hourly rainfall series in southern Italy is becoming a pressing priority. Therefore, the aim of this thesis work is to investigate time series of sub-daily annual maximum rainfall depths (1, 3, 6, 12 and 24 hours) in the period 1970-2020 in order to detect potential trends. For this reason, the database of rainfall annual maxima was constructed using all available records and extend by using spatial gap-filling procedures. This extended database enabled the assessment of rainfall trends, thereby reducing the statistical uncertainties, and the analyses of the influence of the spatial and temporal scale on observed trends.

The findings of this study are expected to improve the understanding of the effects of climate change on short-durations rainfall events in terms of frequency and intensity at the southern Italy scale.

Chapter 2. Hydrology in data scarce environments: methods and techniques

2.1 State of the art on gap-filling techniques

The availability of long-term data on precipitation occurrence, intensity, amount, and spatio-temporal distribution is crucial for the design of hydrologic structures, water supply, water quality modelling, and other hydrologic studies. Additionally, the analysis of extreme rainfall data is essential to investigate changes in the frequency and intensity of extreme weather events in response to the warming climate conditions.

However, in many regions worldwide, long-term gap-free precipitation data at temporal resolutions of day or less, required to perform such analyses, are often non completely available. Often hydrologists encounter the problem of missing data because of systematic and/or random errors. The uneven and fragmented records are typically due to the activation and dismissal of stations, service interruptions, inability of operator to collect data, replacement/renewal of the sensor, changes in the ownership of the monitoring network, and relocation of the equipment (with changes in location and elevation).

When dealing with not-continuous time-series two approaches can be adopted: i) precautionary approach, that consist in excluding all the series with a length shorter than a threshold and ii) a conservative approach, focused on the identification of methodologies aimed at reconstructing missing data by using all the available information even from the shorter records.

The second approach turns out to be more complex and can lead to severe errors in estimating the data. Nevertheless, it is the most widely followed because dense, serially complete and reliable series are needed to understand precipitation processes (Pappas et al., 2014). Therefore, reconstruction methods are required to fill the gaps with appropriate values to obtain a serially complete dataset.

Data filling techniques are normally selected based on location and desired accuracy required for the hydrologic analyses and are divided in spatial or temporal interpolation methods. The first group uses observations available at different stations in a region for infilling the data at a site with missing data (i.e., base station), while the second one employs only data from the base site itself to infill data. Spatial interpolation methods depend on the existence of strong spatial correlation between any stations and the base site, while temporal interpolation on the presence of serial autocorrelation in the time-series.

Several interpolation methods have been frequently employed to interpolate rainfall data from rain-gauge stations to estimate missing precipitation data. Examples of such methods are: temporal interpolation methods, simple conventional methods (e.g., Thiessen polygons [Thiessen, 1911], isohyet mapping [ASCE, 1996]), non-linear interpolation methods (normal-ratio [ASCE, 1996], gauge mean (GM) and single best estimator (SBE) [Xia et al., 1999]), deterministic distance-based weighting methods (i.e., inverse distance weighting (IDW), [ASCE, 1996], coefficient of correlation weighting (CCW), inverse exponential weighting (IEW), nearest neighbour distance weighting (NNDW) [Teegavarapu and Chandramouli, 2005]), regression and time series models (global polynomial interpolation [Wang, 2006], local polynomial interpolation [Loader, 1999], thin-plate spline [Chang, 2004]), and complex geostatistical methods (i.e., kriging, cokriging, kriging with an external drift (KED) [Teegavarapu, 2009], artificial neural networks (ANN) and Kalman filter approaches [Alavi et al., 2006]). More details on the aforementioned methodologies can be found in Koutsoyiannis and Langousis (2011).

Daly et al. (1994) developed a regression model for estimation of precipitation values using different spatial parameters, such as elevation, topography, proximity to coastal area and distances as independent variables.

In recent years, instead, authors have tried to associate stochastic and geostatistical interpolation methods with traditional distance-based weighting techniques in estimating the missing values. For example, Noori et al. (2014), in their work, proposed the integration of the IDW method with a geographic information system (GIS) to calibrate the parameters and then, to estimate the rainfall distribution. By using a total of 25 rainfall stations with 10-years rainfall data series, they showed that, using a search radius of 105 km for all the rainfall stations, the IDW method is a suitable interpolation method to predict the rainfall data in unknown locations.

Ashraf et al. (1997) compared some interpolation methods (kriging, inverse distance and co-kriging) to estimate missing values of precipitation. They showed that kriging method provided the lowest root mean square error (RMSE) related to the reconstruction.

Additionally, a similar study was carried out by Teegavarapu (2005) comparing different estimating methods, such as inverse distance weighting method (IDW), integration of Thiessen polygon approach and inverse distance method (MIDW), coefficient of correlation weighting method (CCW), inverse exponential weighting method (IEW), nearest neighbours weighting method (NNW), revised nearest neighbours weighting method (RNNW), artificial neural networks estimation method (ANN), and kriging estimation method (KEM). The study tested all the methods using daily precipitation data from the state of Kentucky (USA) and demonstrated that the most accurate methods are ANN, and Kriging method.

Several authors (Moral, 2010; Xu et al., 2015) evidenced that geostatistical techniques provide better rainfall estimations than deterministic techniques because they allow for the exploitation of spatial correlation between neighbouring stations to predict attribute values at ungauged locations. Among the geostatistical approaches, kriging prediction technique was widely used because it provided better estimates of rainfall than conventional methods. Additionally, the main advantage of kriging over simpler methods is that the sparseness of recorded observations can be overcome by including secondary attributes that might be more densely sampled. For rainfall measurements, secondary information can be the digital elevation model (DEM). A multivariate extension of kriging, known as cokriging, and another geostatistical technique, kriging with an external drift, were developed to combine both types of information, as shown in the work of Goovaerts (2000). The author tried to interpolate annual and monthly rainfall data using two types of approaches: i) methods that use only rainfall data (i.e., Thiessen polygon, inverse square distance, and ordinary kriging), and ii) algorithms that combine rainfall data with a digital elevation model (linear regression, co-kriging, simple kriging with varying local means, kriging with an external drift, collocated ordinary cokriging). As expected, they demonstrated that the larger reconstruction errors were obtained for the two algorithms (inverse square distance, Thiessen polygon) that ignore both the elevation and rainfall records at neighbouring stations. Ordinary kriging (without elevation) outperforms the linear regression, which ignores the importance of accounting for the information provided by surrounding stations when the correlation between rainfall and elevation is moderate. The author highlighted that to account for both elevation and spatial correlation in interpolating rainfall data, the multivariate geostatistical algorithms are the best predictors, despite the complexity of implementing them.

A similar study was carried out by Pellicone et al. (2018) in Calabria (a region of southern Italy), in which several geostatistical and deterministic approaches of rainfall spatial interpolation were applied and the results compared in order to choose the best method for reproducing the actual precipitation field surface. In particular, a deterministic (inverse distance weighting, IDW) and four geostatistical (ordinary kriging, OK; kriging with external drift, KED; ordinary co-kriging COK and empirical Bayesian kriging, EBK) methods were applied to interpolate monthly rainfall observations using as auxiliary variables in the multivariate models the elevation and distance to coastline. They indicated that geostatistical methods outperform inverse distance, confirming findings by other researchers (Goovaerts, 2000). Additionally, among these methods, the kriging with an external drift showed the smallest error of prediction in that region.

Therefore, it is clear how challenging it is to identify the best interpolation method for a particular study area because the performance depends on several factors, such as geomorphological characteristics of the study area, sampling density and spatial distribution of rain gauges, and rainfall data variance.

2.2 SIMPLE RECONSTRUCTION METHODS

These methods are conceptually simple and use regional rainfall information from nearby rain gauges to estimate missing values at the base point (i.e., station where missing data need to be estimated). In particular, gauge mean estimator (GME) uses an average value of observations from the nearby rain gauges, single best estimator (SBE) uses observations from one rain gauge, and climatological mean estimator (CME) uses mean of historical observations available for that specific temporal period at the base rain gauge. These methods are often used as benchmark methods to serve as a comparison point for advanced spatial interpolation methods and to evaluate their performances.

2.2.1 Gauge Mean Estimator (GME) method

Gauge Mean Estimator (GME) method uses the mean of all observations at several gauges near the base site to provide an estimate of the missing value. The method is a special case of IDW in which the weights are raised to an exponent of zero. Estimate of missing precipitation value using GME is given by the following equation:

$$h_m = \frac{\sum_{i=1}^{n_r} h_i}{n_r - 1} \qquad [1]$$

where h_m is the missing observation at the base station m, h_i is the observation at station i, n_r is the number of rain gauges including the gauge at which missing precipitation data is estimated.

2.2.2 Sigle Best Estimator (SBE) method

The Single Best Estimator (SBE) method uses data from the gauges closest to the site where missing data need to be reconstructed. This closest rain gauge may be selected by Euclidean distance or by using information about the strongest positive correlation which requires long-term historical data. The precipitation estimates using SBE are given by:

$$h_m = h_i^* \tag{2}$$

where h_m is the missing observation at the base station m and h_i^* is the observation value from a specific gauge selected as an SBE.

2.2.3 Climatological Mean Estimator (CME) method

The Climatological Mean Estimator (CME) method estimates a missing value using the climatological mean for the day based on the available historical record at the gauge. This method requires at least one available measurement for each day of the year. When this one measurement is not available, one can use the following or previous day's value or an average centred on the estimation day. The estimate of missing precipitation value using CME is given by:

$$h_m = \frac{\sum_{k=1}^{n_0} h_k}{n_0} \tag{3}$$

where h_m is the missing observation at the base station m, h_k is the observation at the year k, n_0 is the number of years.

2.3 DETERMINISTIC RECONSTRUCTION METHODS

Distance-based weighting methods are the most commonly used deterministic approaches for the estimation of missing data in hydrological time-series. In the USA, Inverse Distance Weighting (IDW) approach is often referred to as national weather service (NWS) method and is regularly used for the estimation of missing rainfall data (ASCE, 1996).

Several variants of IDW were developed by researchers with a focus mainly on the weighting schemes because the arbitrariness in the choice of weighting parameter and the definition of the neighbourhood are two critical limitations of the method.

2.3.1 Inverse Distance Weighting (IDW) method

Inverse Distance Weighting (IDW) approach (Simanton and Osborn, 1980) is the most commonly used deterministic spatial interpolation method for the estimation of missing data to ungauged points by computing an average value for unsampled locations using distance-based weighted values from nearby gauged locations. Therefore, the value to be estimated at a location is function of data recorded at the surrounding stations and the distance of each gauged station from the ungauged point. The used weights are proportional to the proximity of the sampled points to the ungauged location and are specified by the IDW power coefficient (n). The IDW method for estimating a missing value, h_m, using the recorded values at other stations, is given by:

$$h_m = \frac{\sum_i h_i d_{m,i}^{-n}}{\sum_i d_{m,i}^{-n}} \qquad [4]$$

where h_m is the missing observation at the base station m; h_i is the observation at station i; $d_{m,i,}$ is the distance from the station i to the station m; and n is power coefficient. Following Goovaerts (2000) the most common power value power is 2.

According to Brimicombe (2003), a key step to implement the IDW algorithm is the selection of the optimal number of neighbours (N) and neighbourhood size (R), i.e., N is the minimum number of gauged stations existing within the radius R centred on the given point where missing data need to be reconstructed.

2.3.2 Coefficient of Correlation Weighting (CCW) method

The success of the IDW method strongly depends on the existence of strong positive spatial autocorrelation. This correlation might be assessed by estimating the coefficient of correlation (CC) between any two data obtained from two locations. Since the coefficient of correlation is one way of quantifying the strength of spatial autocorrelation, Teegavarapu and Chandramouli (2005) tried to replace the IDW weighting power factor by the correlation coefficient, developing the Coefficient of Correlation Weighting (CCW) method. The estimation method is given by:

$$h_m = \frac{\sum_i h_i CC_{m,i}}{\sum_i CC_{m,i}} \qquad [5]$$

where $CC_{m,1}$ is the coefficient of correlation, obtained by using the data at station m and any other station i.

2.3.3 Inverse Exponential Weighting (IEW) method

The Inverse Exponential Weighting (IEW) method uses a negative exponential function replacing the reciprocal-distance as weight in the traditional IDW method. The estimation method is given by:

$$h_m = \frac{\sum_i h_i e^{-nd_{m,i}}}{\sum_i e^{-nd_{m,i}}} \qquad [6]$$

The most commonly used value for *n* is 2.

2.4 ARTIFICIAL NEURAL NETWORKS (ANN) METHOD

In recent years, Artificial Neural Networks (ANN) have been applied extensively for estimation and forecasting of hydrological variables (Tanty and Desmukh, 2015).

The architecture of ANN might be a feed-forward network and consists of hidden layers with neurons. The hidden layer neurons are selected using a trial and error procedure. The input neurons use values from all the gauged stations and output neuron of the ANN provides the missing value at the ungauged station of interest. The neural network training is done using standard error, supervised back-propagation training algorithm with a fixed learning rate, momentum factor and activation function. The learning rate is a factor that determines the amount by which the connection weight is changed according to error gradient information. The momentum parameter governs the weight change in the current iteration of the algorithm due to change in the previous iteration. The activation function is used for modelling the transformation of values across the layers. These factors are obtained by trial and error method and can significantly impact the training and final results.

2.5 GEOSTATISTICAL RECONSTRUCTION METHODS

In recent years, application of geostatistical interpolation methods on climatic variables have been extensively performed, as shown in Webster and Oliver (2007). In the following sections, a brief description of the two most widely used methods (ordinary kriging and ordinary co-kriging) is provided.

2.5.1 Ordinary Kriging (OK) method

Ordinary Kriging (OK) (Isaaks and Srivastava, 1990) approach is the most widely used geostatistical method for rainfall data interpolation since it considers the spatial correlation between data points and provides unbiased estimates with a minimum variance.

The two main assumptions for kriging to provide best unbiased prediction are:

- stationarity (the joint probability distribution does not vary across the study space and, therefore, the same variogram model is assumed to be valid across the study space)
- isotropy (uniformity in all directions).

However, there are various forms of kriging that allow the strictest form of these assumptions to be relaxed. Thus, several forms of kriging interpolators have been developed (e.g., ordinary kriging, universal kriging, simple kriging, block kriging, kriging with anisotropy etc.). Focusing on the Ordinary Kriging (OK) interpolation method, it can be understood as a two-step process: i) the variographic analysis, which consists of determining the spatial covariance structure of the gauged points by fitting a variogram model; ii) the kriging implementation, in which the weights, derived from this covariance structure, are used to interpolate values for unsampled points across the study area.

Kriging is a geostatistical interpolation method based on spatially dependent variance. The degree of spatial dependence is generally expressed as a variogram. The semi-variogram is a representation of the covariance between each pair of points in the considered time series. For each pair of points, the semi-variance (half-square difference between pairs of values at a fixed distance) is plotted against the distance (lag) between them. The general expression that is used to estimate the semi-variogram is given by:

$$V_y(d) = \frac{1}{2n(d)} \sum_{i=1}^{n(d)} (h(i) - h(i+d))^2 \qquad [7]$$

where $h(i)$ and $h(i+d)$ are the observations time-lagged by lag-distance d and $n(d)$ represents the number of pairs of the sample separated by lag d.

The experimental variogram is the plot of observed values, while the theoretical variogram is the model that best fits the recorded data. The semi-variogram must be fitted with a mathematical function or model. Depending on the shape of semi-variogram, several mathematical models are possible, such as spherical (Eq. [8]), exponential (Eq. [9]), and Guassian (Eq. [10]).

$$\gamma_{spherical}(h) = c_0 + c_1 \left(1.5\frac{d}{a} - 0.5\frac{d^3}{a^3}\right) \qquad [8]$$

$$\gamma_{exponential}(h) = c_0 + c_1 \left(1 - \exp\left(-3\frac{d}{a}\right)\right) \qquad [9]$$

$$\gamma_{gaussian}(h) = c_0 + c_1 \left(1 - \exp\left(-\frac{(3d)^2}{a^2}\right)\right) \qquad [10]$$

where d is the lag-distance, c_0 and a are respectively the nugget and the range, while the summation of c_0 and c_1 is referred to as sill. A typical spherical semi-variogram is shown in Figure 22.

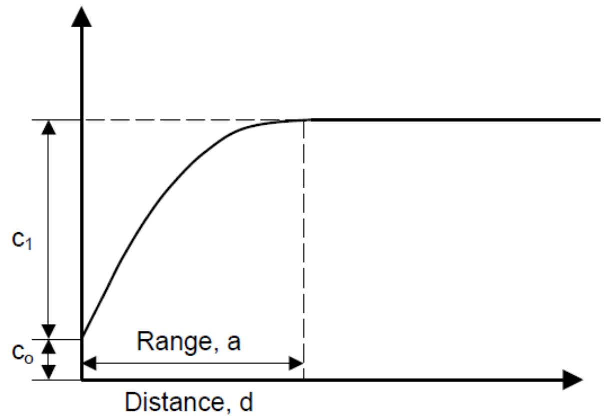

Figure 22 *- Typical spherical semi-variogram with the characteristic parameters. Sources: Teegavarapu and Chandramouli (2005)*

In kriging approach, the weights are based not only on the distance between the measured points and the ungauged location, but also on the overall spatial correlation among the measured points and their values. The weights mainly depend on fitted model (i.e., semi-variogram). The general equation for estimating missing values is given by:

$$h_m = \sum_i h_i \lambda_i \qquad [11]$$

where h_m is the missing observation at the base station m, h_i is the observation at station i, λ_i is the weight obtained from the fitted semi-variogram. It is clear that the observed data are used twice, once to estimate the semi-variogram and then to interpolate the values.

However, kriging methods are plagued by several limitations. Selection of variogram model, assignment of arbitrary values to sill and nugget parameters, and distance intervals are a few difficulties associated with this method.

2.5.2 Ordinary Co-Kriging (COK) method

Ordinary Co-Kriging (COK) method is an extension of the basic kriging algorithm that allows to predict the value at unsampled locations by using the main variable and an auxiliary variable. In particular, it is appropriate when the main variable is sparse but related secondary information is abundant. COK requires the same conditions as kriging but demands more variographic analyses, modelling, and computation time. The general equation for two-variable cokriging for estimating missing values is given by:

$$h_m = \sum_i h_i \lambda_i + \sum_j \beta_j t_j \qquad [12]$$

where h_m is the missing observation at the base station m, h_i is the first regionalized variable at station i, λ_i is the weight obtained from the fitted semi-variogram, t_j is the second regionalized variable that is co-located with h_i, β_j is the undetermined weight assigned to t_j.

2.5.3 Location-based variants of the Ordinary Kriging method

Over the years, several variants of the ordinary kriging method have been developed.

In Sicily region (southern Italy), Liuzzo et al. (2016) tried to fill the gaps in the monthly rainfall dataset, covering the period 1921-2012, using a geostatistical spatial interpolation technique, the residual ordinary kriging (Odeh et al., 1995), which allows to identify two different types of spatial variability, i.e., deterministic (trend) and stochastic. Stochastic variability may be further split into spatially dependent and spatially independent components. The spatially dependent component is generally evaluated through a variogram, while the spatially independent component is linked to measurement imprecision and can often be neglected. Therefore, the missing rainfall data at a given location can be evaluated as the sum of the deterministic component and the spatially dependent stochastic component. The deterministic component is estimated by using a geographically weighted regression, while the determination of the stochastic component is a two-step procedure: i) identification of the residuals, ii) application of the ordinary kriging to the residuals.

They demonstrated that the errors related to the estimation of missing data by residual ordinary kriging resulted to be lower than those produced by other methods, such as inverse distance weighting, ordinary kriging and multiple linear regression.

Teegavarapu (2009), instead, proposed an association rule mining (ARM) based on a spatial interpolation approach, namely an integrated technique that combines the power of data mining techniques (Zhang and Zhang, 2002) and the ordinary kriging interpolation method. ARM is one of the most popular data mining methods mainly aimed at extracting correlations, patterns, associations or causal structures among data available in databases and at formulating rules based on spatial and temporal associations among observed time-series. The author demonstrated that the rules allow for improving the precipitation reconstruction obtained by spatial interpolation methods.

A further revised variation of the OK method is that proposed by Libertino et a. (2018a), named “patched kriging”. The methodology consists in applying the ordinary kriging equations sequentially to the values recorded annually in order to create a homogeneous dataset of synthetic series with uniform lengths. They applied this technique to a case study in the north-western Italy (Piemonte region) in order to reconstruct missing data in the local dataset of sub-daily rainfall annual maxima.

In implementing the procedure, first they removed the possible correlation between rainfall and elevation by performing a linear regression on precipitation vs. elevation. Then, once assessed the regression significance, de-trended at-station precipitation values were calculated by subtracting the regressed elevation effect from the rainfall data.

Regarding the variographic analysis, they calculated a sample variogram averaged over all the considered years and based on the number of data available in each year. In detail, for each year, y, the annual sample variogram $V_y(d)$ is computed using Eq. [7]. Then, a global mean sample variogram was obtained by averaging the annual sample variogram, weighted by the number of active stations ($S_{att,y}$) in the considered year, as given by:

$$V_{global} = \frac{\sum_y V_y(d) * S_{att,y}}{\sum_y S_{att,y}} \qquad [13]$$

The estimated global experimental variogram, V_{global}, was converted to an analytical function. Then, for each cell of the gridded domain, the fitted variogram was used to weight the values recorded at the nearest cells. The sequential kriging application led to the development of a set of grids (as many as the considered years), named cube, containing the estimated values of precipitation maxima for each location of the study area. By accessing the cube at a specific point, they obtained the complete time-series for that location. The last step of the procedure was to identify a suitable correction factor for increasing the variability of the estimated series.

In this thesis, a new spatial reconstruction approach based on ordinary kriging is proposed, namely "Spatially-Constrained Ordinary Kriging" (SC-OK) (Avino et al., 2021), which combines deterministic and geostatistical methods. In particular, the procedure allows for the reconstruction of missing data by means of the ordinary kriging equations, but only in the locations identified by the spatial parameters of the inverse distance weighting technique (further details can be found in the 3.4.1 section).

Chapter 3. Reconstruction of the rainfall database of southern Italy

3.1 DESCRIPTION OF THE STUDY AREA

The area under investigation is the southern Italy, namely a large portion of the Italian peninsula, including Apulia, Basilicata, Calabria, Campania, and Molise regions, and covering an area of 63000 km^2, about 20% of the whole Italian territory. Southern Italy is located within the Mediterranean basin, surrounded by the Adriatic Sea to the east, the Ionian Sea to the south-east and the Tyrrhenian Sea to the west. The area is mostly hilly-mountainous. Indeed, it is crossed from north to south by the Apennines. It is largely characterized by the typical Mediterranean climate made up of mild and rainy winters and hot and dry summers, which dominates especially the coastal areas. Only along the Apennine mountains the climate is continental, with cold and snowy winters and mild summers.

Apulia region is an area of approximately 19541 km^2; 54.2 % of the country reaches altitudes ranging from 0 to 300 m a.s.l., 44.4 % of the region has altitudes from 300 to 600 m a.s.l., and only the 1.4 % has altitudes exceeding 600 m a.s.l. Thus, most of the regional territory is flat except for the Mount Gargano area situated in the North-East, and the Sub-Apennine part located in the North-West of the region, where the altitude is greater than 1000 m (Polemio and Lonigro, 2015). The climate is semi-arid with hot and dry summer and mild and rainy winter season.

Basilicata region is located between 15°20' and 16°53' latitude and 39°54' and 41°8' longitude. It is an area of 10073 km^2, covered for 70% by the Apennines. The altitude ranges from 0 to 2400 m a.s.l. The Apennine chain represents a barrier for Atlantic currents from the Mediterranean Sea dividing the Tyrrhenian basins from the Ionian ones. The climate over the entire region is characterized by cold winters and relatively warm summers.

Calabria region is located between 15°36' and 17°13' latitude and 37°54' and 40°10' longitude. It covers an area of 15222 km^2 with a coastline of 738 km divided between the Tyrrhenian Sea on the west side and the Ionian Sea on the southeast side. Calabria is mainly mountainous, with more than 40% of the territory located over 500 m a.s.l. The climate is typically temperate with mild winters and dry and warm summers (Coscarelli and Caloiero, 2012). In particular, the Ionian side, impacted by African warm air currents, presents high temperatures and short and heavy rainfall, while the Tyrrhenian area is characterized by lower temperatures and high precipitation. Instead, the inner areas present cold winters and fresh summers.

Campania region extends from the Tyrrhenian Sea to the Southern Apennine Chain, covering an area of about 13671 km^2. The area is characterized by a complex orography that represents a physical barrier for meteorological phenomena originating from the Tyrrhenian Sea (Cuomo et al., 2011; Pelosi and Furcolo, 2015). The inner portion is characterized by the presence of a central mountain ridge extending for more than 200 km in a NW–SE direction, with maximum peak heights reaching 2000 m a.s.l. On its western side, the chain is bounded by a concave area and the landscape is characterized by a wide flat area with isolated volcanic reliefs. Close to the coast there are two volcanic massifs: Vesuvius (1277 m) and Campi Flegrei. The eastern side of the region is dominated by a hilly landscape. The region is characterized by typical Mediterranean climate, with dry summers and wet winters.

Molise region covers an area of 4461 km^2. The western area is characterised by a mountainous landscape, while the central and eastern zone are dominated by a hilly morphology.

To sum up, the study area is characterized by a complex orography (Figure 23) that represents a physical barrier for meteorological phenomena and, therefore, has a strong impact on the precipitation regime. In fact, the geographic position and mountainous nature lead to high climatic variability and a precipitation gradient between the Tyrrhenian, Ionian, and Adriatic side. Therefore, the rainfall patterns widely vary over the regions with relevant local effects due to the presence of orography and the proximity of the sea.

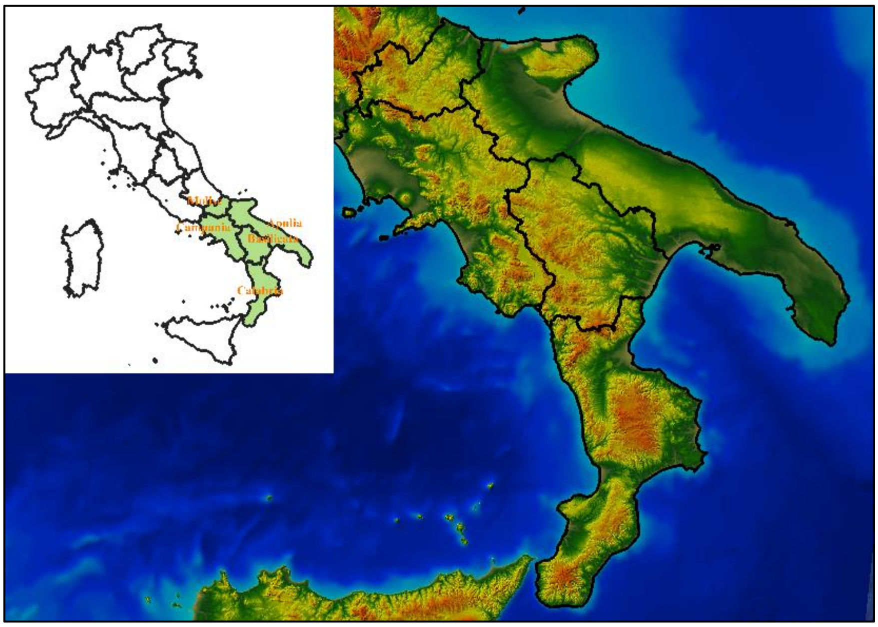

Figure 23 *- Study area with the digital elevation model (DEM). Sources: TINITALY DEM (Tarquini et al., 2012)*

3.2 STRUCTURE OF THE RAINFALL MONITORING NETWORK

This section aims at describing the set-up of the hydrological monitoring system in southern Italy, highlighting how the rainfall monitoring network has operated intermittently with changes in both the number and location of rain gauges.

The monitoring network has been managed, over the years, by two different agencies: initially, the National Agency for Hydro-Meteorological Monitoring (SII/SIMN) and, subsequently, the Regions and the Department of Civil Protection.

The Italian Hydrographic Service (SII, Legislative Decree 2187/1917) and the National Hydrographic and Mareographic Service (SIMN, Legislative Decree 183/1989) were in charge of hydrological monitoring from 1917 to about 2002. Initially, the SII was made up of the Central Administration in Rome and ten local Departmental Offices (Venezia, Parma, Pisa, Roma, Napoli, Catanzaro, Chieti, Bologna, Palermo, Cagliari) that were in charge of a specific Compartments, namely a portion of the national territory comprising entire river basins. After many changes, the Decree 85/1991 stated the definitive structure of the SIMN: i) the Central Administration located in Roma, ii) ten Compartmental Offices located in Venezia, Parma, Bologna, Pescara, Bari, Catanzaro, Napoli, Roma, Pisa e Genova, iii) four independent Hydrographic Services hosted in Bolzano, Trento, Cagliari and Palermo and coordinated by the SIMN. The final configuration of the SIMN is shown in Figure 24.

Figure 24 *- The structure of the SIMN under the Decree 85/1991. Sources: ISPRA*

The activities of the SIMN included the systematic publication of observed and validated variables in the Hydrological Yearbook, which contains data for a given year and for the area of competence of the Departmental Office, which is responsible for editing and publishing the data concerned. The Hydrological Yearbooks from 1950 onwards and for most of the previous years are divided into two parts: Part I: thermometry and pluviometry; Part II: rainfall, hydrometry, hydrological capacities and budgets, groundwater levels, sediment loads, surveys, ideological studies, and exceptional events, tide measurement, and marigraphy. Figure 25 shows the first pages of Part I and II of the Hydrological Yearbook.


PRESIDENZA DEL CONSIGLIO DEI MINISTRI
SERVIZI TECNICI NAZIONALI

UFFICIO IDROGRAFICO E MAREOGRAFICO DI NAPOLI
PER I BACINI CON FOCE NEL LITORALE TIRRENICO DAL GARIGLIANO AL BUSSENTO E NEL TRATTO COMPRESO TRA LA FOCE DEL NOCE E LA FOCE DEL GARIGLIANO

Direttore: Dott. Ing. ANTIMO DE BLASIO

ANNALI IDROLOGICI

1993

PARTE PRIMA

a)

ROMA
ISTITUTO POLIGRAFICO DELLO STATO
LIBRERIA
1997

PRESIDENZA DEL CONSIGLIO DEI MINISTRI
SERVIZI TECNICI NAZIONALI

UFFICIO IDROGRAFICO E MAREOGRAFICO DI NAPOLI
PER I BACINI CON FOCE NEL LITORALE TIRRENICO DAL GARIGLIANO AL BUSSENTO E NEL TRATTO COMPRESO TRA LA FOCE DEL NOCE E LA FOCE DEL GARIGLIANO

Direttore: Dott. Ing. ANTIMO DE BLASIO

ANNALI IDROLOGICI

1993

PARTE SECONDA

b)

ROMA
ISTITUTO POLIGRAFICO DELLO STATO
LIBRERIA
2001

Figure 25 *- a) Part I and b) Part II of the Hydrological Yearbook of the Compartmental Office of Napoli of the National Hydrographic and Mareographic Service for the year 1993.*

With the Legislative Decree 112/1998 and subsequently, the D.P.C.M. (i.e., ministerial decree) of July 2002, the monitoring activities (data collection and management tasks) carried out by the Compartmental Offices of the National Hydrographic and Mareographic Service were delegated to the regions and then, to local Agencies. In particular, in recent years the hydrological monitoring activities are ensured by the Department of Civil Protection and the Regions through the network of Functional Centres, which consists of a Central Functional Centre (CFC) based at the Civil Protection Department and of Regional Functional Centres. Therefore, the Regional Functional Centres took over the competences of the Compartmental Offices of the National Hydrographic and Mareographic Service.

In the transfer process, the historical network was partly dismissed and partly re-located for the new functions, that are primarily directed towards early warning purposes. Thus, the dismantlement of SIMN resulted in an initial depletion of the main gauging network, which in some cases was flanked by additional monitoring networks that are still not integrated in the official regional network.

To understand the evolution of the rainfall monitoring network in Italy over the years, the case of the Basilicata region is representative. The pluviometric network is extremely fragmented because several regional or local agencies have been involved in its management, leading to uneven spatial and temporal coverage over the years. Additionally, different private and public authorities tried to overcome this problem by installing new rain gauges, ending up with increased inhomogeneity in the management. Manfreda et al. (2015) tried to recreate the evolution experienced by the rainfall monitoring system in the region since the early 1900s. The public agencies that have been involved and are still partly in charge of hydrological monitoring in Basilicata are: National Hydrographic and Mareographic Service (SIMN), the Regional Agency for Environmental Protection of Basilicata (ARPAB), the Department of Civil Protection of the Basilicata, Apulia and Campania regions, the Lucanian Agency for Development and Innovation in Agriculture (ALSIA), Agrobios Metapontum, the Ente per lo Sviluppo dell'Irrigazione e la Trasformazione Fondiaria in Puglia, Lucania ed Irpinia (EIPLI), and the University of Basilicata (UNIBAS). By 2015, the rainfall monitoring network was made up of 133 stations, of which 43% belonged to the Civil Protection, 34% to ALSIA, 15% to ARPAB, and the remaining 7% were divided between the University of Basilicata, the Province of Potenza, EIPLI, and Agrobios Metapontum. In Figure 26 is depicted the evolution of the monitoring network in terms of the number of active stations over the years.

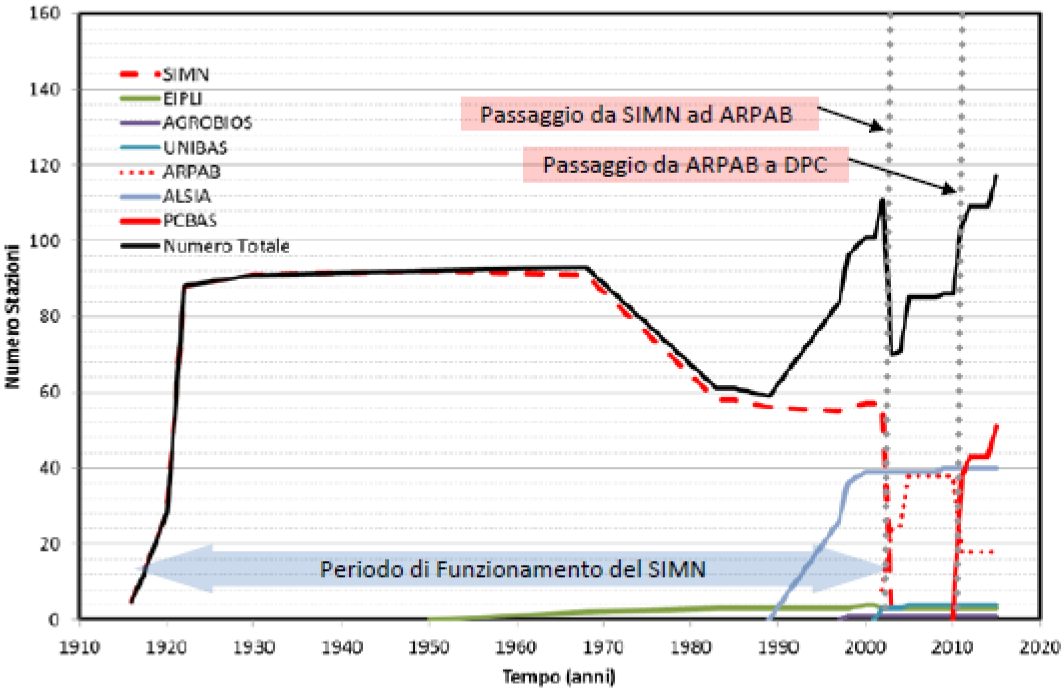

Figure 26 - *Graphical representation of the changes in the number of rainfall stations with a label based on the managing agencies. Sources: Manfreda et al. (2015)*

The changes experienced by the Basilicata pluviometric network are typical of all regional monitoring systems.

However, in this thesis we considered only the official monitoring network. In detail, the regional agencies in Southern Italy involved in data collection and management tasks after the dismantlement of SIMN are reported in Table 1, while in Figure 27 is depicted the spatial distribution of the existing and previous rainfall networks operating in the considered regions.

Table 1 - *Regions of Southern Italy with the related local Managing Centre and information on the availability of data.*

Regions	Monitoring Agencies	Data Availability
Apulia	Department of Civil Protection Apulia region	available at [1]
Basilicata	Department of Civil Protection Basilicata region	available at [2]
	ALSIA - Lucanian Agency for Development and Innovation in Agriculture	available upon request
Calabria	ARPACAL - Functional Centre of Civil Protection Calabria region	available at [3]
Campania	Functional Centre of Civil Protection Campania region	available upon request [4]
Molise	Functional Centre of Civil Protection Molise region	available upon request

[1] Hydrological Yearbooks - Part I: https://protezionecivile.puglia.it/annali-idrologici-parte-i-documenti-dal-1921-al-2021

[2] Manfreda et al. (2015) and
Hydrological Yearbooks - Part I: http://www.centrofunzionalebasilicata.it/it/annali1.php

[3] Hydrological Yearbooks - Part I: http://www.cfd.calabria.it/index.php/dati-stazioni/dati-storici (password-protected website, access granted upon request)

[4] Data provided by the Department for Territorial Policies - General Directorate for Public Works and Civil Protection - U.O.D. 53.08.05 Functional Centre

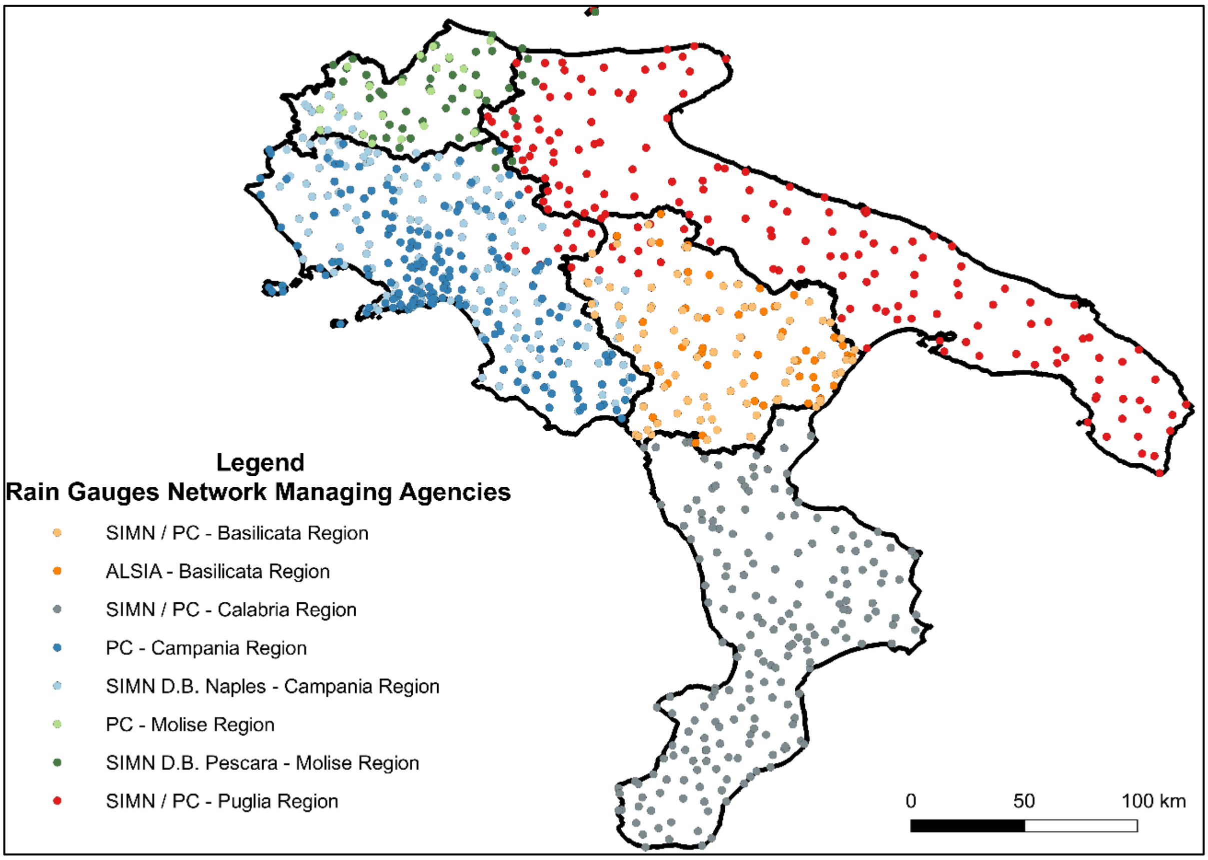

Figure 27 *- Spatial distribution of the rainfall stations over the Southern Italy with references to the local Monitoring Agency involved in data collection and management tasks.*

Two main aspects can be understood by analysing Figure 27. First of all, in some regions (Calabria, Campania and Molise) the rain gauges of the SII/SIMN monitoring network were removed and relocated with changes in location, elevation, and sensor type. Most of the new rainfall stations managed by the Civil Protection have been installed on high elevation sites to obtain more representative estimates of rainfall amounts due to the abundance of orographic precipitation, thus missing the opportunity to build continuous time series. For this reason, in the aforementioned regions two different rainfall station networks are considered (the SIMN and the Civil Protection ones). Only for the Apulia region the spatial continuity of the rain gauges was preserved because there was no need to relocate stations in order to collect orographic precipitation as most of the territory is flat.

Secondly, it was possible to gather data from the ALSIA monitoring network in the Basilicata region. ALSIA is the acronym for the Lucanian Agency for Development and Innovation in Agriculture, which is the agency of the Basilicata Region for the research and innovation in agriculture and the agri-food industry. The ALSIA monitoring network, managed by the SAL (Lucanian Agrometeorological Service), is composed by 42 electronic stations, operating since 1996, that send data to the collection centre to be validated and published. The inclusion of the ALSIA network allowed to increase the spatial density of rain gauges in Basilicata region, thus overcoming the issue of small number of stations that make up the main network managed by Civil Protection.

To sum up, the assembled database consists of around 910 stations, including SIMN stations that have been removed, SIMN rain gauges currently managed by the Civil Protection, the new rainfall stations officially managed by the Civil Protection and a few stations of secondary networks operated by agro-meteorological offices that are still not integrated in the official regional system.

3.3 Sub-daily rainfall annual maxima dataset

Hourly rainfall frequency assessment and large-scale trend analyses require an update, continuous and quality-controlled dataset of extreme rainfall data. One of the first efforts to collate a homogeneous database of short-duration rainfall at global scale was that of Lewis et al. (2019). They developed a global database, the Global Sub-Daily Rainfall Dataset (GSDR), based on gauged observations of about 23687 stations. Figure 28 maps the location of the rain gauges included in the GSDR with a zoom on the European continent. It is evident that no stations were enlisted in Italy (except for Sicily region) because of the difficulty in collecting data, as records are often subjected to restricted access by the regional authorities that are in charge of the monitoring activities.

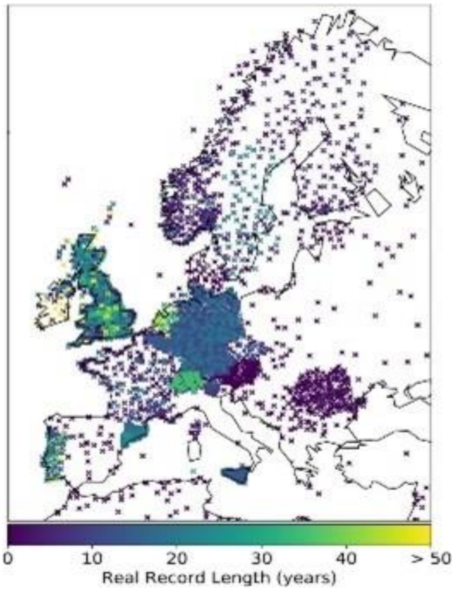

Figure 28 *- Locations and length of available sub-daily precipitation time-series from the GSDR database. Sources: Lewis et al. (2019)*

A first comprehensive and updated dataset of annual maximum rainfalls of short duration in Italy, referred to as the Italian Rainfall Extreme Dataset (I-RED), was gathered by Libertino et al. (2018b), including more than 4500 stations across the country and covering the period between 1916 and 2014.

In this thesis, a database of short-durations (1, 3, 6, 12 and 24 hours) annual maximum rainfall depths in the period 1930-2020 was assembled for the five considered regions (Apulia, Basilicata, Calabria, Campania and Molise).

The historical data, which were collected before the dismantlement of SIMN and published in the SII/SIMN Hydrological Yearbooks, are freely available. Indeed, the ISPRA's "Yearbook project" (ISPRA, 2012) involved the digitization of all data published in the Hydrological Yearbooks since 1921 in order to create a national database. This project is still ongoing and just a PDF archive has been published (http://www.bio.isprambiente.it/annalipdf/).
Instead, since the administration changes, some agencies have not published the data (raw or validated), and only make them available upon formal request. Therefore, the different agencies have been contacted, requesting their annual maxima dataset for sub-daily duration or the raw series at instrumental resolution (1, 5, or 10 minutes).

The different Regions provided different type of dataset, with different temporal coverages and spatial reference systems. The type and format of the data are described below.

The Apulia, Basilicata and Calabria regions provide a complete and merged SIMN-postSIMN database. In detail, Apulia and Basilicata regions publish the Hydrological Yearbooks stored in pdf files on a yearly basis. These data were digitized using optical character recognition (OCR) software. For Calabria region, the data are available (as a scanned copy in pdf format) on a password-protected website; but the access is granted upon request.

The Lucanian Agency for Development and Innovation in Agriculture (ALSIA), instead, provided the raw series at instrumental resolution (1 hour) for the 42 stations in the period 1998-2020. The annual maxima, for the fixed durations, were extracted using the "sliding time windows" method (Papalexiou et al., 2016) implemented in an ad-hoc MATLAB code.

Finally, Campania and Molise regions provided just the postSIMN data, i.e., the observations recorded from the network they actually manage. In detail, they provided the raw series at the instrumental resolution (10 minutes, Campania; 1 or 15 minutes, Molise). The annual maxima, for the fixed durations, were extracted using the "sliding time windows" method. For these two regions, the constructed datasets were merged with the SIMN database, extracted from the Hydrological Yearbooks stored in pdf files on a yearly basis.

Merging the different datasets was a long and tricky procedure. It is important to highlight that almost every hydrological agency also has rainfall stations in nearby regions, as a result of the joint management of interregional basins. The values reported in the database were therefore checked by comparing the time series of each rain gauge with all the other ones: this check allowed for the identification of the stations located along the regional boundaries that had been included twice (sometimes with the same station name, sometimes not) with similar positions and the same rainfall values. The visual data check was of fundamental importance to avoid data duplication. Stations with the same name, similar coordinates and with a time overlap were merged if the rainfall measurements were the same, otherwise they were considered as different stations. The data merging and harmonizing was accompanied by ad-hoc quality-check performed manually, by visually screening all the collected data. In addition, a simple procedure was implemented to verify that rainfall values (for each station and each year) corresponding to increasing durations were valid (i.e., the annual maxima related to a 1 hour duration is lower or at least equal to the 3 hours one and so on).

Some aspects of the assembled database are reported in Figure 29, that shows the number of active rainfall stations per year and the maximum number (over the entire period of analysis) of simultaneously operating rain gauges for the five considered regions.

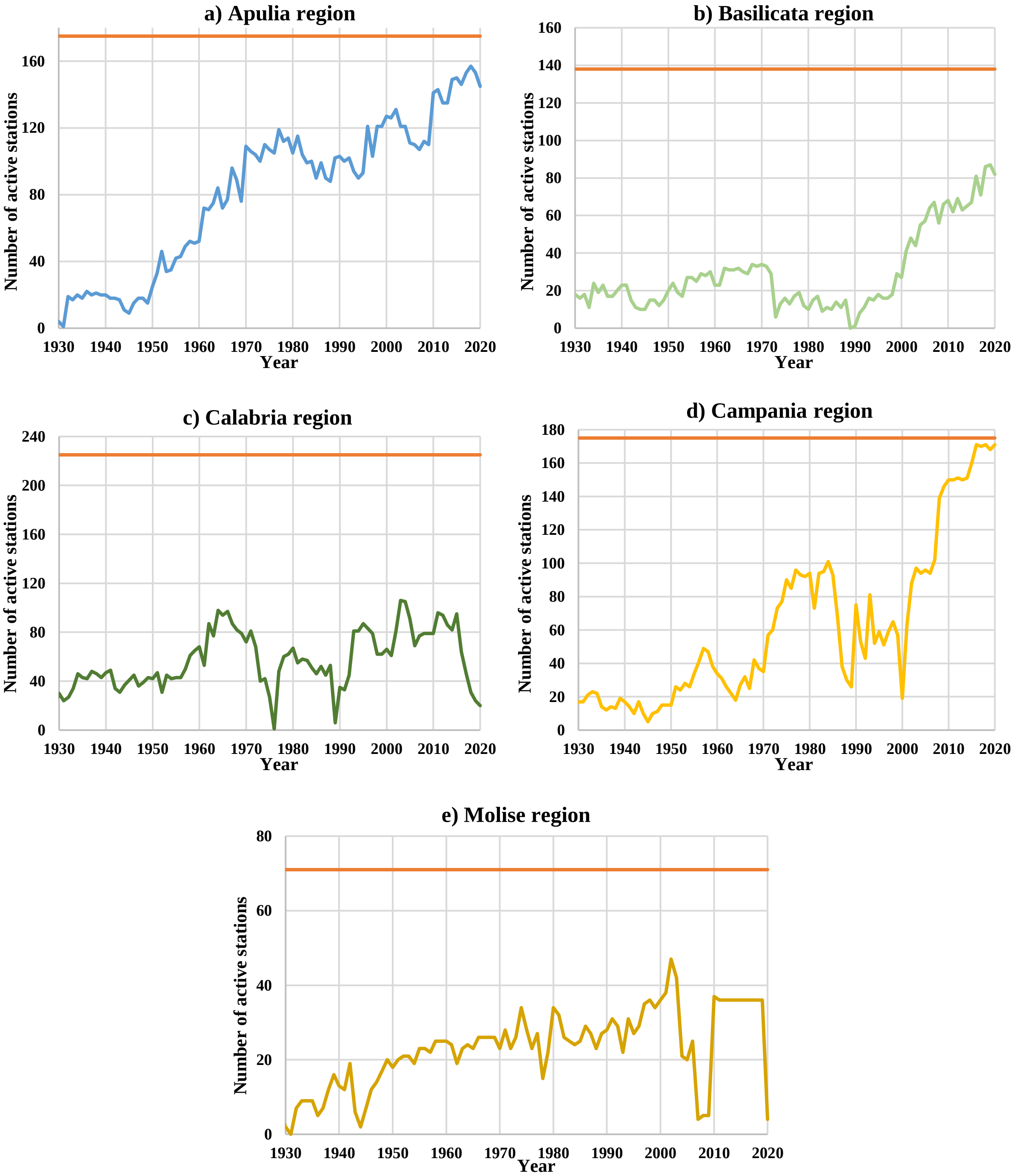

Figure 29 *- Number of active rainfall stations per year and the maximum number (over the entire period of analysis) of simultaneously active rain gauges for the five considered regions: a) Apulia, b) Basilicata, c) Calabria, d) Campania, and e) Molise.*

As shown in Figure 29, the lack of a considerable number of measurements between 1930 and 1950 is due to the Second World War. Moreover, until 1970, the number of available observations was limited due to a fledgling monitoring network and the several complexities of managing the old mechanical tipping-bucket rain gauges. Indeed, in that interval, the percentage of active stations was very low (about 20%), especially in Apulia, Basilicata, and Campania regions. Therefore, for the above reasons, we decided to limit the analysis to the period 1970-2020, considered a suitable time window to assess any changes in the rainfall regime.

A final quality-check was performed concerning the highest values measured in each station, which were defined as “Extraordinary Extreme” (Pelosi et al., 2020). These maxima were analysing, for all the stations and all the durations, in order to possibly identify further errors in the data, which had not been detected in the data digitization and in the record merging process. By examining these values, it was indeed possible to detect unrealistically high annual maxima.

The assessment was carried out by calculating an empirical index based on the highest k-th sample values. In a record of size *n*, the n-th order statistic is the maximum value of the record (x_n), while the (n-1)-th order statistic is the second-highest value (x_{n-1}). By extracting the n-th and the (n-1)-th order statistics of the annual maxima for each rain gauge, we were able to calculate a non-dimensional index, named the “Order Statistic Ratio” (Adler, 2015), as:

$$OSR = \frac{x_n}{x_{n-1}} \tag{14}$$

The spatial distribution of the rain gauges with the higher OSR values (greater than 2), computed for the 24-h duration, is reported in Figure 30.

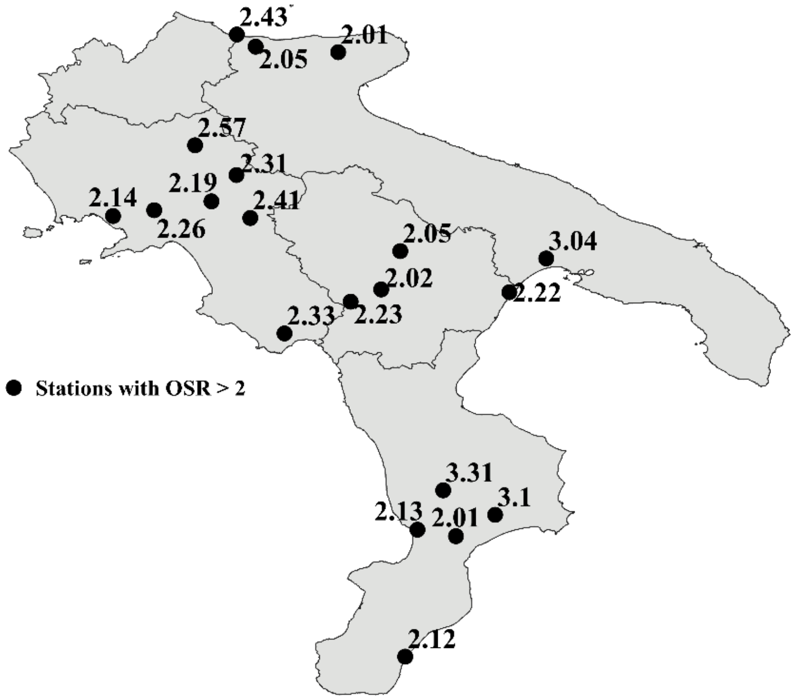

Figure 30 *- Spatial distribution of rain gauges characterized by greater OSR than 2 for the 24-h duration.*

Higher OSR values were observed to range from 2 to 3.3, which implies that there were no outliers in the assembled database. In addition, the spatial distribution of these points is not uniform (as displayed in the work of Mazzoglio et al., 2020), but some cluster can be identified (in the central part of Calabria and along the Campano Apennines). Such analysis was performed for all durations.

Thus, the considered database for the statistical analysis consists of annual maximum rainfall depths series for sub-daily durations (1, 3, 6, 12, and 24 hours) in the period 1970-2020. It is made up of around 910 rain gauges, for a total of 17040 records, representing the 36.8% of the total number of data that would be available if all stations had complete time series. By dividing the number of records by the number of stations, it is possible to obtain the average length of the time series, which is equal to 18.8 years.

Some characteristics of the rainfall stations included in the database are reported in Figure 31 and 32. Figure 31a, in particular, maps the location and length of each rain gauge in the period 1970-2020, while Figure 31b shows the number of active rainfall stations per year for the five considered regions (further information can be found in Appendix B). Instead, Figure 32 depicts the percentage of series per length class for each region (32a) and for the entire study area (32b).

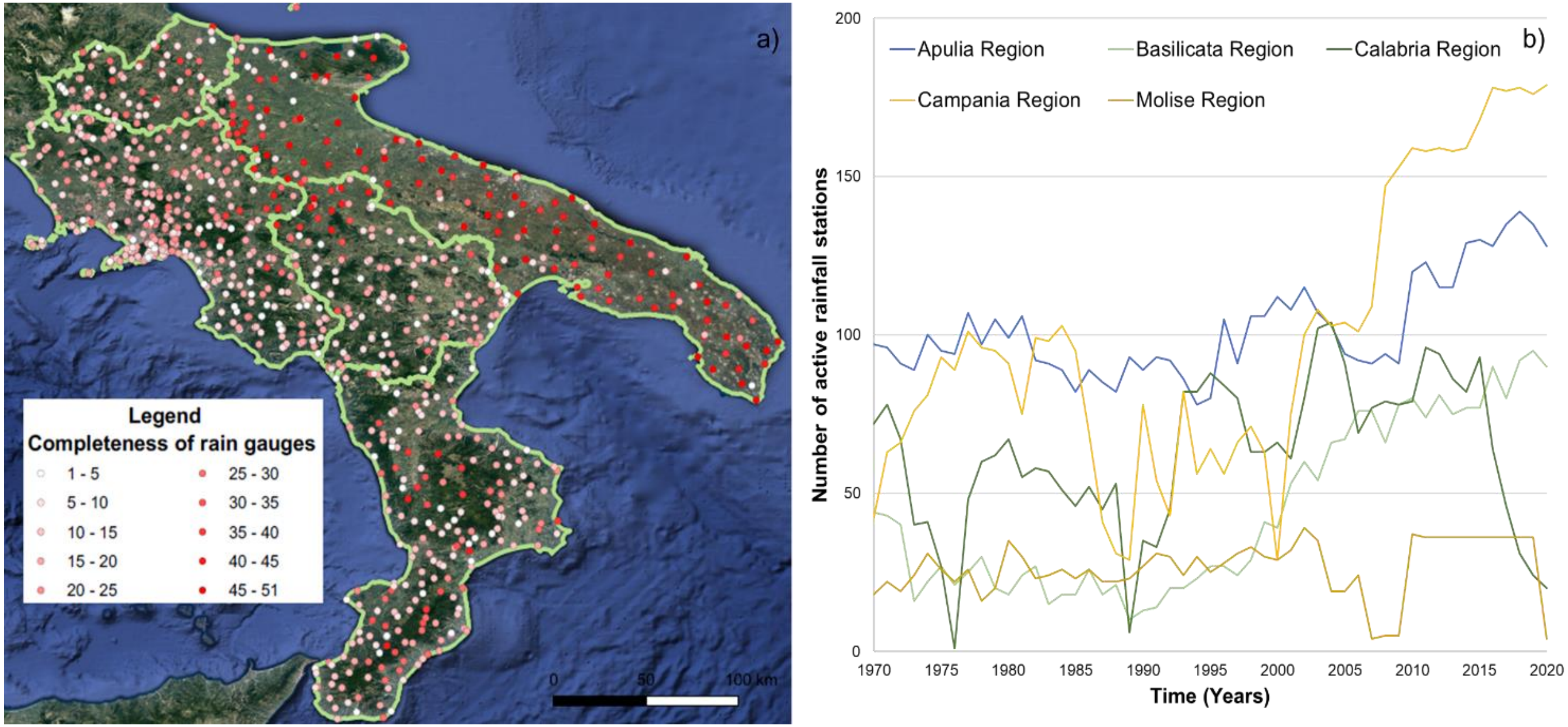

Figure 31 *- a) Spatial distribution of the rain gauges over the study area. The colour refers to the length of the time series; b) Number of active rainfall stations per year for the five considered regions.*

As shown in Figure 31b, the number of observations per year has increased over time as more stations have been installed in recent years. In addition, the apparent reduction in the number of rain gauges between 1990 and 2000 was mainly induced by the effect of the dismissing of SIMN: in those years, some regions decided not to upgrade or repair the old rainfall stations, and most of the old mechanical tipping-bucket rain gauges were progressively substituted by automatic ones. Finally, the decreasing number of stations that emerges in recent years in Calabria and Molise region is due to the fact that, for the most recent years, measurements are not yet fully available for all stations.

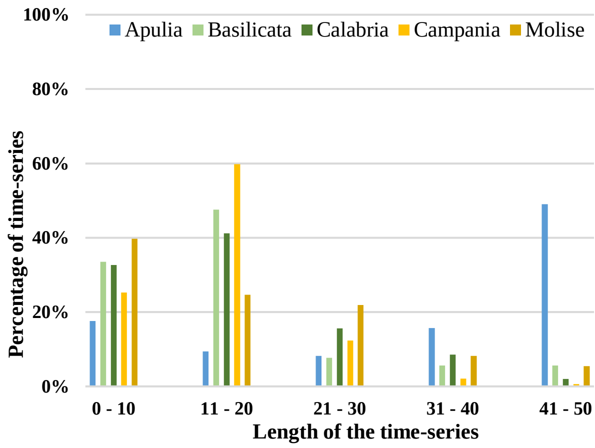

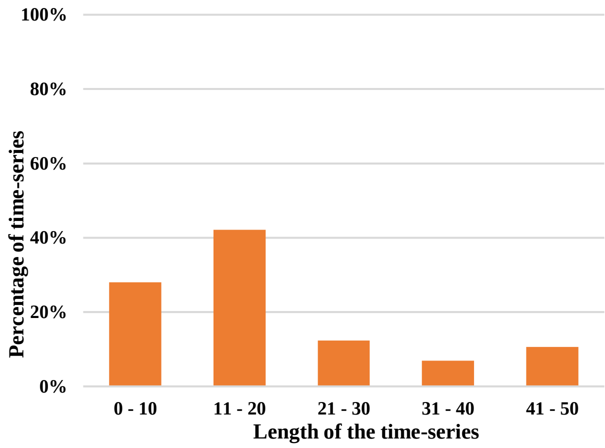

Figure 32 *- Percentage of series per length class in the recorded databases for a) each region (Apulia, Basilicata, Calabria, Campania and Molise); b) for the southern Italy study area (comprising around 910 rain gauges).*

By analysing Figure 32, it is worth noting that at the study area scale:

- 653 rain gauges (72% of the total) have a time series longer than 10 years.
- 271 rain gauges (30% of the total) have a time series longer than 20 years.
- 159 rain gauges (18% of the total) have a time series longer than 30 years.
- 96 rain gauges (11% of the total) have a time series longer than 40 years.
- 3 rain gauges have a time series without missing data.

It is important to highlight that only 136 stations (15% of the total) are characterized by a time series with at least 35 years of measurements (corresponding to the 70% of the completeness), which we identified as the minimum length suitable for trend analyses. However, as highlighted in Figure 31a and 32a, in Apulia region almost all stations have mostly complete series; in particular, more than 85% of the rainfall stations have a completeness of at least 35 observations. Thus, if we exclude those stations, the number of series with 70% completeness falls from 15% to 3%. This means that in the other four regions, no station has a complete series. In Table 2 is reported the number and percentage of stations, within the administrative boards of each region, with at least 35 data in the last 50 years (1970-2020).

Table 2 *- Number and percentage of stations, within the administrative boards of each region, with at least 35 data (annual maximum rainfall depths) in the period 1970-2020.*

Region	**Number of stations***	**Percentage of stations***
Apulia	99	85%
Basilicata	12	8%
Calabria	10	5%
Campania	8	2%
Molise	7	10%
Southern Italy	136	15%

* with at least 70% completeness (i.e., at least 35 records of rainfall annual maximum in the period 1970-2020)

The evolution in the management of the rain gauge network is one of the main factors that has led to short, uneven and fragmented rainfall series in Italy. Although the most recent stations were installed to locally increase the network density, they unfortunately still provide little suitable information for these types of analysis. The inhomogeneity of the record length is also influenced by the different degrees of accuracy adopted by each regional agency. In fact, some agencies recorded small relocations of the station position (i.e., Apulia), which do not break the series, while others did not (as already pointed out in Section 3.2).

Some further features of the considered rain gauges are reported in Figure 33 that shows the kriged maps of the mean value of rainfall annual maxima for each station spatially interpolated with QGIS software by applying an ordinary kriging with a spherical semi-variogram and variable windows (a maximum value of 30 km was set to find at least 5 rain gauges).

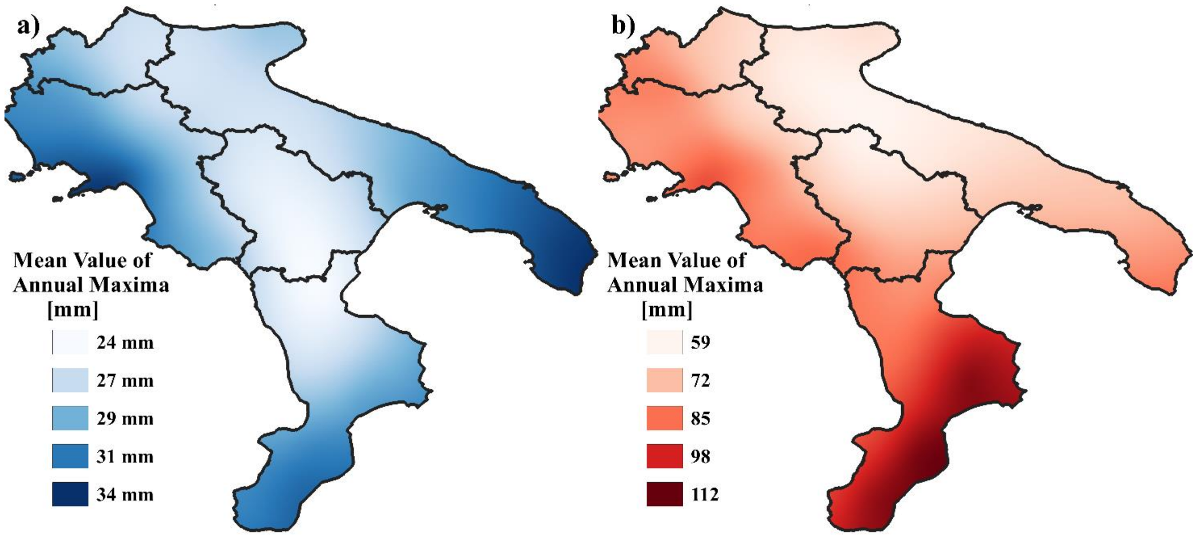

Figure 33 *- Kriged maps of mean values (over the period 1970-2020) of annual maxima, spatially interpolated by applying an ordinary kriging with the GIS software, for two durations: a) 1 hour and b) 24 hours. The maps are characterized by a 1×1 km spatial resolution.*

For the 1-h duration (Figure 33a), the highest values are observed along the northern coastal belt of Campania and in the southern part of Apulia and Calabria regions, while the lowest values are detected along the Apennine chain. Instead, for 24-h interval (Figure 33b) the lowest values are recorded in Apulia, Basilicata and Molise regions, middle values in Campania and the highest one in large part of Calabria.

In summary, during this activity, we developed an updated and quality-controlled dataset of the annual maximum rainfall events for sub-daily durations (1, 3, 6, 12, and 24 hours) that may be used for statistical analysis and to investigate and highlight the areas that are more exposed to extreme rainfall.

3.4 MISSING RAINFALL DATA RECONSTRUCTION

The assembled database made up of annual maximum rainfall observations is extremely fragmented and irregular. As described in section 3.3, most of the rainfall series contain gaps, and more than 85% of the considered rain gauges have records shorter than 35 years (over the period 1970-2020) due to the frequent changes (location, type of sensor, and managing agency) experienced in the gauging network. Uneven series are not suitable for exploring the variability in precipitation patterns and detecting the presence of trends at different spatial and temporal resolutions. Additionally, the heterogeneity and discontinuity of rainfall series could affect or invalidate the statistical analysis of extreme rainfall events. Thus, the estimation of missing precipitation data was a mandatory step to obtain unbiased results from the statistical assessment. Therefore, gap-filling procedures were implemented in order to reconstruct annual maximum rainfall depths over given durations (1, 3, 6, 12, and 24 hours) in ungauged locations. These procedures allow for the use of all the information available from the recorded series to obtain estimates of extreme rainfall in locations where only a few or no data are accessible.

In several works, the estimation of missing values in ungauged points is preceded by the identification and removal of the possible correlation between precipitation and elevation, especially in areas characterized by a complex orography. Different approaches have been adopted in the literature for dealing with this problem; for example, Chua and Bras [1982] and Dingman et al. [1988] proposed to perform a linear regression on precipitation versus elevation, subtract the regressed orographic effect and apply the equations for the reconstruction to the elevation-adjusted data.

It is important to note that, in this thesis, analyses to investigate the impact of orography on precipitation data were also conducted. In particular, the relation between the average annual maximum precipitation, h_d, and elevation, z, is assumed to follow the equation:

$$h_d = m_0 + mz \qquad [15]$$

where m is the slope of the regression line (called orographic factor) and m_0 is the intercept. In Table 3 the slope values for each considered region and duration are reported.

Table 3 *- Parameters of the relation between the average annual maximum precipitation, h_d, and elevation, z: slope of the regression line (orographic factor), m, and the determination coefficient R^2 for each region and duration.*

Regions	**d [h]**	**m ± Std. Error**	**R^2**
Apulia	1	-0.0042 ± 0.0022	0.0223
	3	-0.0057 ± 0.0029	0.0236
	6	-0.0040 ± 0.0034	0.0088
	12	-0.0003 ± 0.0040	0.0008
	24	+0.0072 ± 0.0043	0.0175
Basilicata	1	-0.0036 ± 0.0014	0.0437
	3	-0.0050 ± 0.0018	0.0501
	6	-0.0043 ± 0.0024	0.0224
	12	-0.0041 ± 0.0033	0.0108
	24	-0.0007 ± 0.0046	0.0002
Calabria	1	-0.0010 ± 0.0015	0.0022
	3	+0.0040 ± 0.0025	0.0127
	6	+0.0012 ± 0.0035	0.0567
	12	+0.0025 ± 0.0049	0.1174
	24	+0.0041 ± 0.0068	0.1563
Campania	1	-0.0015 ± 0.0013	0.0045
	3	-0.0016 ± 0.0019	0.0022
	6	+0.0009 ± 0.0025	0.0004
	12	+0.0055 ± 0.0034	0.0078
	24	+0.0010 ± 0.0042	0.0165
Molise	1	+0.0045 ± 0.0021	0.0641
	3	+0.0084 ± 0.0030	0.0989
	6	+0.0011 ± 0.0044	0.0796
	12	+0.0016 ± 0.0060	0.0905
	24	+0.0024 ± 0.0080	0.1106

By analysing Table 3, no apparent relationship between annual rainfall maxima and altitude was discovered. Therefore, procedures based on de-trended data (i.e., those obtained by removing any altitude dependence) or other multivariate geostatistical reconstruction methods, such as co-Kriging, were excluded. Thus, in this thesis, first we tried to apply the inverse distance weighting (IDW) and ordinary kriging (OK) approaches. However, since the performances, in terms of estimation error, were not so acceptable, we developed a new reconstruction framework, the “Spatially-Constrained Ordinary Kriging” (SC-OK) method (Avino et al., 2021), which is a mixed procedure that adopts the OK approach coupled with the same spatial constraints of the IDW method. The SC-OK method exploits the advantages of both the IDW and OK techniques, as detailed in the next subsection (3.4.1).

3.4.1 Spatially-Constrained Ordinary Kriging (SC-OK) reconstruction method

In the Spatially-Constrained Ordinary Kriging (SC-OK) method, ordinary kriging (OK) and inverse distance weighting (IDW) approaches are combined in order to exploit their characteristics.

The feasibility of the IDW method depends mainly on the existence of positive spatial autocorrelation (Griffith, 1987). Instead, negative autocorrelation may become a restriction in the application of the method. Moreover, the main conceptual limitation of the distance-based weighting methods is that Euclidean distance is not always a proper measure of the correlation among spatial data point.

In ordinary kriging, instead, the weights are based not only on the distance between the measured points and the prediction location, but also on the overall spatial pattern among the gauged points and their values. The recorded data are used to detect the degree and form of the spatial correlation, which is modelled by means of the semi-variogram and then used to assess the weight of the different observations.

Kriging approaches allow to preserve spatial variability that would be lost using a simpler method. In addition, this method enable to minimize the estimation variance at points where measurements are not available in order to obtain unbiased values.

Notably, since the OK method has no spatial limitations, it allows to reconstruct the totality of the missing data, but the estimated annual maxima may be inaccurate especially in locations with limited information in the most positively correlated stations, which are the closest ones. On the contrary, the IDW procedure may fail to reconstruct records at stations that do not have enough neighbouring stations functioning. In the IDW method, estimation of rainfall data is carried out considering only rain gauges within a radius R centered on the given station where rainfall values need to be reconstructed. Thus, the IDW method is spatially constrained by the characteristics of its parameters.

Therefore, in order to remove the effect of long-range extrapolation in the OK, Avino et al. (2021) enforced spatial constraints on the OK method that are the same as in the IDW model. In this way, the SC-OK will reconstruct only the missing data in the same locations identified by the IDW method. As a result, this proposed method fully exploits the OK approach, but at the same time it turns out to be spatially constrained allowing rainfall data to be estimated only at stations with sufficient (at least N within the radius R) neighbouring stations with gauged data.

As reported in Avino et al. (2021), the first step to implement the SC-OK procedure is the selection of IDW parameters: the power coefficient (n), the radius of influence of each rainfall station (R) and the minimum number of rain gauges (N) within the radius R centred on the ungauged station. However, to consider that the rain gauges are located at different elevations (ranging from 1 to 1500 meters above sea-level), R is calculated as the Euclidean distance in three dimensions (x and y on the ground and z the elevation).

To simplify the computational steps, we added a fourth parameter, ρ, defined as the minimum density of rainfall stations required to perform the reconstruction, given by:

$$\rho = \frac{N}{\pi R^2} \tag{16}$$

where N is the minimum number of rain gauges existing within the radius R centred on the given station where the missing data need to be reconstructed. As ρ varied, only the values of n and N were optimized using a genetic algorithm (Goldberg, 1989), whereas R was calculated from Eq. [16].

In practice, for each region (*Reg* = Apulia, Basilicata, Calabria, Campania and Molise) and duration (d = 1, 3, 6, 12 and 24 hours) a matrix, $M_{Reg,d}$ of size $n_r \times Y$ was assembled consisting of the observed annual maxima; n_r represents the number of rainfall stations within the administrative borders of each region and Y (= 51) the years in the considered period (1970-2020). The optimization of the IDW parameters was carried out in a three-step procedure: i) the 10% of the rainfall data in the $M_{Reg,d}$ matrix was randomly removed; ii) the root mean square error (RMSE) related to the IDW reconstruction of the deleted data was computed; iii) the three parameters (i.e., n, N, R) were selected as those that minimize the RMSE value.

In detail, as ρ varied (from 0.0005 to 0.01, step 0.0005; it represents the minimum density of rainfall stations required to perform the reconstruction and, in particular, the number of stations within an area of 1 km^2), the three parameters were estimated by means of the genetic algorithm minimizing the RMSE related to the reconstruction of the removed rainfall data with the IDW method. Table 4 presents the results of the optimization step for the Basilicata region, showing for each value of ρ the optimal values of R and N. The tables for all regions can be found in the Appendix A (Table A.1 - A.4).

Table 4 *- Results of the optimization step for the Basilicata region. In particular, for each value of ρ, the optimal value or R and N is reported.*

ρ	**1h**		**3h**		**6h**		**12h**		**24h**	
	R [km]	**N**	**R [km]**	**N**	**R [km]**	**N**	**R [km]**	**N**	**R [km]**	**N**
0.0005	61.80	6	50.46	4	94.41	14	50.46	4	50.46	4
0.0010	56.42	10	35.68	4	35.68	4	39.89	5	39.89	5
0.0015	43.70	9	35.68	6	41.20	8	41.20	8	41.20	8
0.0020	35.68	8	37.85	9	37.85	9	41.84	11	41.84	11
0.0025	42.22	14	35.68	10	42.22	14	40.68	13	42.22	14
0.0030	35.68	12	35.68	12	35.68	12	35.68	12	39.89	15
0.0035	36.93	15	33.04	12	31.63	11	19.07	4	33.04	12
0.0040	19.95	5	25.23	8	29.59	11	19.95	5	25.23	8
0.0045	16.82	4	26.60	10	26.60	10	30.32	13	27.89	11
0.0050	15.96	4	26.46	11	26.46	11	26.46	11	22.57	8
0.0055	15.22	4	20.13	7	20.13	7	20.13	7	25.23	11
0.0060	17.84	6	20.60	8	28.21	15	24.16	11	14.57	4
0.0065	15.65	5	15.65	5	14.00	4	26.18	14	26.18	14
0.0070	22.37	11	22.37	11	15.08	5	25.23	14	25.23	14
0.0075	15.96	6	14.57	5	21.61	11	21.61	11	21.61	11
0.0080	19.95	10	14.10	5	14.10	5	21.85	12	12.62	4
0.0085	14.99	6	14.99	6	12.24	4	14.99	6	22.90	14
0.0090	14.57	6	13.30	5	11.89	4	14.57	6	14.57	6
0.0095	14.18	6	14.18	6	15.31	7	15.31	7	15.31	7
0.0100	16.93	9	14.93	7	14.93	7	12.62	5	14.93	7

Then, for each value of ρ, the missing rainfall data in matrix $M_{Reg,d}$ were estimated using the IDW method coupled with the optimized parameters. Thereby, the number and percentage of reconstructed data were calculated. The tables reporting the number of the observed (OD), reconstructed (RD) and total (TD) data and the percentage ratio between RD and OD, for all regions and durations, can be found in the Appendix A (Apulia, Table A.5 - A.9; Basilicata, Table A.10 - A.14; Calabria, Table A.15 - A.19; Campania, Table A.20 - A.24; Molise, Table A.25 - A.29). It is worth noting that the percentage of reconstruction using the SC-OK and IDW method is equivalent because the same spatial constraints (to select the position in which the reconstruction is admissible) were used in both gap-filling procedures.

At this step, to get an acceptable reconstruction in terms of series completeness, values of ρ with the number of reconstructed data less than a threshold, equal to 30% of the recorded data numerosity, were discarded.

The next step in the procedure is aimed at identifying the optimal value of ρ and, therefore, of R and N in applying the SC-OK method. In detail, 10 different matrices were drawn from $M_{Reg,d}$ by randomly removing the 10% of the recorded data. For each value of ρ, the deleted data were reconstructed by means of SC-OK method and the RMSE related to reconstruction was calculated. Then, the statistics concerning the RMSE values were assessed. As an example, the statistics for the Basilicata region are reported in Figure 34 by means of the boxplot, that provides the representation of the following indicators: maximum and minimum value, 75^{th}, 50^{th} and 25^{th} percentile, the mean value, and the outliers. The box-plot graphs for the other regions can be found in the Appendix A (Apulia, Figure A.1; Calabria, Figure A.2; Campania, Figure A.3; Molise, Figure A.4).

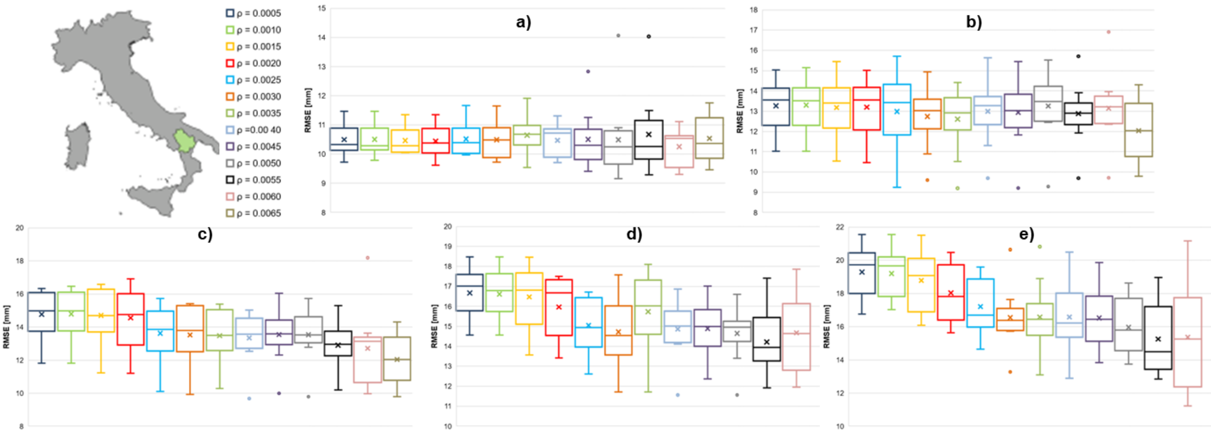

Figure 34 *- Box-plot of RMSE (root mean square error) values in relation to ρ (minimum density of rainfall stations required to perform the reconstruction) for the Basilicata region and for each considered duration: a) 1h, b) 3h, c) 6h, d) 12h, e) 24h. The box-plot provides the representation of the following statistics: maximum and minimum (whiskers), 75th percentile and 25th percentile (rectangle edges), median or 50th percentile (horizontal line in the rectangle), mean (x symbol), outliers (o symbol).*

Within this context, the optimal value of ρ was selected as that with the minimum average RMSE. For the Basilicata region, the selected value was 0.006, which corresponded to a value of R equal to 17.84 km and N equal to 6 and an average reconstruction error of 10 mm (RMSE).

The calibration procedure of the SC-OK method to spatially reconstruct missing rainfall data is summarised in the flow chart in Figure 35.

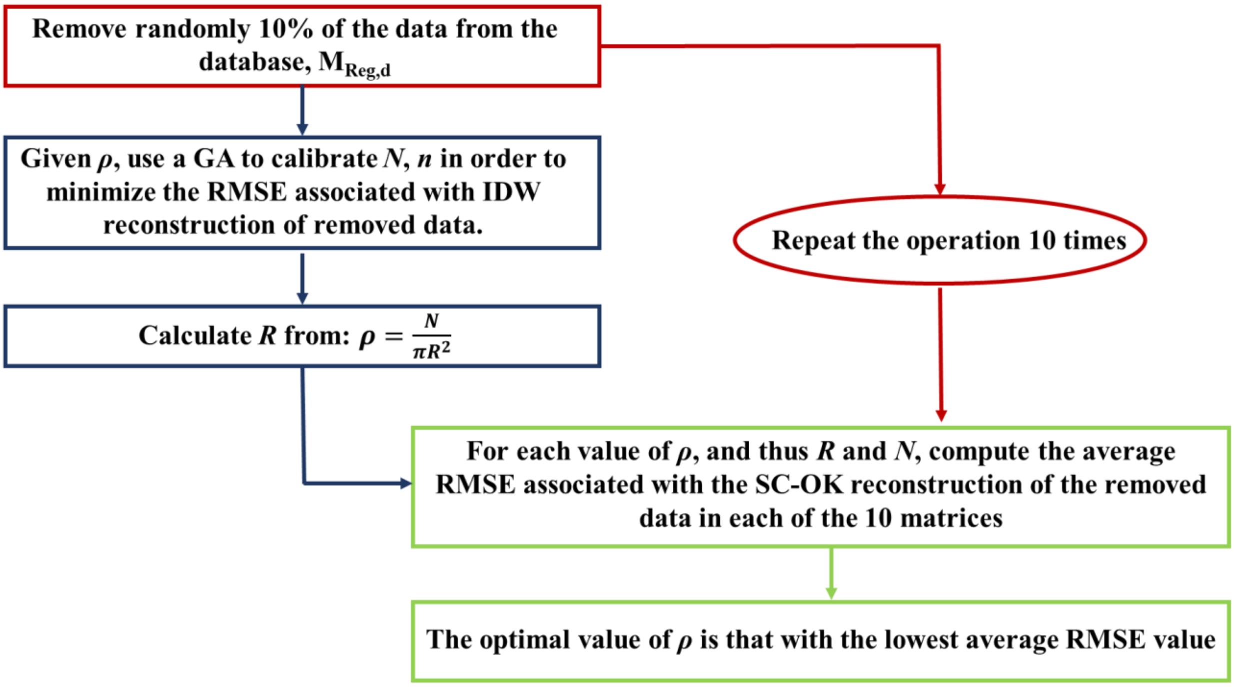

Figure 35 *- Flow chart for the calibration of the spatially-constrained ordinary kriging (SC-OK) method for the missing data reconstruction.*

This procedure (Figure 35) for the calibration of the SC-OK method parameters was applied independently to all durations (1, 3, 6, 12, and 24 hours) and all the considered regions (Apulia, Basilicata, Calabria, Campania, Molise) and the results (the optimal value of ρ and the corresponding values of N and R) are presented in Table 5.

Table 5 *- The optimal value of ρ (the minimum density of rainfall stations required to perform a suitable reconstruction) and the corresponding optimal values of R (the radius of influence centred on the rainfall station), N (the minimum number of rain gauges within the radius R), the average value of RMSE (root mean square error) and the average value of MAPE (mean absolute percentage error), for each considered duration (1, 3, 6, 12 and 24 hours) and for each region (Apulia, Basilicata, Calabria, Campania and Molise).*

Regions	Parameters	1 hour	3 hours	6 hours	12 hours	24 hours
Apulia	**ρ [N/1km^2]**	0.0035	0.0035	0.0035	0.0035	0.0035
	R [km]	**23.36**	**28.61**	**30.16**	**30.16**	**26.97**
	N	**6**	**9**	**10**	**10**	**8**
	RMSE [mm]	11.66	14.12	14.66	15.36	17.28
	MAPE [%]	39	37	32	28	26
Basilicata	**ρ [N/1km^2]**	0.0060	0.0035	0.0055	0.0055	0.0055
	R [km]	**17.84**	**33.04**	**20.13**	**20.13**	**25.23**
	N	**6**	**12**	**7**	**7**	**11**
	RMSE [mm]	10.25	12.60	12.90	14.21	15.24
	MAPE [%]	38	34	27	25	22
Calabria	**ρ [N/1km^2]**	0.0030	0.0035	0.0045	0.0060	0.0030
	R [km]	**27.25**	**28.61**	**18.81**	**14.57**	**37.14**
	N	**7**	**9**	**5**	**4**	**13**
	RMSE [mm]	10.79	16.99	21.56	25.76	32.71
	MAPE [%]	39	32	32	30	28
Campania	**ρ [N/1km^2]**	0.0075	0.00125	0.0095	0.00125	0.0085
	R [km]	**17.24**	**10.09**	**12.94**	**10.09**	**13.68**
	N	**7**	**4**	**5**	**4**	**5**
	RMSE [mm]	9.19	12.02	14.20	17.50	19.86
	MAPE [%]	29	23	23	22	22
Molise	**ρ [N/1km^2]**	0.0060	0.0070	0.0060	0.0060	0.0085
	R [km]	**26.26**	**22.37**	**27.25**	**27.25**	**12.24**
	N	**13**	**11**	**14**	**14**	**4**
	RMSE [mm]	6.12	8.70	9.30	10.48	13.90
	MAPE [%]	26	23	22	20	20

In addition, to verify the reliability of the reconstructed data, the Kolmogorov-Smirnov (K-S) homogeneity test was carried out at each station. The K-S test allows to quantify the distance between the empirical distribution function of the two series (recorded and reconstructed ones) in order to verify that the two samples are drawn from the same distribution. For the selected values of ρ, it was found the all the reconstructed rainfall series satisfy the test with a 95%

confidence level. This test allowed to verify that the SC-OK interpolation method provides reconstructed time series consistent with the historical ones.

In summary, to reconstruct missing rainfall annual maxima the Spatially-Constrained Ordinary Kriging (SC-OK) model was developed. It is based on the ordinary kringing approach, with an average spherical variogram weighted by the annual number of active stations, coupled with the IDW spatial parameters, calibrated by means of a genetic algorithm and a jack-knife technique.

3.4.2 Data reconstruction with the SC-OK method: characteristics of the updated database

Once the optimal values of R and N were calibrated for the considered durations, the assembled rainfall database was reconstructed using the SC-OK method (ordinary kriging with an average spherical variogram weighted by the annual number of active stations) coupled with spatial parameters in order to estimate only the data in the position identified by the IDW.

Therefore, by using the SC-OK method, we reconstructed rainfall series of annual maxima for each region within the study area (southern Italy). A summary of the completeness of the rainfall database before and after the reconstruction is reported in Table 6.

Table 6 *- The number of measurements and record completeness in the database before and after the reconstruction and the reconstruction percentage, for each duration (1, 3, 6, 12 and 24 hours) and for each region (Apulia, Basilicata, Calabria, Campania and Molise).*

Regions	d [h]	Number of Data	Record Completeness [%]	Number of Data	Record Completeness [%]	Reconstruction Percentage [%]
		Database before reconstruction		Database after reconstruction		
	1	5209	64.24	6770	83.49	**19.25**
	3	5255	64.80	6720	82.87	**18.07**
Apulia	6	5287	65.20	6741	83.13	**17.93**
	12	5318	65.58	6771	83.50	**17.92**
	24	5345	65.91	6856	84.55	**18.64**
	1	2267	31.08	3127	42.88	**11.80**
	3	2272	31.15	4171	57.19	**26.04**
Basilicata	6	2274	31.18	3191	43.75	**12.57**
	12	2274	31.18	3191	43.75	**12.57**
	24	2271	31.14	3208	43.99	**12.85**
	1	3163	31.17	6227	61.36	**30.19**
	3	3161	31.15	5363	52.84	**21.69**
Calabria	6	3162	31.16	4922	48.50	**17.34**
	12	3162	31.16	4253	41.91	**10.75**
	24	3161	31.15	5632	55.49	**24.34**
	1	5044	29.70	8507	50.09	**20.39**
	3	5046	29.71	6908	40.68	**10.97**
Campania	6	5049	29.73	7717	45.44	**15.71**
	12	5049	29.73	6915	40.72	**10.99**
	24	5044	29.70	8248	48.57	**18.87**
	1	1343	36.07	2009	53.96	**17.89**
	3	1343	36.07	1752	47.06	**10.99**
Molise	6	1343	36.07	1972	52.97	**16.90**
	12	1343	36.07	1973	52.99	**16.92**
	24	1343	36.07	1857	49.88	**13.81**

As shown in Table 6, the record completeness after the reconstruction varies between 40% and 80%. As expected, the higher completeness rate (more than 80%) was observed in Apulia region for all durations as the recorded database already had a 65% numerosity. For all the regions, the reconstruction percentage is in the range 10-20% with an average percentage increase of 17%.

The impact of the reconstruction procedure on the rainfall database is detailed in Figure 36, which depicts the total number of rainfall annual maxima per year for both observed and reconstructed series for each studied region (further information can be found in Appendix B), and Figure 37, which maps the number of series per length class for both the databases.

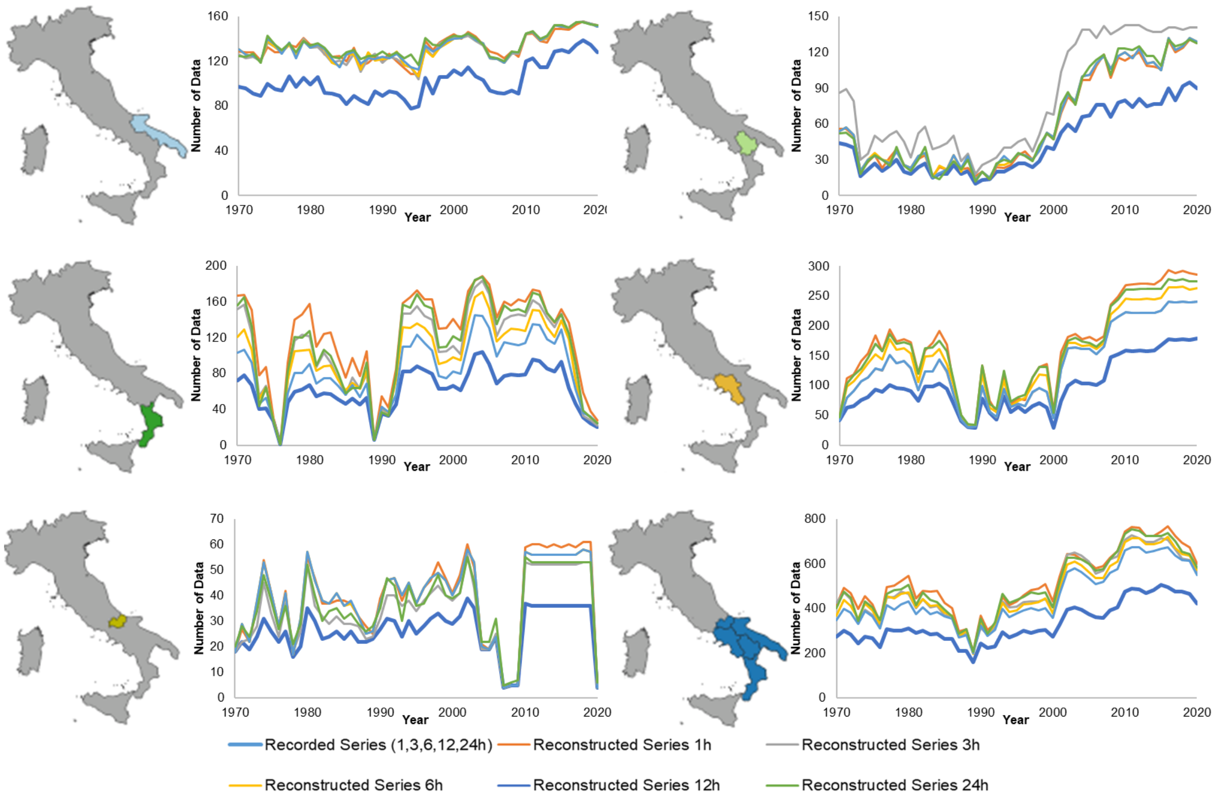

Figure 36 *- Data availability per year in the observed and reconstructed databases for each considered region (Apulia, Basilicata, Calabria, Campania and Molise) and for the entire territory of southern Italy.*

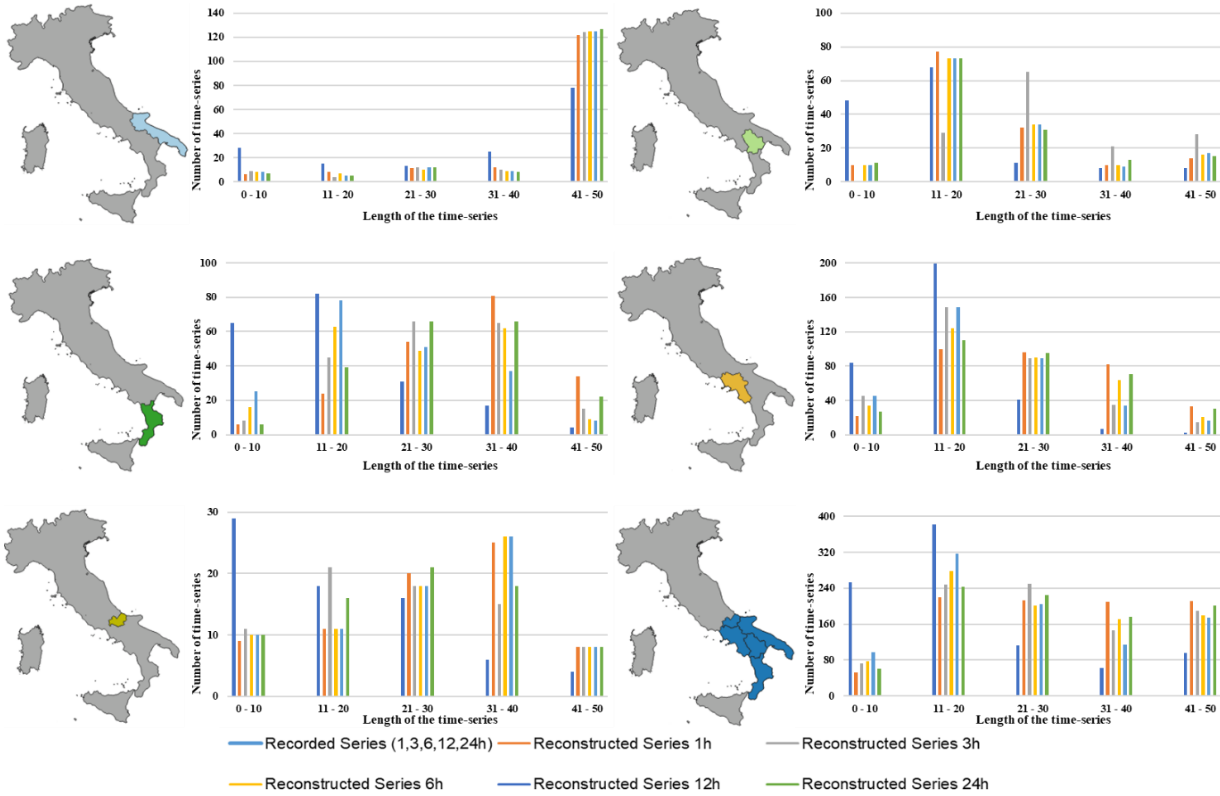

Figure 37 *- Number of series per length class in the recorded (blue bars) and reconstructed (1-h orange, 3-h grey, 6-h yellow, 12-h light blue, 24-h green bars) databases.*

As shown in Table 6 and Figure 36, the implemented procedure allows to extend the length of all recorded series and the procedure is more effective for years with more active stations. Additionally, the majority of observed series had a length in the range 0-20 years of observations, while, after the reconstruction, the number of series with a numerosity in the range 21-40 has significantly increased (Figure 37). Therefore, the SC-OK procedure was successful in reconstructing a reliable database of rainfall data suitable for statistical analysis and trend detection.

Although the completeness of time-series has nearly doubled, we decided to use only the reconstructed series with a completeness of more than 70% to avoid significant gaps. This value was chosen as a compromise between the maximum completeness attained using the proposed method and extent of the examined temporal window (1970-2020). Table 7 lists the number of selected series for each duration and region.

Table 7 *- Number of rainfall series with a completeness of more than 70% of the possible length in the period 1970-2020 for each duration (1, 3, 6, 12 and 24 hours) and for each region (Apulia, Basilicata, Calabria, Campania, and Molise).*

d [h]	**Number of time series analysed**					
	Apulia	**Basilicata**	**Calabria**	**Campania**	**Molise**	**TOT - Southern Italy**
1	132	19	78	71	28	**328**
3	129	36	42	33	16	**256**
6	129	20	33	49	27	**258**
12	129	20	15	33	27	**224**
24	134	20	55	62	22	**293**

Due to the filtering process, there were areas where no rainfall stations could be selected. In particular, no spatial conclusions can be drawn mainly in the northern (the Domitian coastline and the hinterland of Caserta) and southern (the Cilento and Vallo di Diana National Park areas) parts of Campania, the central and southern Basilicata and the norther Calabria. In these areas, the reconstruction was difficult due to the low density of the rain-gauge network (especially in Basilicata) and the small radius that has been selected (in Campania with a value of R ranging from 10 to 17 km) during the calibration step of the SC-Ok procedure. For these reasons, the number of stations meeting the spatial criteria of the SC-OK method is limited and, thus, no rain gauges were considered.

In summary, this section demonstrates that gap-filling procedures allow to overcome the problem of time-series discontinuity. In fact, the OK procedure coupled with a spatial selection criterion allows to obtain an increase in both the number of data and their temporal continuity. Therefore, the increase in the dataset size improves the statistical significance of the trend detection and the frequency analysis of extreme rainfall, which is discussed in the next paragraph (Section 4).

3.4.3 Validation of the SC-OK method

To validate the SC-OK reconstruction method, we decided to test its performance at local scale. In particular, a station randomly drawn from the database (in this section we considered the “Gragnano” rain gauge, in Campania region; for the location see Figure 38) was removed and then reconstructed by using the SC-OK procedure. The reconstruction error (reported in Table

8) was calculated by means of three error indices, namely root mean square error (RMSE), mean absolute error (MAE), and mean absolute percentage error (MAPE), given by:

$$RMSE = \sqrt{\frac{\sum_{i=1}^{N_p}\left(h_{obs,i} - h_{rec,i}\right)^2}{N_p}} \quad [17]$$

$$MAE = \frac{\sum_{i=1}^{N_p}\left|h_{obs,i} - h_{rec,i}\right|}{N_p} \quad [18]$$

$$MAPE = \frac{\sum_{i=1}^{N_p}\left|\frac{h_{obs,i} - h_{rec,i}}{h_{obs,i}}\right|}{N_p} \quad [19]$$

where N_p is the number of considered data, $h_{obs,i}$ and $h_{rec,i}$ are the observed and reconstructed value, respectively.

Table 8 *- Assessment of the reconstruction error by means of the error indices: root mean square error (RMSE), mean absolute error (MAE) and mean absolute percentage error (MAPE). The error values were calculated for recorded and reconstructed rainfall annual maxima for the station under investigation (Gragnano, ID 21789, Campania region).*

d [h]	**RMSE [mm]**	**MAE [mm]**	**MAPE [%]**
1	6.19	4.55	10.0
3	5.88	4.96	8.9
6	9.38	6.79	9.3
12	14.70	10.02	10.2
24	19.96	12.22	9.8

As shown in Table 8, the percentage error related to the reconstruction of the rainfall values ranges between 9% and 10%. Figure 38, instead, depicts the graphical comparison between observed (blue) and reconstructed (red) data for the station under investigation.

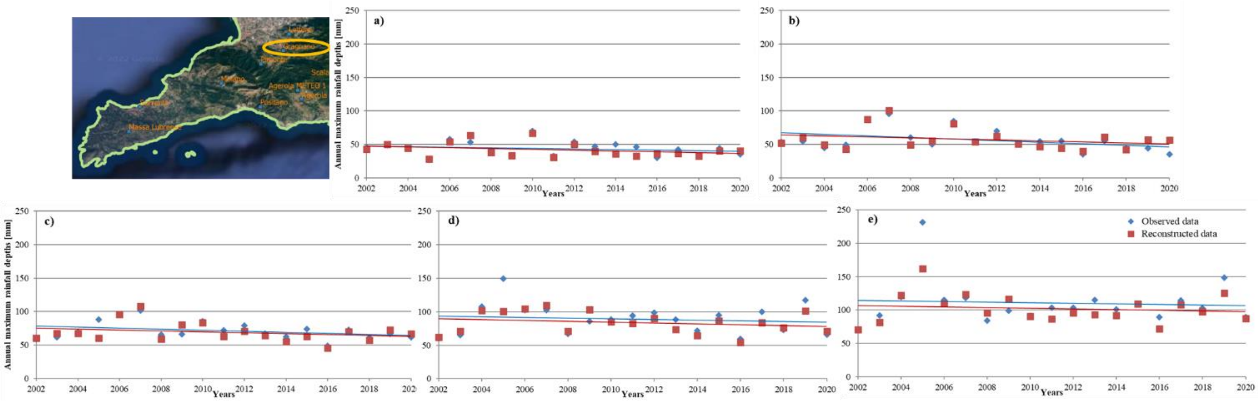

Figure 38 *- Graphical comparison between observed (in blue) and reconstructed (in red) values of the rainfall annual maxima series under investigation (Gragnano, ID 21789, Campania Region) for the five durations: a) 1h, b) 3h, c) 6h, d) 12h, and e) 24h.*

By analysing the Figure 38, it is clear that the majority of the estimated data tends to overlap with the observed data, thus demonstrating the goodness of the reconstruction procedure.

This kind of cross-validation was extended to 10% of randomly chosen stations in the database of each region. The regional performance statistics are shown by means of a box-plot graph for the RMSE (Figure 39), MAE (Figure 40), and MAPE (Figure 41) statistical indices, for the different durations.

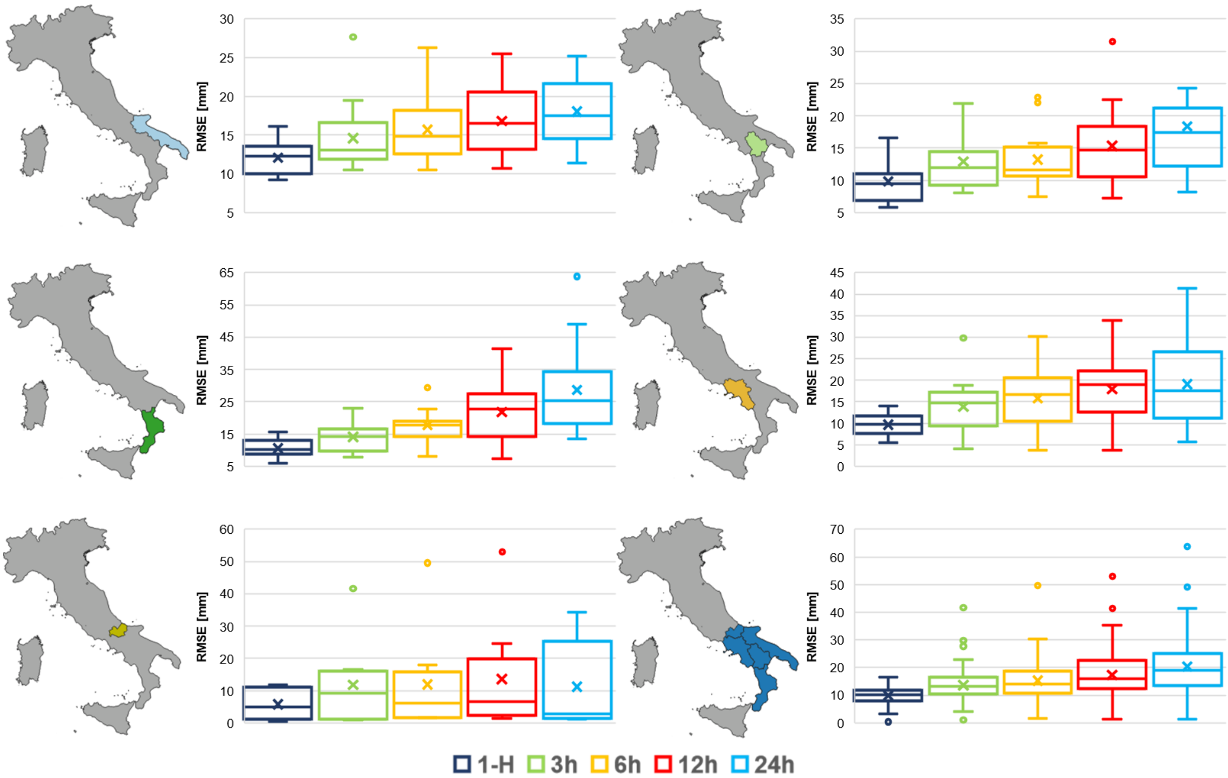

Figure 39 *- Box-plot graph of the root mean square error (RMSE) related to the reconstruction of the rainfall values of 10% of randomly chosen stations in the database of each region and each duration.*

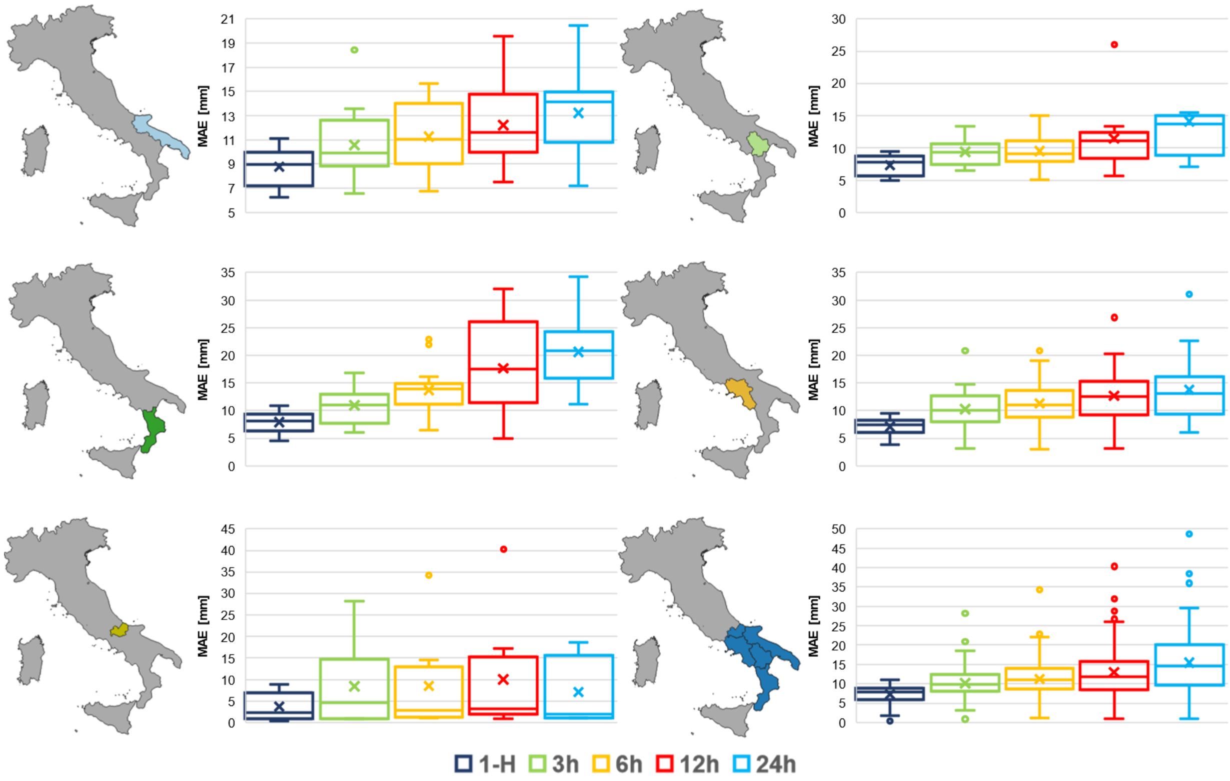

Figure 40 *- Box-plot graph of the mean absolute error (MAE) related to the reconstruction of the rainfall values of 10% of randomly chosen stations in the database of each region and each duration.*

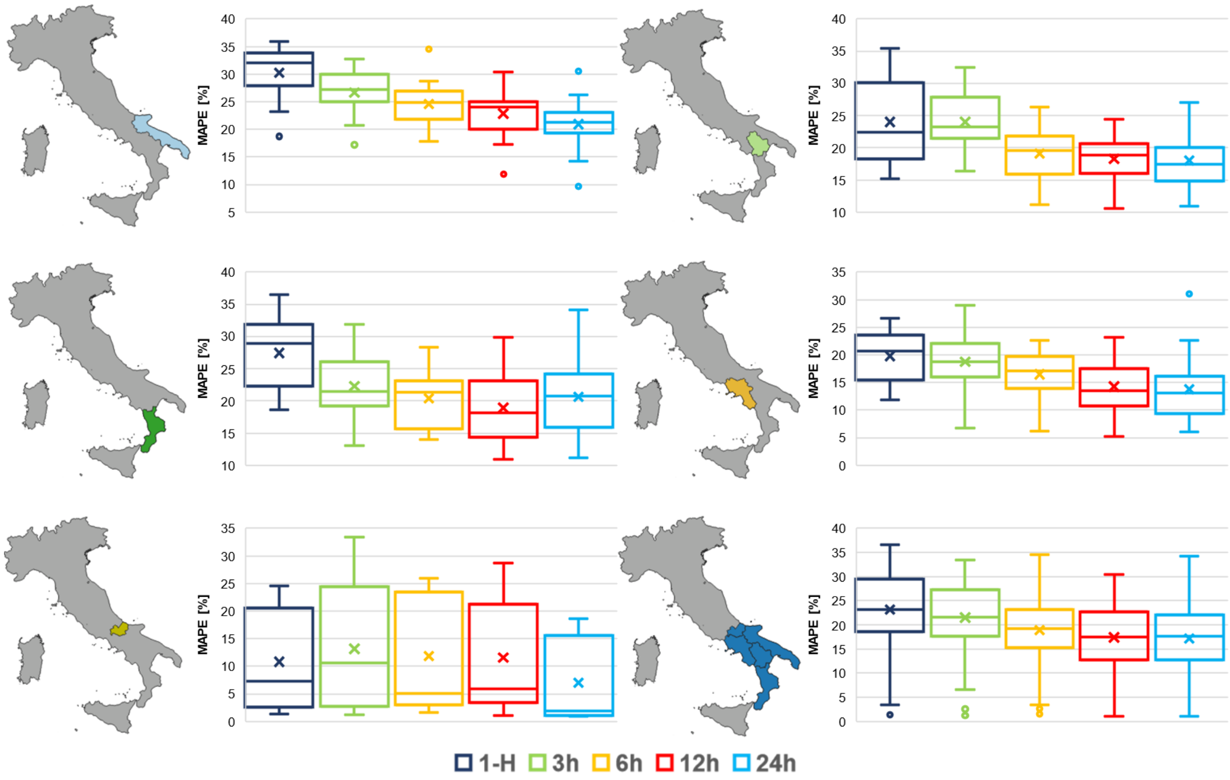

Figure 41 *- Box-plot graph of the mean percentage absolute error (MAPE) related to the reconstruction of the rainfall values of 10% of randomly chosen stations in the database of each region and each duration.*

The main results of the cross-validation analysis are that the mean RMSE at the southern Italy scale (Figure 39) ranges from 10 to 20 mm as the duration increases, while the mean MAPE (Figure 41) passes from 23% at 1-h to 20% at 24-h.

Nevertheless, as the aim of the work is to investigate trends in extreme precipitation, it is relevant to examine how the reconstruction error impacts the trend detection. For this purpose, the non-parametric Mann-Kendall (MK) trend test (Kendall, 1975) was applied to both the observed and reconstructed series. It detected no statistically significant tendency at 5% significance level. Additionally, the slopes of the trends were assessed by means of the Sen's slope test (Sen, 1968). As reported in Table 9, both the tests show similar results for the two different series, except at 6- and 12-h where there are small deviations in terms of trend slope without, however, leading to a different assessment of the general trend according to the MK test.

Therefore, we can confidently state that the error related to the reconstruction of missing data does not significantly affect the trend detection purposes.

Table 9 - *Trend slope, assessed by means of the Sen's slope test, for the observed and reconstructed series for the station under investigation (Gragnano, ID 21789, Campania region).*

d [h]	**1**		**3**		**6**		**12**		**24**	
	Slope	Trend	Slope	Trend	Slope	Trend	Slope	Trend	Slope	Trend
Observed data	-0.54	X	-0.31	X	-0.60	X	-0.64	X	-0.41	X
Reconstructed data	-0.50	X	-0.57	X	-0.34	X	-1.04	X	-0.46	X

Then, as previously described, this validation procedure was carried out to 10% of randomly chosen stations in the database, comparing the Sen's slope of the reconstructed series versus the Sen's slope of the observed series. For long-term series, the ratio between the two values is close to 1.

Therefore, it can be asserted that the reconstruction error, caused by the estimation of the missing data by means of the developed SC-OK method, does not introduce a statistical bias in the trend analysis of the rainfall series.

Chapter 4. Characteristics of rainfall annual maxima of southern Italy in recent years: trends and statistics

4.1 TRENDS DETECTION WITH NON-PARAMETRIC TESTS

The aim of this thesis is to analyse the trends and variability of long-term time series (1970-2020) of rainfall annual maxima by means of different statistical methods (simple non-parametric tests), which do not require any prior assumptions on the statistical proprieties of the data other than the independence of the recorded observations in time. Non-parametric tests are distribution-free methods, more suitable for non-normally distributed, censored, and missing data, which are frequently encountered in hydrological time series (Hirsch et al., 1992).

Six different methodologies have been applied to investigate temporal trends of the reconstructed rainfall series in order to characterize the precipitation regime: i) the at-site Mann-Kendall (MK) test and Sen's slope approach to explore and assess the presence of local trends in the magnitude of rainfall intensity; ii) the at-site Spearman's rho (SR) test to investigate trends in rainfall series; iii) the Regional Kendall test (RKT) to detect the evidence for a general trend over a specific region; iv) the Innovative Trend Analysis (ITA) technique which allows a graphical trend evaluation of the low, medium, and high values in the series; v) the record-breaking analysis to assess regional trends in the frequency of occurrence of record-breaking events; vi) the Pettitt test to identify change-points in the rainfall series.

Therefore, the first three approaches and the Pettitt test allow for exploring the presence of non-stationarities in the magnitude of extreme rainfall annual maxima, while the record-breaking analysis is more focused on the stability of the occurrence frequency of the higher extremes.

The assessment of the variability of long-term extreme rainfall time series using non-parametric tests was preceded by a graphical comparison of the average values of annual maxima for two different time periods. In detail, for each reconstructed rainfall series, the statistical means of the annual maximum rainfall depths over two distinct time windows (1970-1994 and 1995-2020) were calculated to identify the existing trends in the dataset. To obtain a statistically significant value of the mean, series with less than 5 data in a period were excluded. Then, the relative difference in percentage (*H*) was calculated using the following equation:

$$H = \frac{\bar{h}_{1995-2020} - \bar{h}_{1970-1994}}{\bar{h}_{1970-1994}} * 100 \quad [20]$$

where $\bar{h}_{1970-1994}$ is the mean value of the annual maximum rainfall depths in the period 1970-1994 and $\bar{h}_{1995-2020}$ is the mean value of the annual maximum rainfall depths in the period 1995-2020. The values of *H* were spatially interpolated by means of the QGIS software by applying an ordinary kriging with a spherical semi-variogram and variable windows (a maximum value of 30 km was set to find at least 5 rain gauges). The kriged maps, for the five durations, are displayed in Figure 42.

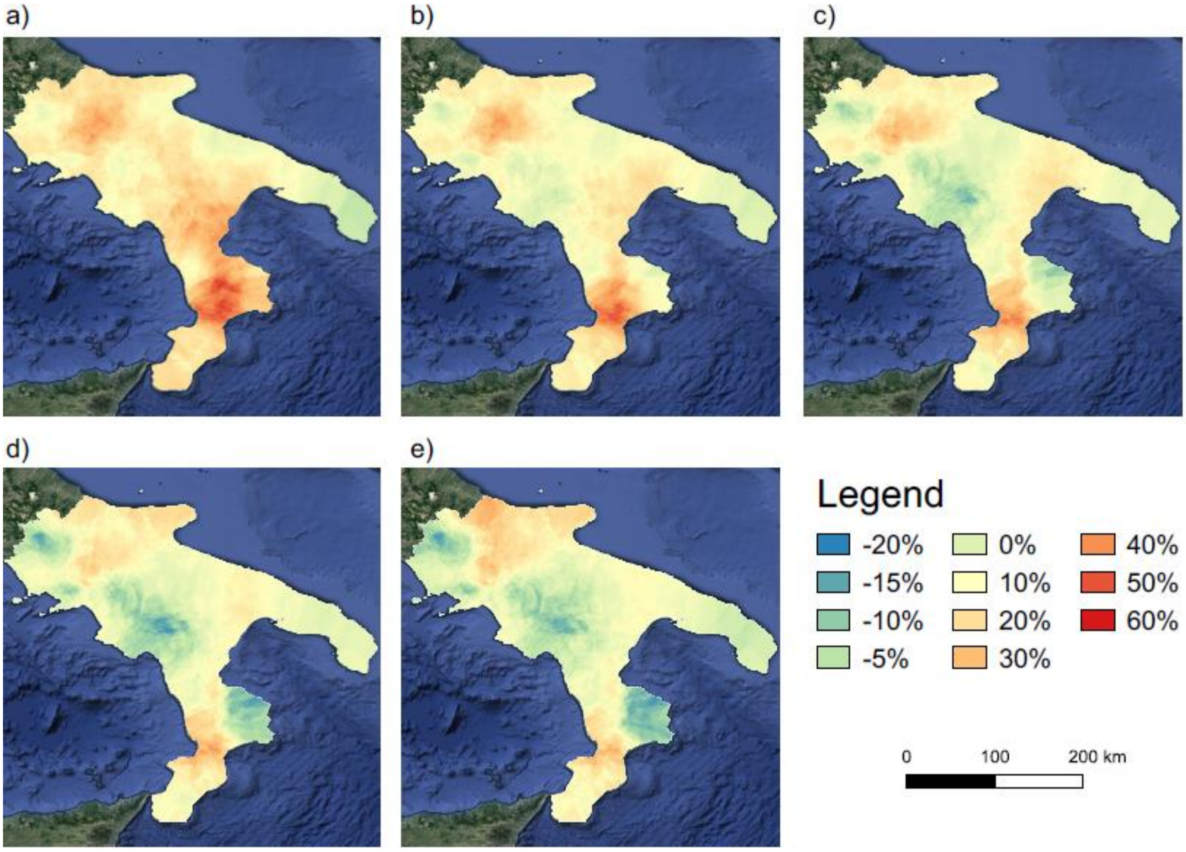

Figure 42 *- Kriged maps of the relative difference of mean values of rainfall annual maxima over two distinct time windows 1970-1994 and 1995-2020 in percentage spatially interpolated for the five durations: a) 1h, b) 3h, c) 6h, d) 12h, e) 24h. The maps are characterized by a 1×1 km spatial resolution.*

The five maps in Figure 42 allow to better understand the changes in rainfall regime, in terms of both spatial and temporal scale, comparing the periods 1995-2020 to 1970-1994. In the recent years, an increase in short-duration rainfall (1-3 hours, respectively; Figures 42a and 42b) was detected in the entire region, with the exception of the southern tip of the Apulia region. In particular, an average increase of 15-20% was estimated for the 1-hour duration, with peak values of 30-40% in the area of the Campano Apennines and Matese Regional Park, on the border between Apulia, Campania, and Molise, and in the Basilicata Ionian. Additionally, 40-50% increases were recorded in the southern part of the Calabria region, namely along the Calabrian Apennines, from the Sila plateau to Aspromonte.

Instead, for longer durations, a generalized decrease was identified, except for the areas mentioned above, the Molise region and the norther Apulia. The most significant decreases were observed in the north of the study area (i.e., on the border with Lazio), south-eastern Campania and the norther Basilicata. Peak values of -20% were detected in the hinterland of Crotone in the Calabria Ionian.

This analysis confirms the well-known theoretical evidence suggesting that, in recent decades, climate changes have resulted in a higher frequency of short-duration (less than 3 hours) and more intense rainfall events.

4.2 MANN-KENDALL (MK) AT-SITE TREND TEST

The non-parametric Mann-Kendall (MK) trend test is a widely used rank-based method for detecting monotonic trends in hydrological time series. The test has been suggested by the World Meteorological Organization (WMO) to assess trends in environmental data time series (WMO, 2014) as the test is suitable for cases where the trend may be assumed monotonic and therefore no seasonal aspects are presented in the data. The MK test allows to assess whether a time series has an upward or downward trend without making assumptions about its distributional properties. The null hypothesis is that there is no trend, while the alternative hypothesis is that there is an upward (or downward) trend in the one-side test. Given a random variable *h*, and a sample of *sl* independent data $h = (h_1, \dots, h_{sl})$, the Kendall S_k statistic (Mann 1945; Kendall 1975) is defined as follows:

$$S_k = \sum_{i=1}^{sl_k - 1} \sum_{j=i+1}^{sl_k} sign(h_j - h_i) \qquad [21]$$

where *h* represents the data values at times *i* and *j*, sl_k is the length of the k^th series and

$$sign(\vartheta) = \begin{cases} 1 \; if \; \vartheta > 0 \\ 0 \; if \; \vartheta = 0 \\ -1 \; if \; \vartheta < 0 \end{cases} \qquad [22]$$

Under the null hypothesis that h is independent and randomly distributed, for $sl_k \geq 8$, the result of Eq. [21] is approximately a normal variable with zero mean and variance that, in the presence of $N_{tg,k}$ tied groups of length $l_{m,k}$, can be expressed as:

$$\sigma_k^2 = \frac{sl_k(sl_k - 1)(2sl_k + 5) - \sum_{m=1}^{N_{tg,k}} l_{m,k}\left(l_{m,k} - 1\right)(2l_{m,k} + 5)}{18} \qquad [23]$$

The standardized test statistic Z_k can be calculated by:

$$Z_k = \begin{cases} \dfrac{S_k - 1}{\sigma} if \; S_k > 0 \\ 0 \qquad if \; S_k = 0 \\ \dfrac{S_k + 1}{\sigma} if \; S_k < 0 \end{cases} \qquad [24]$$

Using this approach, the p-value is evaluated and then, compared with a given significance level. The local p-value for each trend test can be obtained from the following relation:

$$p = 2[1 - \Phi|\mathrm{Z_S}|] \qquad [25]$$

where $\Phi|*|$ denotes the cumulative distribution function of a standard normal variable.
The non-parametric estimate of the magnitude of the trend slope, called Sen's slope (Sen, 1968), in a time series containing W pairs of data is defined as the median of the slopes, β_j, given by:

$$\beta_j = \frac{h_i - h_k}{i - k} \qquad [26]$$

where $j = 1, \ldots, W$ and $i > k$.

MK method is widely used in analysing atmospheric and climatological time series because it offers many advantages, such as missing values are allowed, and the data need not to be conform to any statistical distribution. In detail, the following assumptions underlie the MK test:

- when no trend is present, the measurements obtained over time are independent and identically distributed. The assumption of independence means that the observations are not serially correlated over time.

- the observations obtained over time are representative of the true conditions at sampling times.
- there is no requirement that the measurements be normally distributed or that the trend, if present, is linear.

The MK test can be computed if there are missing values, but the performance of the test will be adversely affected by such event. The assumption of independence requires that the time between samples be sufficiently large so that there is no correlation between measurements collected at different times.

The MK test was applied independently to each reconstructed time series for all durations (from 1 to 24 hours) and for all the considered regions (Apulia, Basilicata, Calabria, Campania and Molise) at 95% confidence interval in order to detect increasing, decreasing or no trend. Application of the MK test to the extended series may indicate possible duration-dependent trend existence in the extreme rainfall events over the study area. However, as a general result, most of the series display no statistically significant tendencies for all the temporal intervals.

It is not possible to compare the results in terms of number of stations showing trends as the number of series used to perform the analysis is quite variable for the different durations and regions. Nevertheless, some overall conclusions can be drawn by considering the percentage of rain gauges with statistically significant (95% confidence interval) positive or negative trends, as reported in Figure 43.

Trend	Duration				
	1h	3h	6h	12h	24h
Increasing	13%	15%	9%	8%	7%
Decreasing	0%	0%	1%	0%	0%
No Trend	87%	85%	90%	92%	93%
Number of stations	132	129	129	129	134

Trend	Duration				
	1h	3h	6h	12h	24h
Increasing	21%	8%	15%	5%	0%
Decreasing	0%	0%	0%	5%	0%
No Trend	79%	92%	85%	90%	100%
Number of stations	19	36	20	20	20

Trend	Duration				
	1h	3h	6h	12h	24h
Increasing	51%	31%	24%	20%	24%
Decreasing	0%	0%	0%	0%	2%
No Trend	49%	69%	76%	80%	75%
Number of stations	78	42	33	15	55

Trend	Duration				
	1h	3h	6h	12h	24h
Increasing	24%	15%	10%	6%	3%
Decreasing	0%	0%	2%	12%	3%
No Trend	76%	85%	88%	82%	94%
Number of stations	71	33	49	33	62

Trend	Duration				
	1h	3h	6h	12h	24h
Increasing	54%	25%	30%	22%	23%
Decreasing	0%	0%	0%	0%	9%
No Trend	46%	75%	70%	78%	68%
Number of stations	28	16	27	27	22

Trend	Duration				
	1h	3h	6h	12h	24h
Increasing	27%	17%	14%	10%	10%
Decreasing	0%	0%	1%	2%	2%
No Trend	73%	83%	85%	88%	88%
Number of stations	328	256	258	224	293

Figure 43 *- Percentage of stations with positive, negative or no trends (detected with Mann-Kendall trend test at 95% confidence interval) and number of rain gauges analysed for each considered duration (1, 3, 6, 12 and 24 hours) and for each region (Apulia, Basilicata, Calabria, Campania, Molise and Southern Italy).*

By analysing the presented results, a general increasing trend is confirmed at shorter durations, which tends to disappear or become less significant for rainfall events of longer durations. In particular, in Basilicata and Campania about 20% (21% and 24% respectively) of the stations show an increasing trend at 1 hour, but that percentage tends to zero at 24 hours. Such behaviour was also observed, in Calabria and Molise where the percentage of series exhibiting an upward tendency decreases from 50% (51% and 54% respectively) at 1 hour to 20% (24% and 23% respectively) at 24 hours. Instead, in Apulia, about 10% of the stations present an upward trend for all durations.

Unfortunately, it was not possible to include sub-hourly durations assessment in this study due to the lack of data, especially in the period before 2000. However, in the near future, analyses may be extended to the smaller time scales by exploiting the hybrid procedure proposed by Pelosi et al. (2022). The innovative methodology allows for integrating databases with different time resolutions in order to achieve an extension of the sample size of data at sub-hourly durations. In particular, the purpose of the procedure is to blend historical time series of annual maxima recorded by mechanical stations (operating at hourly scales) up to the end of the past century with newer time series of annual maxima at higher time resolutions recorded by automatic stations installed over the past twenty years.

Nevertheless, at this stage, extrapolating the presented results to sub-hourly durations might indicate an increase in extreme events relative to such durations, similar to the cases examined by De Toffol et al. (2009), which proved evidence of trends at shorter time intervals.

On the contrary, decreasing trends were only detected at longer durations (12 and 24 hours), but however their percentage is not significant in all the regions, ranging from 0% in Apulia and Basilicata to 2% in Calabria and Campania up to 9% in Molise at 24 hours. Nevertheless, it is worth noting that 12% of the stations in Campania and 5% in Basilicata show a decreasing trend at 12 hours. Therefore, the correlation with the duration is less evident than in the case of positive trend analysis, rather showing almost a constant behaviour with duration.

Similar results were observed in Sicily region by Bonaccorso et al. (2005), that found an increasing trend only at shorter durations (less than 3 hours), while the opposite for events of longer durations. Instead, for the Calabria region the presented findings are not in good agreement with the ones shown by Libertino et al. (2019). In fact, they underlined a general decreasing trend for all durations in the period 1928-2014, even if the regional trend turned out to be significant and homogeneous only at 24 hours. On the contrary, in our work a marked increasing trend was detected for all the durations. This difference may be due to the different completeness of the considered time series and the different temporal window of assessment (we limited the analysed period to the years 1970-2020).

Nevertheless, from the analysis of the observed trends, further considerations can be drawn. In particular, it was noted that the majority of rain gauges in all regions do not exhibit any statistically significant trends. Therefore, it is intriguing to know, for these stations, what the sign of the slope is, if any. Hence, the percentage of stations with positive or negative trends (significant or not at 95% confidence interval) was depicted in Figure 44 (for the five considered regions) and Figure 45 (for the whole Southern Italy).

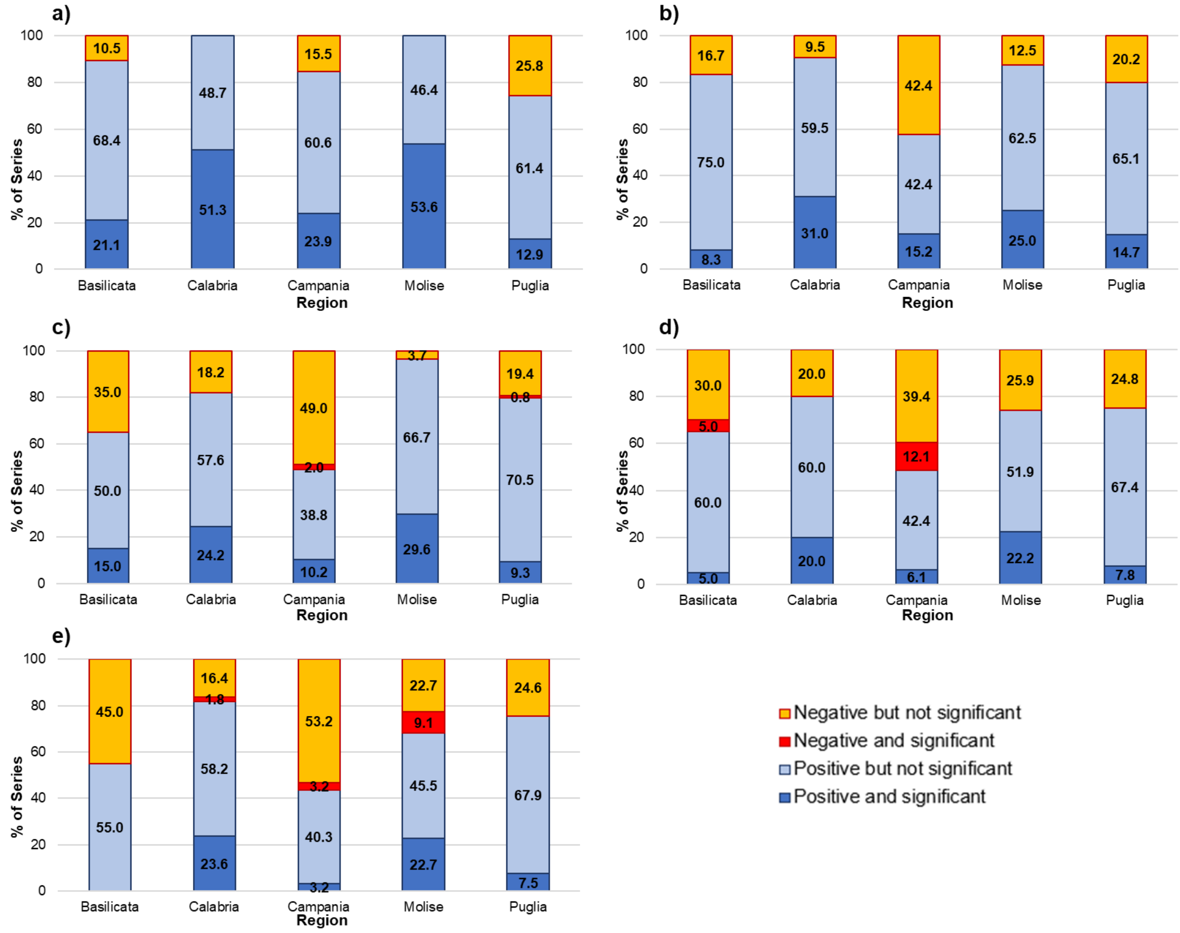

Figure 44 *- Results of the Mann-Kendall (MK) trend test (5% significance level) for the five considered durations: a) 1h, b) 3h, c) 6h, d) 12h, and e) 24h. The percentage of stations with increasing or decreasing trends, statistically significant or not, is reported for the five considered region (Apulia, Basilicata, Calabria, Campania and Molise).*

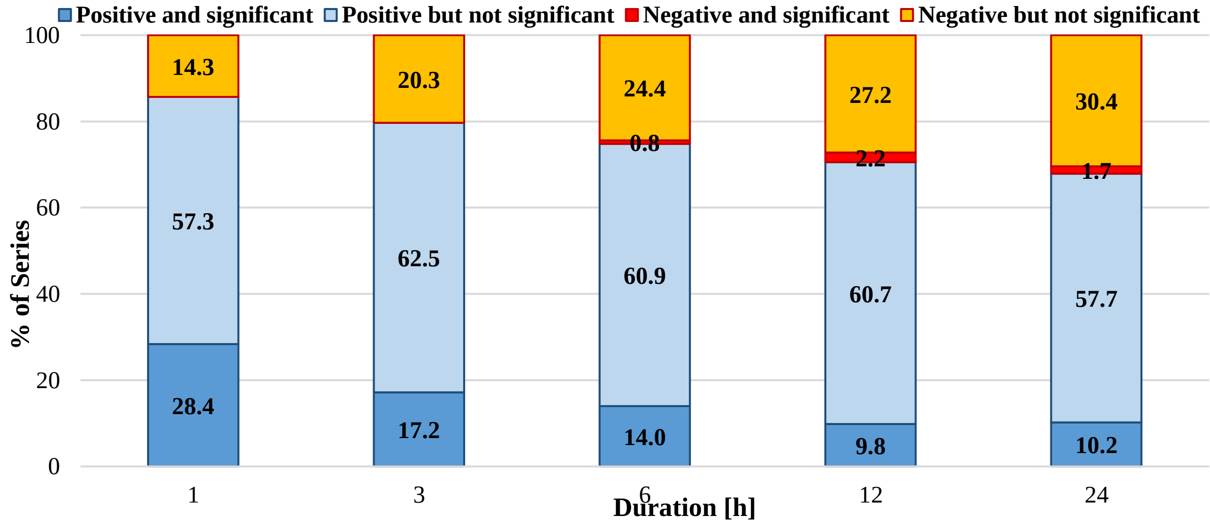

Figure 45 *- Results of the Mann-Kendall (MK) trend test (5% significance level) for the five considered durations (1, 3, 6, 12, and 24 hours). The percentage of stations with increasing or decreasing trends, statistically significant or not, is reported for the southern Italy scale.*

As shown in Figure 44, a prevailing positive increasing trend was found, especially for the shorter durations, in all the regions. In particular, Calabria and Molise regions show the most diffuse positive trend at shorter durations, with the 100% of the considered rain gauges presenting an increasing trend at 1-h duration, even if only the 50% turned out to be statistically significant (as shown previously; Figure 43). This percentage tends to decrease as the duration increases, but it never falls below 70%. Regarding the Apulia region, the ratio of stations with upward and downward trends is nearly constant (4 to 1) at all durations. Instead, Basilicata and Campania display the greatest percentage of stations showing a downward tendency, nearly or even more than 50% for longer durations.

A general behaviour might be derived from the above results, according to which the longer the duration, the lower the percentage of stations with a positive trend. In detail, for the whole study area (Figure 45), that percentage decreases from 86% at 1-h to 68% at 24-h; while the percentage of negative trends increase from 14% to 32%.

In light of this, we can state that when a trend is found, it is typically positive for short durations and both positive and negative for the longer time intervals, even if the majority of rain gauges do not show any statistically significant trend.

It is extremely noteworthy observing the spatial distribution of the rainfall stations that display statistically significant trends. In fact, the spatial representation (Figure 46) might allow to identify local clusters characterized by an increase or decrease in extreme precipitation regime over the period 1970-2020.

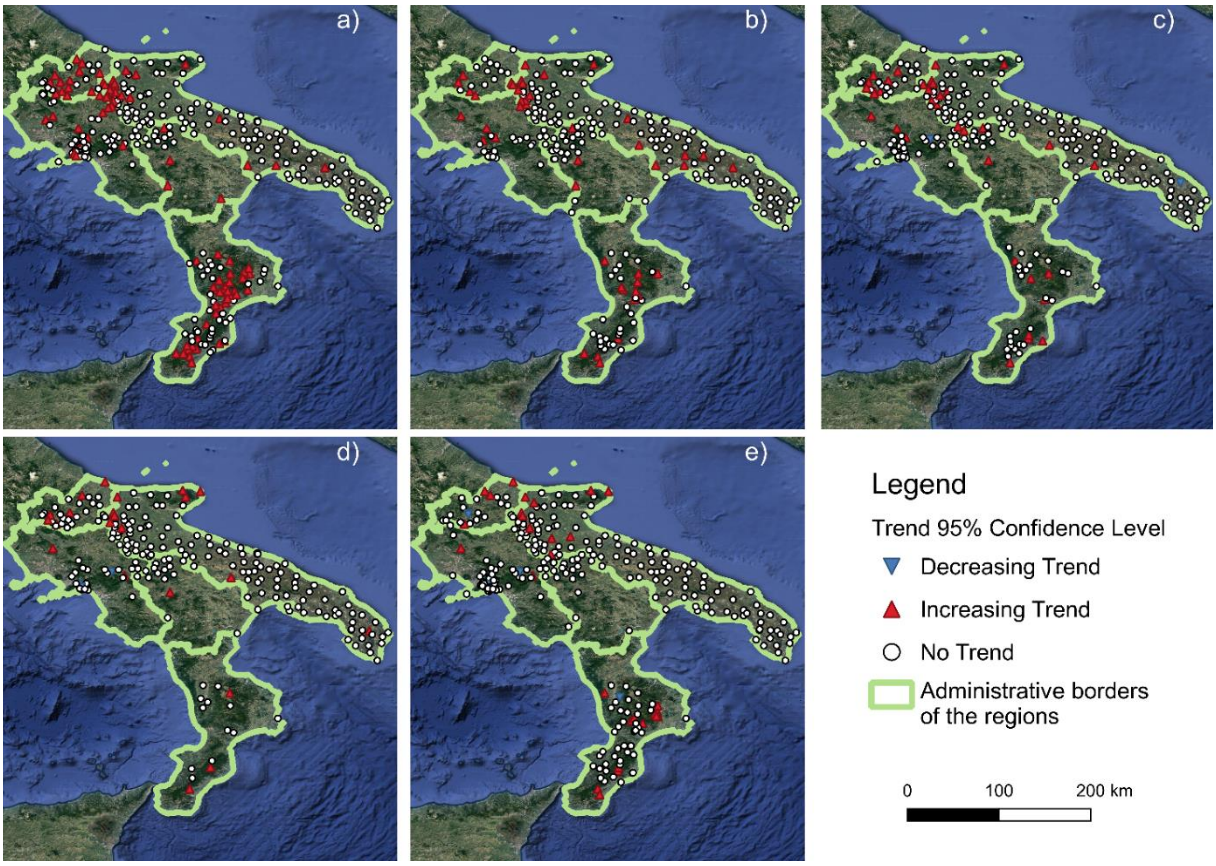

Figure 46 *- Spatial distribution of the local trends for the rainfall annual maxima detected with Mann-Kendall (MK) trend test at 5% significance level for the five durations: a) 1h, b) 3h, c) 6h, d) 12h, e) 24h. The red triangles show an increasing trend, the inverted blue triangles show a decreasing trend, while the white circles represent no statistically significant trend.*

As highlighted in Figure 46, some spatial clusters of increasing trends emerge especially at shorter durations (1 and 3 hours). However, the sparseness of rain gauges did not allow to provide a full analysis of the investigated area. In fact, there are many areas, especially in Campania and Basilicata, where no station with enough data were selected in the previous step of data reconstruction, due to the limited number of observations and the restrictive reconstruction constraints. By analysing the maps, we can state that the overall situation appears very heterogeneous, even if most of study area display no trend at all.

For longer durations, most of the series have no statistically significant trend. Additionally, it was not possible to identify local clusters of change as the few stations with trends are widely scattered over the entire territory.

On the contrary, for shorter durations (1 and 3 hours), three areas exhibiting a well-defined increase in extreme rainfall were identified: from north to south, the central highlands of Molise and the Matese Regional Park, on the border between Campania and Molise; the Campano

Apennines, area on the border between Apulia, Campania, and Molise; the Calabrian Apennines, from the Sila plateau to Aspromonte. In Calabria, some of these local upward trends persist even at longer durations. In addition, it is worth noting the presence of some stations showing increasing trends in Campania at shorter durations along the Monti Lattari and in the area of the Paternio and the Monti Picentini regional park.

It must be stated that most the recent observations (starting from 2000) are recorded with digital rain gauges that offer a higher precision. This may affect the results reported herein especially at the hourly scale. In fact, mechanical stations operating typically at hourly scale may under-estimate annual maxima up to 12%, which may impact on the observed trend (Pelosi et al., 2022). Nevertheless, this impact tends to decrease at larger timescales (i.e., three hours or more) where we still observe a relatively large number of increasing trends.

4.3 Spearman's rho correlation (SR) test

Spearman's rho correlation test (Lehmann, 1975; Sneyers, 1990) is another rank-based non-parametric method used for trend analysis and was applied as a comparison with the Mann-Kendall test. The test is well suited for monotonically related variables, even when their relationship is not linear, as it is required in the case of Pearson's test. Just like the MK test, it does not require prior transformations of the data as it is based on ranks, i.e., the indices denoting the positions occupied by the observations in the sorted sample (increasing or decreasing). The Spearman's correlation coefficient, r_s, (Spearman, 1904) is the non-parametric equivalent of the Pearson correlation coefficient in which the data are converted to ranks and then the difference between the ranks is calculated for each pair of observations. In this test, which assumes that time-series are independent and identically distributed, the null hypothesis (H_0) indicates no trend over time; while the alternate hypothesis (H_1) is that a trend exists and that data increase or decrease over the time. Given a random variable h, and a sample of sl independent data $h = (h_1, \dots, h_{sl})$, the test statistics r_s is defined as:

$$r_s = 1 - \frac{6\sum_{i=1}^{sl} D_i^2}{sl(sl^2 - 1)} \qquad [27]$$

where $D_i = r_i - s_i$, being r_i and s_i the rank of the first (h) and second (time interval, i.e., *year*) variables, respectively, and sl the length of the series.

If the sample size is sufficiently large (approximately *sl* > 20), the Student's t-distribution (with *sl-2* degrees of freedom) can be used after appropriately transforming the r_s value as follows:

$$t_s = \frac{r_s}{\sqrt{\frac{1 - r_s^2}{sl - 2}}} \qquad [28]$$

The positive values of t_s represent an increasing trend across the hydrologic time series; negative values represent the decreasing trend. The critical value of t_s at α significance level of Student's t-distribution table is defined as $t_{(sl-2,1-\frac{\alpha}{2})}$. If $|t_s| > t_{(sl-2,1-\frac{\alpha}{2})}$, the null-hypothesis ($H_0$) is rejected and a significant trend exists in the time-series.

The SR test was applied to each reconstructed time series for all durations (from 1 to 24 hours) and for all the considered regions (Apulia, Basilicata, Calabria, Campania and Molise) separately at 95% confidence interval in order to detect increasing, decreasing or no trend. The results are depicted in Figure 47 (for each region) and in Figure 48 (at the southern Italy scale).

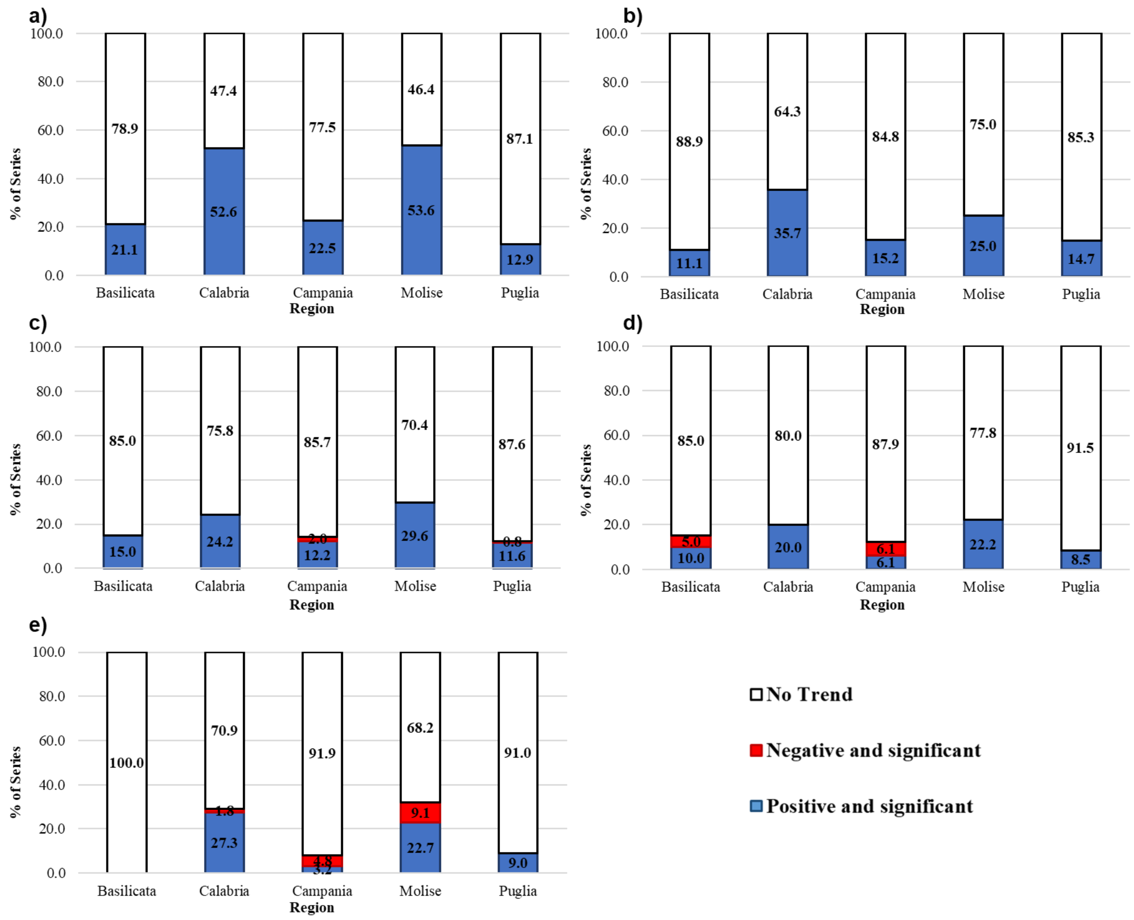

Figure 47 *- Percentage of series with statistically significant positive and negative or no trends (detected with Spearman's rho test at 95% confidence interval) for each duration: a) 1h, b) 3h, c) 6h, d) 12h, and e) 24h.*

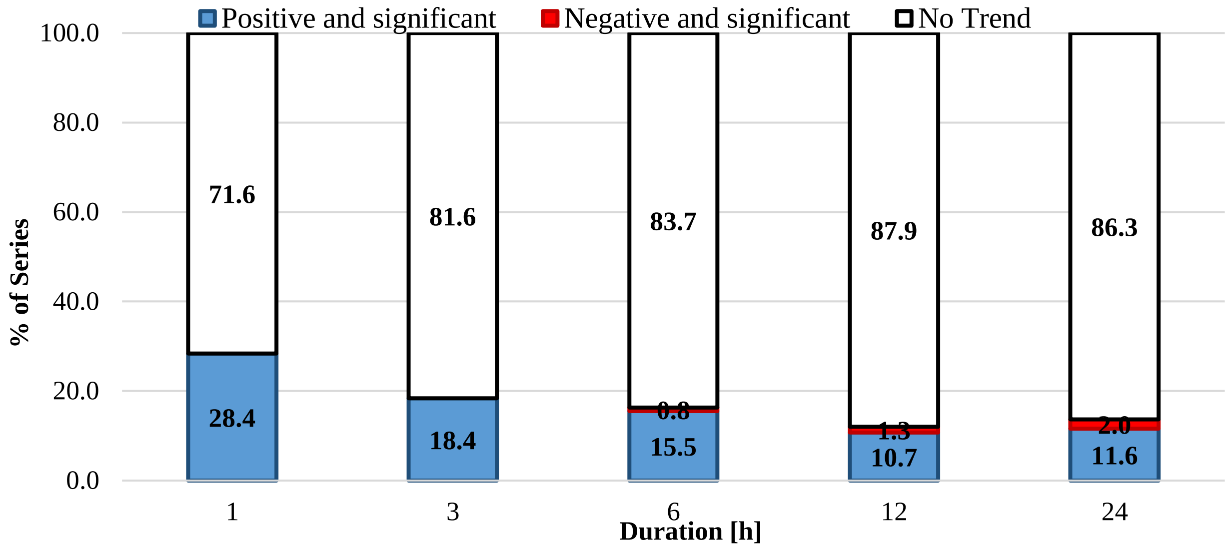

Figure 48 - *Percentage of series with statistically significant positive and negative or no trends (detected with Spearman's rho correlation test at 95% confidence interval) at the southern Italy scale.*

In this work, the Spearman's rho correlation test was applied as a comparison with the Mann-Kendall test, and as expected, the outcomes are almost identical. Therefore, the discussion of the results is identical to that dealt with in Section 4.2.

4.4 Regional Kendall (RK) trend test

Trend results should be consistent between stations. For example, by applying the MK at-site test, each station is dealt with separately, thus the results of trend analysis may not be significant, but when a larger spatial scale is considered as a whole, the trend might be highly significant. Therefore, the Regional Kendall (RK) test was applied to assess the presence of a general trend at the regional scale. The regional Kendall's statistic, S_{reg}, (Helsel and Frans, 2006) was evaluated as the sum of the S Kendall's statistics calculated for each series (k):

$$S_{reg} = \sum_{k=1}^{n_r} S_k \qquad [29]$$

where n_r is the number of rain gauges for each duration, and S_k is the S Kendall's statistics for the k^{th} series. The test statistic, Z_{reg}, was then evaluated using Eq. [24] with $S = S_r$ and $\sigma = \sigma_r$, where:

$$\sigma_r^2 = \sum_{k=1}^{n_r} \frac{sl_k(sl_k - 1)(2sl_k + 5)}{18} \qquad [30]$$

and sl_k represents the number of data in each series.
Additionally, the regional trend slope was calculated as the median of all slopes between data pairs.

Van Belle and Hughes (1984) test we applied to assess the homogeneity of the trends. The test failure means that the considered stations within the considered region have different trend directions, and, therefore, the regional trend slope is statistically incorrect and the region is not climatically homogeneous. The van Belle and Hughes procedure is based on dividing the sum of the squares using the chi-square test to get the trend homogeneity between stations.

$$\chi^2_{homogeneous} = \chi^2_{total} + \chi^2_{trend} \qquad [31]$$

In particular, the equation can be expressed as follows:

$$\chi^2_{homogeneous} = \sum_{k=1}^{n_r} (Z_k)^2 - n_r * \left(\frac{1}{n_r} \sum_{k=1}^{n_r} Z_k \right) \qquad [32]$$

where Z_k is the standardized MK test statistic for k^{th} rain gauge.

If the $\chi^2_{homogeneous}$ exceeds the predefined α (5%) critical value for the Chi-square distribution with $(n_r - 1)$ degrees of freedom, the null hypothesis of homogeneous trend must be rejected and in this case, different stations show dissimilar trends, otherwise, the χ^2_{trend} is referred to the Chi-square distribution with 1 degree of freedom to test a common monotonic trend.

The results of the RK and Van Belle and Hughes tests (at 5% significance level) for each duration are reported in Table 10 (at regional scale) and in Table 11 (at the study area scale, the southern Italy, considering this area as climatically homogeneous).

Table 10 *- Results of the Regional Kendall (RK) and Van Belle and Hughes tests for each duration, carried out at 95% confidence interval. Statistically significant and homogeneous increasing trends are highlighted in green, while in orange upward trends that are statistically significant but not homogeneous.*

Regions	d [h]	RK test	RK Slope	Van Belle-Hughes test
Apulia	1	Increasing Trend	0.085	Non-Homogeneous Trend
	3	**Increasing Trend**	**0.080**	**Homogeneous Trend**
	6	**Increasing Trend**	**0.100**	**Homogeneous Trend**
	12	**Increasing Trend**	**0.107**	**Homogeneous Trend**
	24	**Increasing Trend**	**0.138**	**Homogeneous Trend**
Basilicata	**1**	**Increasing Trend**	**0.162**	**Homogeneous Trend**
	3	**Increasing Trend**	**0.076**	**Homogeneous Trend**
	6	**Increasing Trend**	**0.054**	**Homogeneous Trend**
	12	No Trend	0.050	Homogeneous Trend
	24	No Trend	0.042	Homogeneous Trend
Calabria	**1**	**Increasing Trend**	**0.269**	**Homogeneous Trend**
	3	**Increasing Trend**	**0.333**	**Homogeneous Trend**
	6	**Increasing Trend**	**0.267**	**Homogeneous Trend**
	12	**Increasing Trend**	**0.281**	**Homogeneous Trend**
	24	**Increasing Trend**	**0.559**	**Homogeneous Trend**
Campania	**1**	**Increasing Trend**	**0.154**	**Homogeneous Trend**
	3	Increasing Trend	0.061	Non-Homogeneous Trend
	6	No Trend	-0.010	Non-Homogeneous Trend
	12	No Trend	-0.005	Non-Homogeneous Trend
	24	No Trend	-0.084	Non-Homogeneous Trend
Molise	**1**	**Increasing Trend**	**0.249**	**Homogeneous Trend**
	3	**Increasing Trend**	**0.245**	**Homogeneous Trend**
	6	**Increasing Trend**	**0.262**	**Homogeneous Trend**
	12	**Increasing Trend**	**0.108**	**Homogeneous Trend**
	24	Increasing Trend	0.208	Non-Homogeneous Trend

The RK test revealed a statistically significant increasing trend in Apulia, Calabria and Molise regions for all the analysed time intervals. Furthermore, the detected trend turned out to be homogeneous according to Van Belle and Hughes tests under a 5% significance level for all the durations, except 1-hour in Apulia and 24-hours in Molise. This non-homogeneity is likely due to the non-uniform behaviour of the rainfall station, as different series exhibiting different trend directions. In particular, about 26% of the rainfall series in Apulia and 32% in Molise presents respectively a 1-h and 24-h decreasing tendency, even if not statistically significant (as shown in Figure 43), contrasting the behaviour of the remaining rain gauges.

Instead, a specific attention is needed for Basilicata and Campania regions. A statistically significant and homogeneous increasing trend was only detected at shorter durations (1-, 3- and 6-h in Basilicata and 1- and 3-h in Campania), while for longer time intervals the test revealed no trend, with the regional trend slope tending towards zero as the duration increases. This is likely explained by the absence of statistically significant trends in most of the time series, as shown in Figure 46. However, these results need to be investigated further because they may be affected by the limited number of series selected, which provides inadequate spatial coverage of the area under investigation and may introduce a bias into the regional-scale trend detection.

Table 11 *- Results of the Regional Kendall (RK) and Van Belle and Hughes tests for the whole area of Southern Italy, carried out at 5% significance level. Both tests are. Statistically significant but not homogeneous increasing trends are highlighted in orange.*

d [h]	RK test	RK Slope	Van Belle-Hughes test
1	Increasing Trend	0.156	Non-Homogeneous Trend
3	Increasing Trend	0.115	Non-Homogeneous Trend
6	Increasing Trend	0.115	Non-Homogeneous Trend
12	Increasing Trend	0.106	Non-Homogeneous Trend
24	Increasing Trend	0.137	Non-Homogeneous Trend

Additionally, as shown in Table 11, the RK detected a statistically significant increasing trend for all the durations at southern Italy scale. However, the trend turned out to be non-homogeneous by applying the Van Belle and Hughes' homogeneity test. Two different explanations can be given to justify this result: there may be no trend in most, or all, the series, or some rain gauges may show trends, but not in the same direction. Considering the morphological configuration of southern Italy and its climatic variability, we can state that this non-homogeneity is due to the different contrasting trend directions exhibited by the rain gauges. In fact, although most stations have an upward tendency, there is nevertheless a significant percentage of series with a downward trend (ranging from 14% at 1-h to 32% at 24-h), as shown in Figure 45.

As demonstrated also by Libertino et al. (2019), no statistically homogeneous trend can be identified at the country scale (southern Italy), while significant and convergent regional trends appear when smaller domains are investigated.

4.5 INNOVATIVE TREND ANALYSIS (ITA) METHOD

The Innovative Trend Analysis (ITA) method, introduced by Sen (2012 and 2017), is a graphical trend analysis technique. In the recent years, it has been widely used for detecting trends in hydrological and meteorological variables because it does not require any assumptions (i.e., serial correlation, non-normality, sample number), which are, instead, needed by traditional trend analysis procedures.

In practice, in using ITA method, a time series is divided into two equal halves, and both sub-series were separately sorted in ascending order. In a Cartesian diagram, the first subseries is plotted on the X-axis, and the second subseries on the Y-axis (as shown in Figure 49a). If the data points are clustered on a 1:1 (45°) straight line, it indicates that there is no trend. Data clustered above the 1:1 straight line represent an increasing monotonic trend, while data points below this line indicate a decreasing monotonic trend. The data line is the parallel to the 1:1 line, with the centroid point (s_1, s_2) falling on this line. The vertical difference between the data line and the 1:1 line is related to the slope of the existing trend in the dependent variable.

In addition, the ITA technique allows to investigate trends in the low, medium and high values of a time series, according to the position of the data points. It is necessary to look for low, medium, and high value groups (Figure 49b) when the scatters points are nonparallel with increasing or decreasing trends (non-monotonic trend). Accordingly, patterns of low, medium, and high values are identified through a method based on the percentiles. In detail, low values if $x < \bar{x} - \sigma_x$, medium if $\bar{x} - \sigma_x < x < \bar{x} + \sigma_x$, and high if $x > \bar{x} + \sigma_x$, where x denotes the first half-time series, $\bar{x}$ the mean, and σ_x the standard deviation.

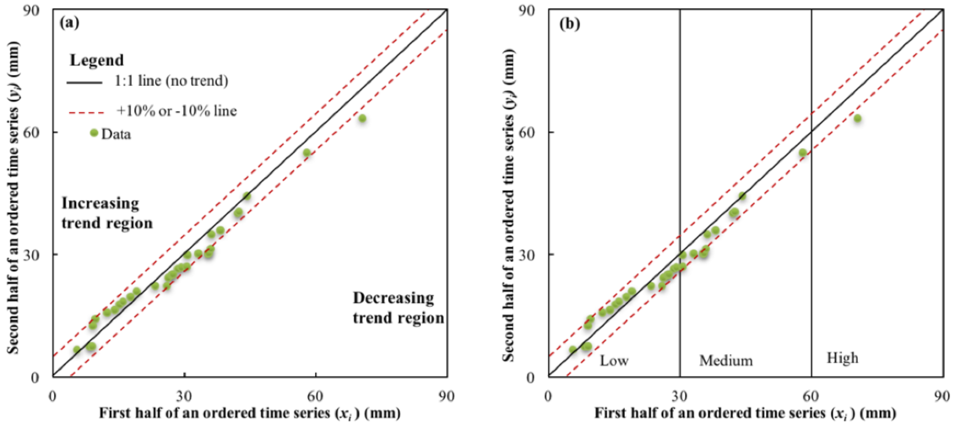

Figure 49 *- Example of the Innovative Trend Analysis (ITA) method for a) monotonic trend and b) trends of each cluster. Sources: Alifujiang et al (2020)*

The statistic of the ITA method is:

$$S_{ITA} = \frac{2(s_1 - s_2)}{sl_k} \quad [33]$$

where s_1 and s_2 are respectively the arithmetic averages of the two sub-series and sl_k is the total number of data points for the kth series. S_{ITA} is the trend slope; a positive value of S_{ITA} means that the time series has an increasing trend, while a negative value means that a decreasing trend is detected. According to the test significance proposed by Sen (2017), the slope of the series is statistically significant if it falls outside the confidence limits (CLs). The CLs of the slope, that follows a Gaussian probability density function with zero mean and standard deviation, are:

$$CL_{(1-\alpha)} = 0 \pm s_{cri}\sigma_s \quad [34]$$

where α is the significance level, s_{cri} is the confidence limit of a standard normal PDF with zero mean and standard deviation σ, and σ_s is defined as follows:

$$\sigma_s = \frac{2\sqrt{2}}{sl_k\sqrt{sl_k}}\sigma\sqrt{1 - \rho_{s_1,s_2}} \quad [35]$$

where ρ_{s_1,s_2} is the correlation coefficient between the two mean values s_1 and s_2 and σ is the standard deviation of the time series.

According to the procedure proposed by Caloiero et al. (2018), the reconstructed series were converted into rainfall anomalies. In detail, for each series, the sample mean was subtracted from the observed precipitation values and then, the difference was divided by the sample standard deviation. An average series of rainfall anomalies was calculated for each duration and region. Thereafter, the ITA method was applied by splitting the series into two sub-periods: 1970-1994 and 1995-2020, and the results are presented in Figure 50, which shows the change graphs of extreme rainfall anomalies obtained according to the ITA method. It is worth pointing out that the blue points are the data points of the two sub-series of rainfall anomalies, the solid orange line represents the no-trend (1:1) line, the solid blue line is the data line, while the red and green dashed lines are respectively 0.25 and 0.5 confidence bounds. In the following, results are discussed considering low, medium and high values which were identified as lower than -0.5, between -0.5 and 0.5 and higher than 0.5, respectively.

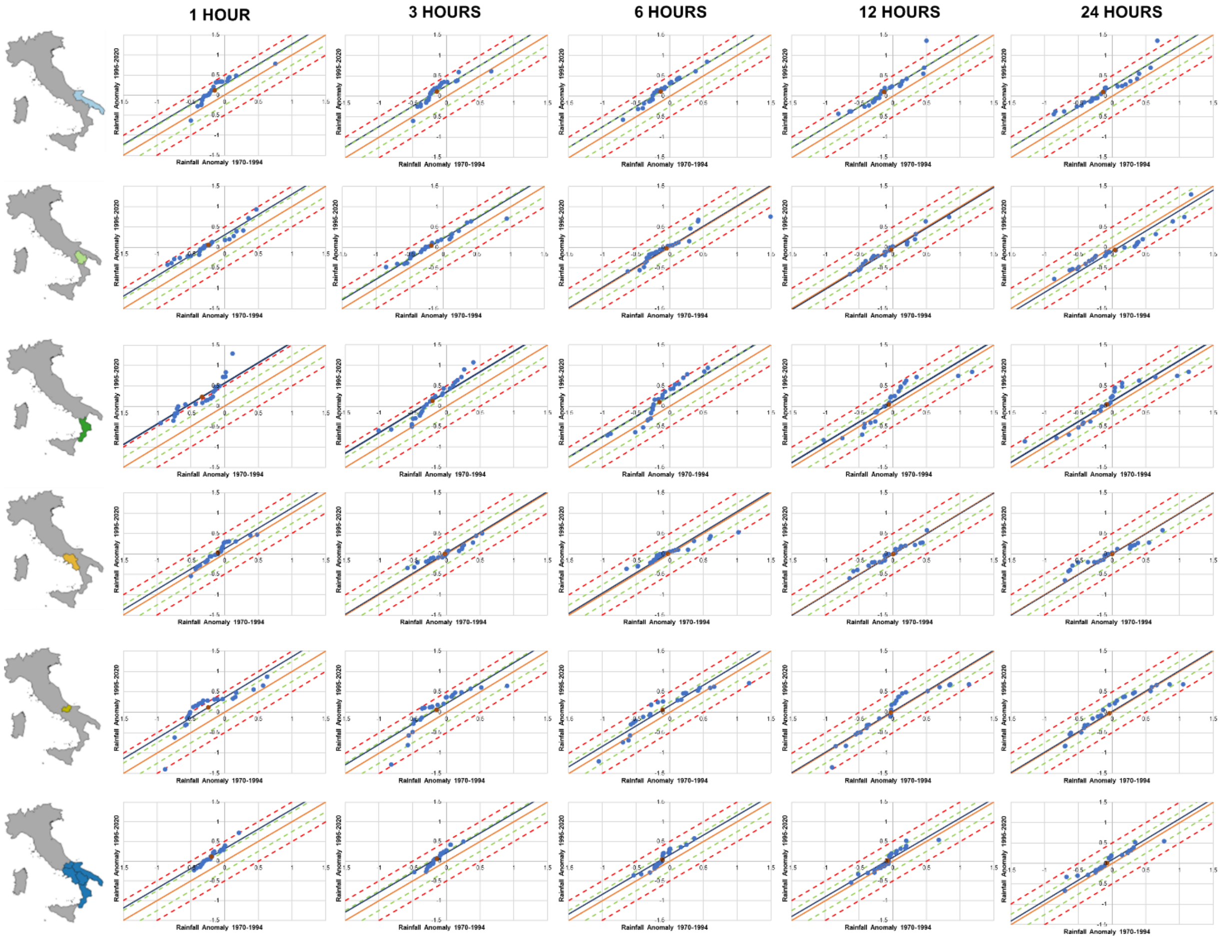

Figure 50 *- Results of the ITA method for the five regions of southern Italy and for the five durations. Blue points are the data points of the two sub-series of rainfall anomalies sorted in ascending order, the brown point is the centroid point, the solid orange line represents the no-trend (1:1) line, the solid blue line is the data line, the red and green dashed lines are respectively 0.25 and 0.5 confidence bounds.*

By analysing Figure 50, we can deduce that increasing trends are prevailing in all regions and for all the durations. However, in more detail we can point out that:

- in Apulia region, there is an upward trend of around 25% in low and high rainfall anomalies and 50% in medium values for shorter durations (1, 3 and 6 hours). Instead, for longer durations an increasing trend of 50% in low values and 25% in medium anomalies was detected. As regard high anomaly values, a positive tendency of 25% was identified at 12-h duration, while a meaningless trend (within the 0.25 bound) prevails at 24-h.
- in Basilicata region, a significant increasing trend of 25-50% in low and medium anomalies and of 25% in high values was detected for 1- and 3-h durations, while the 6-h anomaly values do not show any clear tendency. No trend in low values and a downward tendency of 25% in medium and high ones was observed at 12- and 24-h durations.
- in Calabria region, the clearest result is the positive trend shown by 1-h rainfall anomalies, with most of the data outside the 0.5 bound. Instead, a meaningless trend (within the 0.25 bound) in low values and a significant increasing trend of 25% and 50% in medium and high anomalies respectively was detected for the other durations.
- in Campania region, no clear evidence of general trends could be identified. However, for shorter durations there is a slight increasing trend in low and medium anomaly values, though within the 0.25 bound, and no trend in high values. Instead, for longer time intervals an increasing trend in low anomalies, no trend in medium values and decreasing trend in high ones was detected.
- in Molise region, the ITA method revealed a significant increasing trend in 1-h rainfall anomalies, with most of the medium values outside the 0.5 bound. Additionally, 3- and 6-h anomalies are characterized by positive tendency (within the 0.5 bound) in medium values and variable behaviour in low and high ones. Instead, for longer durations there is no trend in low and medium values, and a meaningless decreasing tendency in high anomalies.

In the last row of Figure 50 the results of the ITA method for the whole study area are reported. First of all, it is worth noting that there is no difference between low, medium and high rainfall anomaly values; this means that a monotonic trend can be detected. In detail, a significant 1-h upward trend was observed, though within the 0.5 bound. Such results are confirmed for all the intervals, even if the date line gets closer to the no-trend (1:1) line as the duration increases.

These findings are further summarised in the Table 12, where the ITA slope of the extreme rainfall anomalies is reported.

Table 12 *- Statistics of the ITA method. In particular, the ITA trend slope, SITA, the confidence limits, CLs, at 95% confidence interval and the detected trend are reported.*

Regions	d [h]	S_{ITA}	Lower CL	Upper CL	Trend
Apulia	1	0.0107	-0.001526	0.001526	Increasing
	3	0.0103	-0.001566	0.001566	Increasing
	6	0.0101	-0.000647	0.000647	Increasing
	12	0.0094	-0.001550	0.001550	Increasing
	24	0.0096	-0.001558	0.001558	Increasing
Basilicata	1	0.0120	-0.001064	0.001064	Increasing
	3	0.0088	-0.001009	0.001009	Increasing
	6	0.0009	-0.001885	0.001885	No Trend
	12	-0.0012	-0.000964	0.000964	Decreasing
	24	-0.0040	-0.001358	0.001358	Decreasing
Calabria	1	0.0227	-0.002083	0.002083	Increasing
	3	0.0138	-0.001162	0.001162	Increasing
	6	0.0100	-0.001558	0.001558	Increasing
	12	0.0044	-0.002285	0.002285	Increasing
	24	0.0050	-0.002025	0.002025	Increasing
Campania	1	0.0053	-0.000855	0.000855	Increasing
	3	0.0010	-0.000676	0.000676	Increasing
	6	0.0015	-0.000734	0.000734	Increasing
	12	-0.0004	-0.001439	0.001439	No Trend
	24	-0.0003	-0.001272	0.001272	No Trend
Molise	1	0.0144	-0.002926	0.002926	Increasing
	3	0.0083	-0.002496	0.002496	Increasing
	6	0.0066	-0.002325	0.002325	Increasing
	12	0.0008	-0.002208	0.002208	No Trend
	24	0.0006	-0.002624	0.002624	No Trend
Southern Italy	1	0.0126	-0.000443	0.000443	Increasing
	3	0.0083	-0.000613	0.000613	Increasing
	6	0.0064	-0.000825	0.000825	Increasing
	12	0.0039	-0.001121	0.001121	Increasing
	24	0.0036	-0.001066	0.001066	Increasing

According to ITA trend slope analysis, increasing trends were observed in Apulia and Calabria regions. Instead, in Campania and Molise there is an upward tendency for shorter durations (1, 3 and 6 hours), while no statistically significant trend for longer one. Finally, in Basilicata an increasing trend at 1- and 3-h, no trend at 6-h and decreasing trend at 12- and 24-h was detected.

These outcomes are fairly in line with the ones obtained by means of RK trend test (Table 10 and 11). In fact, regarding to the southern Italy both methods detected an increasing trend for all durations. Instead, at regional scale, ITA and RK techniques revealed a statistically significant upward tendency in Apulia and Calabria for all the durations and in Basilicata, Campania and Molise at 1 and 3 hours. For longer durations, however, some contrasting findings were observed. In particular, RK test pointed out an increasing trend at 12- and 24-h in Molise in contrast to the ITA method which showed no statistically significant tendency. Similar differences appeared in Basilicata, where RK test identified an increasing trend at 6-h, while ITA test identified no trend; in addition, 12- and 24-h rainfall series presented no trend according to the RK test and decreasing trend according to the ITA method.

Notwithstanding these slight differences (mainly at longer time intervals), both methods proved a significant increase of short-duration extreme rainfall events.

4.6 RECORD-BREAKING (RB) ANALYSIS

The MK and ITA tests are used to investigate the presence of trends in the magnitude of rainfall annual maxima series. Instead, the record-breaking (RB) analysis allows for the detection of trends in terms of occurrence frequency of extreme rainfall events.

The RB events are defined as follows: a value of annual maximum rainfall depth is considered RB if it exceeds all the previous values in its time series. The RB analysis is applied to each series separately. However, to overcome the issue of the spatial and temporal sparseness of RB events and detect changes at a regional scale, the number of RB events was aggregated over the defined region. In detail, considering a $n_r \times Y$ (where n_r is the number of rain gauges and Y the number of years) matrix, M_h, containing recorded annual maxima, two matrices M_{RB} and M_{RBexp}, each of the same size as M_h, were drawn. For each station, if a value of M_h is an RB event the corresponding value of M_{RB} is set to 1, otherwise, it is set to 0. Since the first value of each time series is always a record-breaking event, we started counting record-breaking events at the second time step. M_{RBexp}, on the other hand, was generated by assigning the expected RB probability value under independent and identically distributed (iid) conditions to each non-null element in M_h. Thereby, missing values in M_{RB} are also accounted for in the calculation of M_{RBexp}. With this approach, we assumed that time-series in a stationary climate can be described by independent and identically distributed (iid) values. For iid time series the number of expected record-breaking events at time Y is equal to: $\sum_{y=1}^{Y} \frac{1}{y}$

We subsequently summed up all the values of M_{RB} along the columns producing a vector, RB_{obs}, of length Y giving the total number of record-breaking events per year; additionally, we performed the same summation on M_{RBexp}, resulting in a vector, RB_{exp}, of length Y giving the analytically number of expected record-breaking events assuming a stationary climate. Then, RB_{obs} was normalized with the vector RB_{exp} using the following equation to obtain the vector, RB_{anom}, of record-breaking anomalies.

$$RB_{anom} = \frac{RB_{obs} - RB_{exp}}{RB_{exp}} * 100\ (\%) \qquad [36]$$

where RB_{obs} is the sum of all observed record-breaking events in time series within a given region and, analogously, RB_{exp} is the analytically expected number of record-breaking events summed over the same region.

To test whether the observed number of record-breaking events is significantly different from those in a stationary climate, we applied a field significance bootstrap-based procedure, as suggested by Lehmann et al. (2015), which is based on simulated record-breaking events derived from iid time series. The n_r columns of the M_h matrix were randomly shuffled (bootstrapping along the time axis); this operation preserves the spatial correlation across the stations, while the order in time is lost. The procedure described for the recorded data was therefore applied to the shuffled matrix. The full procedure was repeated 15,000 times in order to create simulated record-breaking anomaly time series under the hypothesis of the iid condition. From these series, the 95% confidence intervals were determined. The observed record-breaking anomalies are deemed to be statistically significant if they fall outside the 95% confidence interval of the distribution of record-breaking anomalies, calculated as previously described. By applying record-breaking analysis, we were interested in observing if record-breaking rainfall events have increased or not, regardless of the changes in the probability distribution. In this way, the number of observed record-breaking events was compared with the number expected in a climate without long-term trends, by assessing the record-breaking anomalies. Figure 51 maps the anomalies in the frequency of record-breaking events at the country and regional scales for each duration.

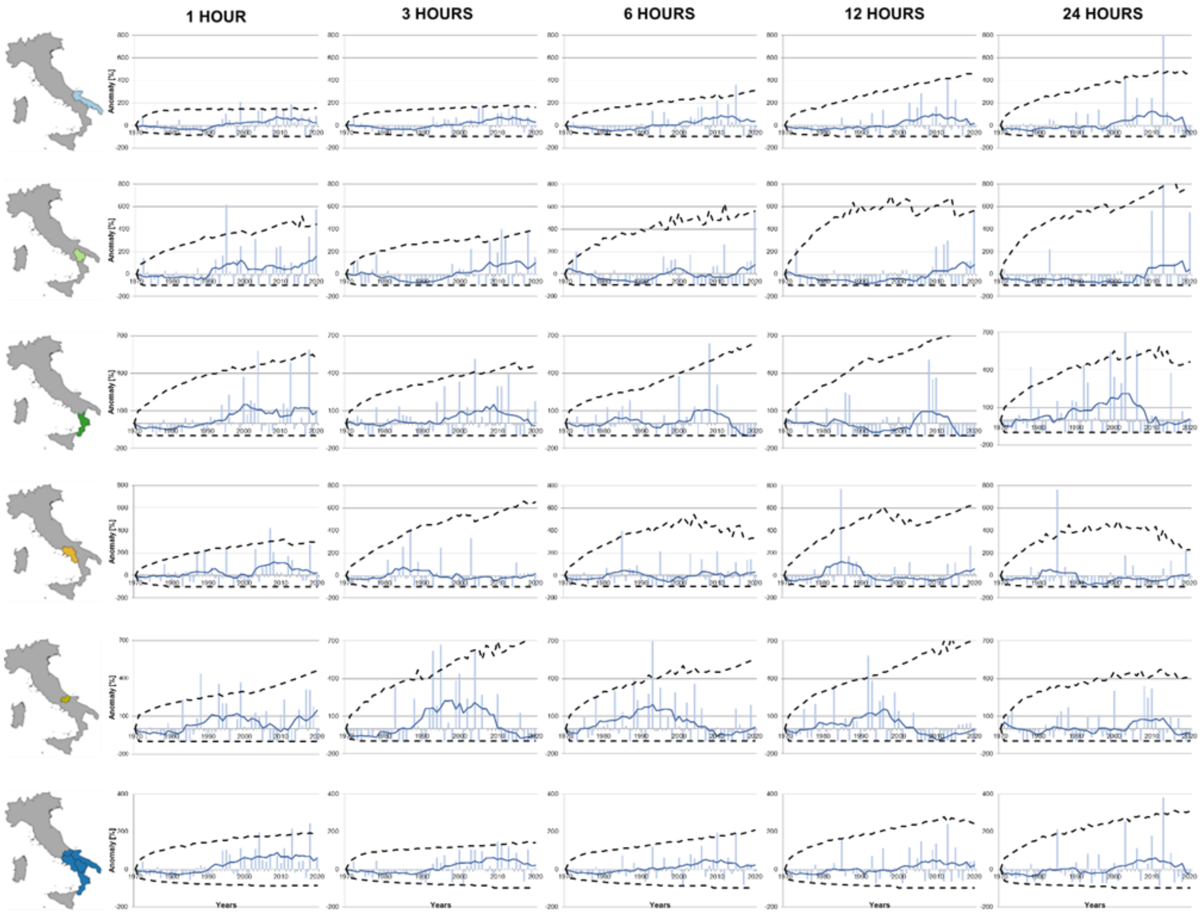

Figure 51 *- Regional annual record-breaking anomaly (light blue bars) for the five considered duration (1, 3, 6, 12 and 24 hours). The long-term non-linear trend in record-breaking anomaly (blue solid line) is calculated using moving average filter with window length of 10 years, while the black dashed lines represent the 5% significance level bounds.*

The long-term record-breaking anomalies are characterized by no statistically significant trend, with periods of negative anomalies (decreasing events) alternating with periods of positive ones (increasing events). In more detail, a comparison of regions is not feasible, as the anomalies have highly fluctuating patterns. Furthermore, even for the same region, there is no pattern of record-breaking anomalies over the different durations.

However, at 1-h duration an increasing trend was observed since 1990 in Apulia, Basilicata and Calabria regions, after 2000 in the Campania region with a peak in 2005. Instead, in Molise region, increasing anomalies became apparent in the period 1980-1995 and after 2010, and they kept growing until the end of the observed period. For longer durations, instead, the signal is less stable and harder to interpret, even if a general stationarity does seem to be prevalent.

Summarising the results at the country scale (southern Italy), the frequency of RB anomalies does not show evidence of a significant non-stationarity, although a slight increasing trend was detected for all the durations in the period 1990-2010 followed by a decreasing trend until the end of the observed period. However, the slope of the trend and the observed peak (in the year 2010) tend to smooth out with increasing duration as shown in the last row of the Figure 51.

Such an analysis was conducted at the global scale by Lehmann et al. (2015) and at the Italian scale by Libertino et al. (2019).

The findings previously discussed agree with those of Lehmann et al., who analysed record-breaking events in maximum 1-day precipitation time-series from HadEX2 database (Donat et al. 2013b), in the period 1901-2010. The results of that study are reported in Figure 52.

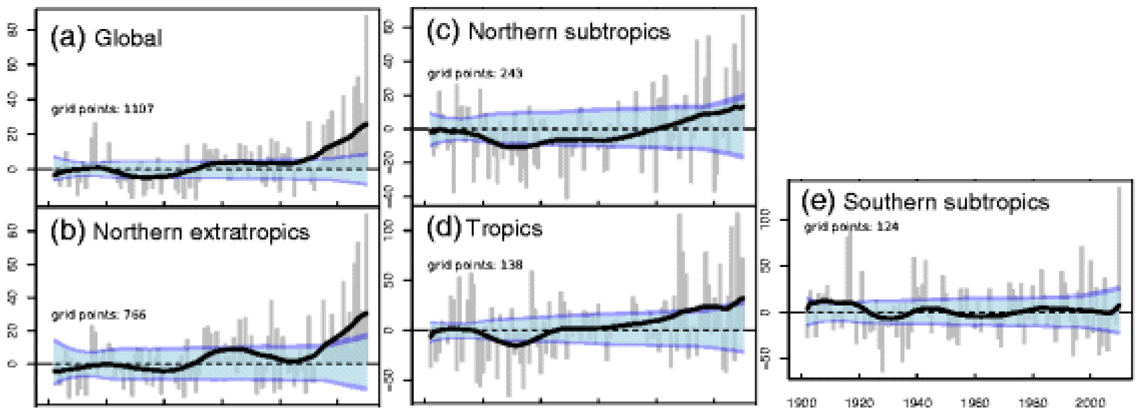

Figure 52 *- Annual record-breaking anomaly (grey bars) for a) global scale and for b) northern extratropic, c) northern subtropics, d) tropics, and e) southern subtropics. The long-term non-linear trend in record-breaking anomaly (black line) is calculated using singular spectrum analysis with window length of 15 years. The shaded areas reflect the 90% (light blue shading) and 95% (dark blue shading) confidence interval. Sources: Lehmann et al. (2015)*

The authors detected a strong and consistent increase in the annual record-breaking anomaly, on a global scale, since the 1980s. The record-breaking anomaly peaks in 2010, which saw +88 % more record-breaking events (grey bars) than expected by the iid case. The long-term non-linear trend of the global record-breaking anomaly significantly increases from 1980 onward reaching +26 % in 2010. The northern subtropics (where southern Italy is located; Figure 52c) presents a not statistically significant upward trend, however the data of the Italian monitoring network are not included in the analysed database.

Therefore, although the considered rainfall duration is different (maximum 1-day precipitation in Lehmann et al., hourly durations in this thesis) both works highlight a positive trend in the annual record-breaking anomaly from 1980-1990 until 2010. In our study, however, a downward trend seems to have prevailed after 2010 until the end of the observed period.

It is worth comparing the results of this thesis with those reported in Libertino et al., who analysed record-breaking anomalies in short-duration (1-, 3-, 6-, 12-, and 24-hr) annual maximum rainfall series from I-RED database (Libertino et al., 2018b) in the period 1928-2014 at the Italian scale. They highlighted the evidence of fluctuating behaviour until the 1980s. Instead, after the 1980s increasing anomalies become apparent for the extremes of shorter durations, overcoming the magnitudes of all the previously recorded positive anomalies, and keep growing until the end of the observed period (2010).

Therefore, the findings presented in this thesis (at the Southern Italy scale) are in excellent agreement with those presented by Libertino et al. (at the Italian scale). Both studies found no evidence of significant non-stationarity in the occurrence frequency of RB events, despite the fact that an increasing trend was observed at shorter time scales from the 1980s to 2010. However, as previously reported in our study, a downward tendency appears to have emerged after 2010, though this has yet to be confirmed, and further research is required to better investigate.

4.7 PETTITT TEST FOR CHANGE-POINT

A change point can be defined as a point in time when any parameter of the data distribution, such as mean, median, variance, and/or autocorrelation, undergoes an abrupt change.

The widely known parametric tests for testing and identifying change-points in hydrological series are Student's t-test, Lepage's test and methods based on Bayesian analysis. Non-parametric tests, on the other hand, are based on the Wilcoxon-Mann-Whitney rank sum test and the most used are Mann-Whitney test (Mann and Whitney, 1947), the CUSUM test (Buishand, 1982), the Kruskal-Wallis test (Kruskal and Wallis, 1952) and the Pettitt test (1979). Pettitt's test is a non-parametric test widely used to detect abrupt changes in the mean of the distribution of the studied variable and, in particular, to identify a single change-point in hydrological series. It tests the following hypothesis H_0: the variables follow one or more distributions having the same location parameter (no change), versus the alternative H_1: there is a single change-point in the series. The non-parametric statistic for a specific year y (with $1 \leq y < Y$, being Y the number of years in the considered time-series) is defined as follows:

$$U_{y,Y} = \sum_{i=1}^{y} \sum_{j=y+1}^{Y} sign(h_i - h_j) \quad [37]$$

where h represents the data values at times i and j, and Y the number of years in the analysed period (which in our case is the length of the time-series).

The most probable change point y will be the one that satisfies the following equation:

$$K_y = \max_{1 \leq y < Y} \left| U_{y,Y} \right| \quad [38]$$

Based on asymptotic arguments about the test statistic, Pettitt (1979) defines the following approximate p-value of the test:

$$p \approx 2e^{\left(\frac{-6K_y^2}{Y^3+Y^2}\right)} \quad [39]$$

Thus, given a significance level α, if $p < \alpha$, the null hypothesis, H_0 (the two distributions are equal), is rejected.

In order to detect non-homogeneity and to identify the possible year of change in the short-duration rainfall series, the Pettitt test was applied independently to all reconstructed series. The results of the Pettitt test in terms of number of stations with a specific year as change-point are reported in Figure 53 for all the considered regions and Figure 54 for the southern Italy scale.

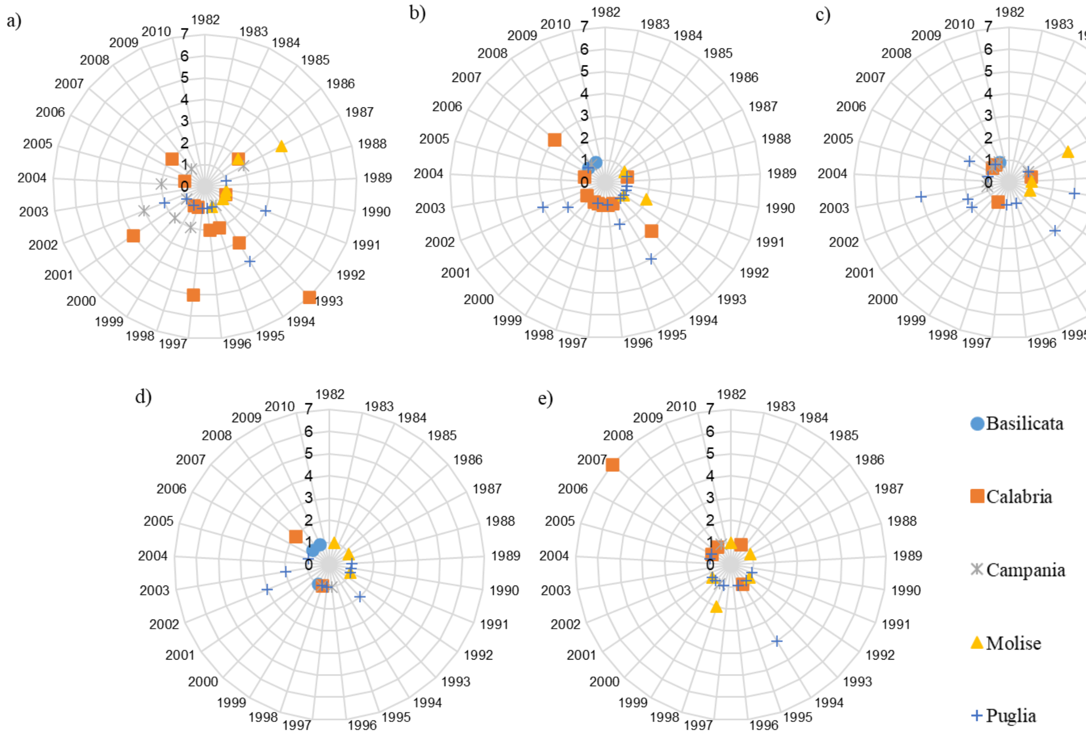

Figure 53 *- Graph assigning to each year the number of stations (for each considered region) having that year as change-point. Each map refers to a specific duration: a) 1h, b) 3h, c) 6h, d) 12h, e) 24h.*

By analysing Figure 53, we observed that the highest number of change points were identified at the shortest durations in all regions. It is worth highlighting that in Calabria the most likely change-point years are 1993 at 1- and 3-hours, and 2007 at 12-h and 24-hours. Additionally, the years 1987-1988 in Molise, while 1993-1994 and 2002-2003 in Puglia were identified as change-point years for all the durations. No conclusions can be drawn for Campania and Basilicata as there are few stations exhibiting a significant trend among those selected in the study.

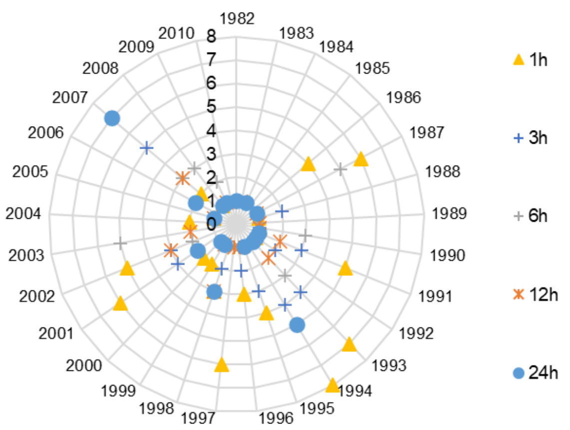

Figure 54 *- Graph assigning to each year the number of stations (within the study area) having that year as change-point.*

Figure 54 shows that the most probable change-point years for the analysed extreme hourly rainfall series at the southern Italy scale are: 1993-1994 and 2001-2002 at 1-h, 1993-1994 and 2007 at 3-h, 1994 and 2007 at 24-h duration. Less clear, however, is the signal at 3-h and 6-hours duration.

However, it is to be considered that these results may be affected not only by the different number of stations examined in each region and duration but also by the fact that the investigated series contain gaps, albeit limited in number.

General conclusions

The present research investigates local dynamics of extreme annual rainfall over a poorly monitored region.

In details, the aim of the work is to provide the characterization of extreme rainfall phenomena in southern Italy highlighting the observed changes at the local and regional scales in the period 1970-2020. The impact of climate change on rainfall process is difficult to quantify given its strong spatial and temporal heterogeneity, therefore, they cannot be investigated on individual hydrological time-series but must be assessed on a regional and/or district scale. To this purpose, a statistical analysis of short-duration extreme rainfall time-series was carried out to detect potential trends at different spatio-temporal levels. For this reason, a database of sub-daily rainfall annual maxima was constructed exploiting all available records and extended by applying reconstruction procedures.

The thesis describes the efforts made to advance the definition of a general framework for working in data-scarce environments in order to improve rainfall statistical analysis at different spatial scales in gauged and ungauged locations.

Chapter 1 reviews the observation-based studies focusing on the detection of trends in extreme rainfall intensities both at global and national scales. Several studies have demonstrated a strong link between the intensity of extreme rainfall and the atmospheric temperature. Therefore, given that there has been approximately 1°C of atmospheric warming during the 20th and early 21st centuries, in this chapter we try to investigate the evidence that rainfall extremes have intensified in this period by reviewing the scientific literature. The first relevant aspect is that the majority of the observation-based studies are based on data recorded at annual, seasonal, or, at most, daily time resolution and demonstrate that extreme precipitation events have increased in intensity and/or frequency at global scales. We can state that globally the number of regions that have experienced an increase in extreme daily rainfall events is greater than the number of regions that have experienced a decrease during the 20th, although these trends are often statistically non-significant and spatially inconsistent. In particular, several studies agree in showing changes toward more intense precipitation over the south-central America as well as over large parts of northern and eastern Europe, Asia, and same regions of South America.

Instead, regions with trends showing less frequent and intense precipitation are located in the Mediterranean area, in Southeast Asia, and the north-western part of North America.
Additionally, in a large part of the globe there have been changes of the same sign (increasing or decreasing) in both the total and the maximum 1-day precipitation events, while some areas (south-western Australia, northern Japan and south-eastern Africa) registered only an increase in the frequency of 1-day heavy precipitation events. Such behaviour has also been observed in the Mediterranean region (primarily in Italy and Spain).

Few studies are available on sub-daily rainfall extremes and are often focused on the analysis of local sites or small regions. The relative scarcity in literature of large-scale studies investigating trends in hourly rainfall extremes is largely due to the lack of long-term, high-quality observations at sub-daily time scales and, therefore, the absence of an international repositories for data. In fact, records are often subjected to restricted access by the national authorities and, when available, they are often unevenly distributed and with missing data.

At the national scale, the majority of the studies agree about a decrease of the total annual precipitation throughout the Italian territory, except for the Northern Italy. Additionally, winter monthly negative precipitation trends were registered for several regions, while different tendencies were observed at other seasons. As at the global scale, there are limited number of studies analysing short-duration rainfall events also in Italy due to the lack of a consolidate national dataset.

Chapter 2 provides an overview of the widely used gap-filling procedures existing in the literature that allow for the reconstruction of missing data in hydrological series. Several studies have demonstrated that geospatial techniques (i.e., ordinary kriging) outperform simple and deterministic methods (i.e., distance-based weighting approaches). Furthermore, over time, different variants of geospatial methods (i.e., multivariate techniques) have been developed to identify the best predictor with the lowest reconstruction error.

Chapter 3 is divided in two main parts: i) description of the assembled database of rainfall annual maxima for short duration over the southern Italy; ii) description a robust statistical framework for dealing with uneven and fragmented rainfall records on a non-uniform spatial domain, in order to reconstruct missing data in gauged sites or estimate rainfall extremes in ungauged sites.

The assembled Hourly Rainfall Database for southern Italy consists of around 910 stations, including SIMN stations that have been removed, SIMN rain gauges currently managed by the Civil Protection, the new rainfall stations officially managed by the Civil Protection and a few stations of secondary networks operated by agro-meteorological offices that are still not integrated in the official regional network. The gathered rainfall time-series turned out to be extremely uneven and fragmented due to the frequent changes (location, equipment and managing agency) experienced in the gauging network. For this reason, a new procedure to reconstruct missing rainfall data has been developed.

The proposed "Spatially-Constrained Ordinary Kriging" technique exploits all available information from recorded series, regardless of length, and provides annual extreme rainfall estimates at ungauged sites or points with missing data. The methodology combines the ordinary kriging approach with the same spatial constraints as the IDW method. Additionally, the optimal parameters of the IDW method were identified by means of a genetic algorithm with a jack-knife technique minimizing the error related to the reconstruction.
Thus, the procedure allows for the reconstruction of missing data by means of the ordinary Kriging equations, but only in the locations identified by the spatial parameters of the IDW technique (i.e., those with enough neighbouring operating stations). In this way, the main limitation of the OK approach was overcome, i.e., the absence of spatial limitations. Notably, the method does indeed allow the reconstruction of the totality of the missing data, but the estimated annual maxima may be inaccurate, especially in locations with limited information at the most positively correlated stations, which are the closest ones. Therefore, in order to remove the effect of long-range extrapolation, we enforced spatial constraints on the OK method that are the same as in the IDW model.

The procedure allowed to reconstruct most of the missing data in the Hourly Rainfall Database for southern Italy with an average reconstruction error of 20%. However, in the validation step, it was demonstrated that this error does not significantly influence the trend detection purposes.

The reconstructed rainfall time-series were analysed by means of non-parametric trend tests, as reported in Chapter 4. The analysis was performed investigating both the magnitude of the rainfall intensities and the frequency of occurrence of very extreme events in order to check the potential non-stationarity in the extreme precipitation series.

The presence of trends in hourly rainfall intensities was explored through the Mann-Kendall test at local and regional scale. The results of the at-site trend analysis show that most of the observed trends are not statistically significant for all durations; however, when a trend is detected, it is typically positive for short durations and either positive or negative for longer durations. Often, upward trends, detected at shorter durations in specific locations, tends to disappear or becomes less significant for rainfall events of longer durations. In general, most of the considered regions displays no trend for longer durations, while some clusters of increasing trends emerge at shorter durations, but the sparseness of rain gauges does not allow to provide a full coverage of the investigated area.

Instead, the regional test detected a statistically significant increasing trend in the rainfall intensities for all the durations. However, the trends turned out to be non-homogeneous due to the different trend directions exhibited by individual stations. These findings are corroborated by the outcomes of the ITA trend method, emphasising the importance of investigating hydrological trends at different spatial (from local to regional up to southern Italy) and temporal scales.

With regard to the frequency of occurrence of extreme precipitation events, record-breaking analysis was carried out at the regional scale. For all the investigated durations, the record-breaking anomalies series do not present statistically significant trends, thus suggesting no evidence of non-stationarity in extreme events occurrences. In fact, the record-breaking anomalies have highly fluctuating patterns and therefore no clear pattern can be drawn. These results suggest that further analysis need to be performed in order to better investigate whether or not there is really a stationarity in the frequency of occurrence of extreme events.

On the basis of the findings presented in this thesis, in our future research we intend to focus on the frequency analysis of rainfall extremes in southern Italy, assessing the performance of different statistical approaches. Therefore, the next stage will be the fitting of a probability distribution to the rainfall data, comparing the results obtained from the use of different models, such as Gumbel distribution, Generalized Extreme value (GEV) distribution, Two-Component Extreme Value (TCEV) distribution and Generalized Pareto (GP) distribution.

Simultaneously with the statistical analyses, the idea is to design and implement, on a web-GIS platform, an integrated, freely accessible, and geo-referenced database of the reconstructed precipitation series for southern Italy. The GIS-based dataset will provide an interactive application tool for presenting rainfall data and details about the monitoring networks in the study area, such as identification number, location, elevation, and managing agency of the rain gauges. Additionally, the aim is to implement a user-friendly reporting service for selecting, displaying, and downloading rainfall values for a selected area, which will allow scientists, professionals, private users, and public bodies to consult the results obtained in this thesis and to acquire the data for the design of hydraulic systems and infrastructures as well as for scientific research.

References

Adler, A. (2015). Strong laws for ratios of order statistics from exponentials. Bulletin of the Institute of Mathematics, Academia Sinica, Vol. 10, No. 1, pp. 101-111.

Alavi, N., Warland, J.S., and Berg, A.A. (2006). Filling gaps in evapotranspiration measurements for water budget studies: Evaluation of a Kalman filtering approach. Agricultural and Forest Meteorology, 141(1), pp. 57-66. https://doi.org/10.1016/j.agrformet.2006.09.011

Alexander, L.V., Zhang, X., Peterson, T.C., Caesar, J., Gleason, B., Klein Tank, A.M.G., Haylock, M., Collins, D., Trewin, B., Rahimzadeh, F., Tagipour, A., Rupa Kumar, K., Revadekar, J., Griffiths, G., Vincent, L., Stephenson, D.B., Burn, J., Aguilar, E., Brunet, M., Taylor, M., New, M., Zhai, P., Rusticucci, M., and Vazquez-Aguirre, J.L. (2006). Global observed changes in daily climate extremes of temperature and precipitation. Journal of Geophysical Research, 111, D05109. https://doi.org/10.1029/2005JD006290

Alexander, L.V. (2016). Global observed long-term changes in temperature and precipitation extremes: a review of progress and limitations in IPCC assessments and beyond. Weather and Climate Extremes, 11, pp. 4-16. https://doi.org/10.1016/j.wace.2015.10.007

Alifujiang, Y., Abuduwaili, J., Maihemuti, B., Emin, B., and Groll, M. (2020). Innovative Trend Analysis of Precipitation in the Lake Issyk-Kul Basin, Kyrgyzstan. Atmosphere, 11, 332. https://doi.org/10.3390/atmos11040332

Allen, M., and Ingram, W. (2002). Constraints on future changes in climate and the hydrologic cycle. Nature, 419, pp. 224-232. https://doi.org/10.1038/nature01092

Alpert, P., Ben-Gai, T., Baharad, A., Benjamini, Y., Yekutieli, D., Colacino, M., Diodato, L., Ramis, C., Homar, V., Romero, R., Michaelides, S., and Manes A. (2002). The paradoxical increase of Mediterranean extreme daily rainfall in spite of decrease in total values. Geophysical Research Letters, 29(11). https://doi.org/10.1029/2001GL013554

Arnone, E., Pumo, D., Viola, F., Noto, L.V., and La Loggia, G. (2013). Rainfall statistics changes in Sicily. Hydrology and Earth System Sciences, 17(7), pp. 2449-2458. https://doi.org/10.5194/hess-17-2449-2013

Asadieh, B., and Krakauer, N. Y. (2015). Global trends in extreme precipitation: Climate models versus observations. Hydrology and Earth System Sciences, 19, pp. 877-891. https://doi.org/10.5194/hess-19-877-2015

ASCE (1996). Hydrology Handbook, 2nd ed. American Society of Civil Engineers ASCE, New York.

Ashraf, M., Loftis, J.C., Hubbard, K.G. (1997). Application of geostatistics to evaluate partial weather station networks. Agricultural and Forest Meteorology, 84, pp. 255-271. https://doi.org/10.1016/S0168-1923(96)02358-1

Avino, A., Manfreda, S., Cimorelli, L., and Pianese, D. (2021). Trend of annual maximum rainfall in Campania region (southern Italy). Hydrological Processes, 35(12), e14447. https://doi.org/10.1002/hyp.14447

Barbero, R., Fowler, H., Lenderink, G., and Blenkinsop, S. (2017). Is the intensification of precipitation extremes with global warming better detected at hourly than daily resolutions? Geophysical Research Letters, 44, pp. 974-983. https://doi.org/10.1002/2016GL071917

Bonaccorso, B., Cancelliere, A., and Rossi, G. (2005). Detecting trends of extreme rainfall series in Sicily. Advances in Geosciences, 2, pp. 7-11. https://doi.org/10.5194/adgeo-2-7-2005

Brimicombie, A. (2003). GIS, Environmental Modeling and Engineering. Taylor and Francis, London.

Brunetti, M., Maugeri, M., and Nanni, T. (2000). Variations of temperature and precipitation in Italy from 1866 to 1995. Theoretical and Applied Climatology, 65, pp. 165-174. https://doi.org/10.1007/s007040070041

Brunetti, M., Colacino, M., Maugeri, M., and Nanni, T. (2001). Trends in the daily intensity of precipitation in Italy from 1951 to 1996. International Journal of Climatology, 21, pp. 299-316. https://doi.org/10.1002/joc.613

Brunetti, M., Buffoni, L., Mangianti, F., Maugeri, M., and Nanni, T. (2004). Temperature, precipitation and extreme events during the last century in Italy. Global and Planetary Change, 40, pp. 141-149. https://doi.org/10.1016/S0921-8181(03)00104-8

Brunetti, M., Maugeri, M., Monti, F., and Nanni, T. (2006). Temperature and precipitation variability in Italy in the last two centuries from homogenised instrumental time series. International Journal of Climatology, 26, pp. 345-381. https://doi.org/10.1002/joc.1251

Brunetti, M., Caloiero, T., Coscarelli, R., Gullà, G., Nanni, T. and Simolo, C. (2012). Precipitation variability and change in the Calabria region (Italy) from a high resolution daily dataset. International Journal of Climatology, 32, pp. 57-73. https://doi.org/10.1002/joc.2233

Buffoni, L., Maugeri, M., and Nanni, T. (1999). Precipitation in Italy from 1833 to 1996. Theoretical and Applied Climatology, 63, pp. 33-40. https://doi.org/10.1007/s007040050089

Buishand, T.A. (1982). Some methods for testing the homogeneity of rainfall records. Journal of Hydrology, 58(1-2), pp. 11-27. https://doi.org/10.1016/0022-1694(82)90066-X

Caloiero, T., Coscarelli, R., Ferrari, E., and Mancini, M. (2011a). Precipitation change in Southern Italy linked to global scale oscillation indexes. Natural Hazards and Earth System Sciences, 11, pp. 1683-1694. https://doi.org/10.5194/nhess-11-1683-2011

Caloiero, T., Coscarelli, R., Ferrari, E., and Mancini, M. (2011b). Trend detection of annual and seasonal rainfall in Calabria (Southern Italy). International Journal of Climatology, 31, pp. 44-56. https://doi.org/10.1002/joc.2055

Caloiero, T., Coscarelli, R., and Ferrari, E. (2018). Application of the Innovative Trend Analysis Method for the Trend Analysis of Rainfall Anomalies in Southern Italy. Water Resources Management, 32, pp. 4971-4983. https://doi.org/10.1007/s11269-018-2117-z

Caloiero, T., Coscarelli, R., Gaudio, R., and Leonardo, G.P. (2019). Precipitation trend and concentration in the Sardinia region. Theoretical and Applied Climatology, 137, pp. 297-307. https://doi.org/10.1007/s00704-018-2595-1

Caloiero, T., Filice, E., Coscarelli, R., and Pellicone, G. (2020). A Homogeneous Dataset for Rainfall Trend Analysis in the Calabria Region (Southern Italy). Water, 12, 2541. https://doi.org/10.3390/w12092541

Cannarozzo, M., Noto, L. V., and Viola, F. (2006). Spatial distribution of rainfall trends in Sicily (1921-2000). Physics and Chemistry of the Earth, 31(18), pp. 1201-1211. https://doi.org/10.1016/j.pce.2006.03.022

Caporali, E., Lompi, M., Pacetti, T., Chiarello, V., and Fatichi, S. (2020). A review of studies on observed precipitation trends in Italy. International Journal of Climatology, 41, pp. 1-25. https://doi.org/10.1002/joc.6741

Chang, K.-T. (2004). Introduction to Geographic Information Systems. McGraw-Hill Higher Education, Boston.

Chiaravalloti, F., Caloiero, T., and Coscarelli, R. (2022). The Long-Term ERA5 Data Series for Trend Analysis of Rainfall in Italy. Hydrology, 9, 18. https://doi.org/10.3390/hydrology9020018

Chua, S.-H., and Bras, R.L. (1982). Optimal estimators of mean areal precipitation in regions of orographic influence. Journal of Hydrology, 57 (1-2), pp. 23-48. https://doi.org/10.1016/0022-1694(82)90101-9

Coscarelli, R., and Caloiero, T. (2012). Analysis of daily and monthly rainfall concentration in Southern Italy (Calabria region). Journal of Hydrology, 416-417, pp. 145-156. https://doi.org/10.1016/j.jhydrol.2011.11.047

Crisci, A., Gozzini, B., Meneguzzo, F., Pagliara, S. and Maracchi, G. (2002) Extreme rainfalls in the changing climate: regional analysis and hydrological implications in Tuscany. Hydrological Processes, 16, pp. 1261-1274. https://doi.org/10.1002/hyp.1061

Cuomo, A., Guida, D., and Palmieri, V. (2011). Digital orographic map of peninsular and insular Italy. Journal of Maps, pp. 447-463. https://doi.org/10.4113/jom.2011.1209

Daly, C., Neilson, R.P., Phillips, D.L. (1994). A statistical topographic model for mapping climatological precipitation over mountainous terrain. Journal of Applied Meteorology, 33, pp. 140-158. https://doi.org/10.1175/1520-0450(1994)033<0140:ASTMFM>2.0.CO;2

De Toffol, S., Laghari, A. N., and Rauch, W. (2009). Are extreme rainfall intensities more frequent? Analysis of trends in rainfall patterns relevant to urban drainage systems. Water Science and Technology, 59, pp. 1769-1776. https://doi.org/10.2166/wst.2009.182

Dingman, S.L., Seely-Reynolds, D.M., and Reynolds, R.C. (1988). Application of kriging to estimating mean annual precipitation in a region of orographic influence. Journal of the American Water Resources Association, 24 (2), pp. 329-339. https://doi.org/10.1111/j.1752-1688.1988.tb02991.x

Diodato, N. (2007). Climatic fluctuations in southern Italy since the 17th century: reconstruction with precipitation records at Benevento. Climatic Change, 80, pp. 411-431. https://doi.org/10.1007/s10584-006-9119-1

Donat, M. G., Alexander, L. V., Yang, H., Durre, I., Vose, R., and Caesar J. (2013a). Global land-based datasets for monitoring climatic extremes. Bulletin of the American Meteorological Society, 96, pp. 997-1006. https://doi.org/10.1175/BAMS-D-12-00109.1

Donat, M. G., Alexander, L. V., Yang, H., Durre, I., Vose, R., Dunn, R.J.H., Willett, K.M., Aguilar, E., Brunet, M., Caesar, J., Hewitson, B., Jack, C., Klein Tank, A.M.G., Kruger, A.C., Marengo, J., Peterson, T.C., Renom, M., Oria Rojas, C., Rusticucci, M., Salinger, J., Elrayah, A.S., Sekele, S.S., Srivastava, A.K., Trewin, B., Villarroel, C., Vincent, L.A., Zhai, P., Zhang, X., and Kitching, S. (2013b). Updated analysis of temperature and precipitation extreme indices since the beginning of the twentieth century: The HadEX2 dataset. Journal of Geophysical Research: Atmospheres, 118, pp. 2098-2118. https://doi.org/10.1002/jgrd.50150

Donat, M.G., Lowry, A.L., Alexander, L.V., O'Gorman, P.A., and Maher, N. (2016). More extreme precipitation in the world's dry and wet regions. Nature Climate Change, 6, pp. 508-513. https://doi.org/10.1038/nclimate2941

Dunn, R.J.H., Willett, K.M., Thorne, P.W., Woolley, E.V., Durre, I., Dai, A., Parker, D.E., and Vose, R.S. (2012). HadISD: a quality-controlled global synoptic report database for selected variables at long-term stations from 1973–2011. Climate of the Past, 8, pp. 1649-1679. https://doi.org/10.5194/cp-8-1649-2012

Dunn, R.J.H., Alexander, L.V., Donat, M.G., Zhang, X., Bador, M., Herold, N., Lippmann, T., Allan, R., Aguilar, E., Barry, A.A., Brunet, M., Caesar, J., Chagnaud, G., Cheng, V., Cinco, T., Durre, I., Guzman, R., Htay, T.M., Wan Ibadullah, W.M., … Bin Hj Yussof, M.N.A. (2020). Development of an updated global land in situ-based data set of temperature and precipitation extremes: HadEX3. Journal of Geophysical Research-Atmospheres, 125(16), e2019JD032263. https://doi.org/10.1029/2019JD032263

Easterling, D. R., Evans, J.L., Groisman, P.Y.A., Karl, T.R., Kunkel, K.E., and Ambenje, P. (2000). Observed variability and trends in extreme climate events: A brief review. Bulletin of the American Meteorological Society, 81(3), pp. 417-426. https://doi.org/10.1175/1520-04772

Fatichi, S., and Caporali, E. (2009). A comprehensive analysis of changes in precipitation regime in Tuscany. International Journal of Climatology, 29(13), pp. 1883-1893. https://doi.org/10.1002/joc.1921

Fischer, E.M., and Knutti, R. (2016). Observed heavy precipitation increase confirms theory and early models. Nature Climate Change, 6, pp. 986-991. https://doi.org/10.1038/nclimate3110

Fowler, H.J., Lenderink, G., Prein, A.F., Westra, S., Allan, R.P., Ban, N., Barbero, R., Berg, P., Blenkinsop, S., Do, H.X., Guerreiro, S., Haerter, J.O., Kendon, E.J., Lewis, E., Schaer, C., Sharma, A., Villarini, G., Wasko, C., and Zhang, X. (2021). Anthropogenic intensification of short-duration rainfall extremes. Nature Reviews Earth & Environment, 2, pp. 107-122. https://doi.org/10.1038/s43017-020-00128-6

Gentilucci, M., Barbieri, M., Lee, H.S., and Zardi, D. (2019). Analysis of Rainfall Trends and Extreme Precipitation in the Middle Adriatic Side, Marche Region (Central Italy). Water, 11, 1948. https://doi.org/10.3390/w11091948

Gimeno, L., Sorí, R., Vázquez, M., Stojanovic, M., Iago Algarra, I., Eiras-Barca, J., Gimeno-Sotelo, L., and Nieto, R. (2022). Extreme precipitation events. WIREs Water, 9(6), e1611. https://doi.org/10.1002/wat2.1611

Goldberg, D.E. (1989). Genetic algorithms in search, optimization and machine learning. Addison-Wesley.

Goovaerts, P. (2000). Geostatistical approaches for incorporating elevation into the spatial interpolation of rainfall. Journal of Hydrology, 228(1-2), pp. 113-129. https://doi.org/10.1016/S0022-1694(00)00144-X

Griffith, D.A. (1987). Spatial Autocorrelation: A primer. Association of American Geographers, Washington DC.

Groisman, P.Y.A., Karl, T.R., Easterling, D.R., Knight, R.W., Jamason, P.F., Hennessy, K.J., Suppiah, R., Page, C.M., Wibig, J., Fortuniak, K., Razuvaev, V.N., Douglas, A., Førland, E., and Zhai, P.M. (1999). Changes in the Probability of Heavy Precipitation: Important Indicators of Climatic Change. In: Karl, T.R., Nicholls, N., Ghazi, A. (eds). Weather and Climate Extremes, Springer, pp. 243-283. https://doi.org/10.1007/978-94-015-9265-9_15

Groisman, P.Y., Knight, R.W., Easterling, D.R., Karl, T.R., Hegerl, G.C., and Razuvaev, V.N. (2005). Trends in intense precipitation in the climate record. Journal of Climate, 18, pp. 1326-1350. https://doi.org/10.1175/JCLI3339.1

Gu, X., Zhang, Q., Singh, V.P., Liu, L., and Shi, P. (2017). Spatiotemporal patterns of annual and seasonal precipitation extreme distributions across China and potential impact of tropical cyclones. International Journal of Climatology, 37(10), pp. 3949-3962. https://doi.org/10.1002/joc.4969

Guerreiro, S.B., Fowler, H.J., Barbero, R., Westra, S., Lenderink, G., Blenkinsop, S., Lewis, E., and Li, X.-F. (2018). Detection of continental-scale intensification of hourly rainfall extremes. Nature Climate Change, 8(9), pp. 803-807. https://doi.org/10.1038/s41558-018-0245-3

Helsel, D.R., and Frans, L.M. (2006). Regional Kendall test for trend. Environmental Science & Technology, 40(13), pp. 4066-4073. https://doi.org/10.1021/es051650b

Hirsch, R.M., Helsel, D.R., Cohn, T.A., and Gilroy, E.J. (1992). Statistical analysis of hydrologic data. Handbook of Hydrology. McGraw-Hill: New York.

Ingram, W. (2006). Increases all round. Nature Climate Change, 6, pp. 443-444. https://doi.org/10.1038/nclimate2966

IPCC, Intergovernmental Panel on Climate Change (1995). Radiative Forcing of Climate Change. Cambridge University Press, New York.

IPPC, Intergovernmental Panel on Climate Change (2014). Climate Change 2014: Mitigation of Climate Change. Contribution of Working Group III to the Fifth Assessment Report of the Intergovernmental Panel on Climate Change [Edenhofer, O., Pichs-Madruga, R., Sokona, Y., Farahani, E., Kadner, S., Seyboth, K., Adler, A., Baum, I., Brunner, S., Eickemeier, P., Kriemann, B., Savolainen, J., Schlömer, S., von Stechow, C., Zwickel, T. and Minx, J.C. (Eds.)]. Cambridge University Press, Cambridge, United Kingdom and New York, NY, USA.

IPCC, Intergovernmental Panel on Climate Change (2021). Climate Change 2021: The Physical Science Basis. Contribution of Working Group I to the Sixth Assessment Report of the Intergovernmental Panel on Climate Change [Masson-Delmotte, V., Zhai, P., Pirani, A., Connors, S.L., Péan, C., Berger, S., Caud, N., Chen, Y., Goldfarb, L., Gomis, M.I., Huang, M., Leitzell, K., Lonnoy, E., Matthews, J.B.R., Maycock, T.K., Waterfield, T., Yelekçi, O., Yu, R., and Zhou, B. (eds.)]. Cambridge University Press, Cambridge, United Kingdom and New York, NY, USA. In press.

Isaaks, E.H., and Srivastava, M.R. (1990). An Introduction to Applied Geostatistics. Oxford University Press, USA.

ISPRA (2012). Progetto Annali. Available online: http://www.bio.isprambiente.it/annalipdf/

ISPRA (2012). Inquadramento storico del monitoraggio idro-meteografico e delle relative competenze.

ISPRA (2020). ReNDis, La difesa del suolo in vent'anni di monitoraggio ISPRA sugli interventi per la mitigazione del rischio idrogeologico. Rapporto 328/2020.

Jakob, D., Karoly, D.J., and Seed, A. (2011). Non-stationarity in daily and sub-daily intense rainfall - Part 1: Sydney, Australia. Natural Hazards and Earth System Sciences, 11(8), pp. 2263-2271. https://doi.org/10.5194/nhess-11-2263-2011

Kendall, M.G. (1975). Rank correlation methods. Griffin, London.

Kiktev, D., Sexton, D.M.H., Alexander, L., and Folland, C. K. (2003). Comparison of modelled and observed trends in indices of daily climate extremes, Journal of Climate, 16, pp. 3560-3571. https://doi.org/10.1175/1520-0442(2003)016<3560:COMAOT>2.0.CO;2

Koutsoyiannis, D., and Langousis A. (2011). Precipitation. Treatise on Water Science, pp. 27-78, Academic Press, Oxford.

Kruskal, W.H., and Wallis, A.W. (1952). Use of ranks in one-criterion variance analysis. Journal of the American Statistical Association, 47(260), pp. 583-621. https://doi.org/10.1080/01621459.1952.10483441

Kundzewicz, Z. W. (2019). Changes in flood risk in Europe. CRC Press.

Kunkel, K.E., and Frankson, R.M. (2015). Global land surface extremes of precipitation: data limitations and trends. Journal of Extreme Events, 2, 1550004. https://doi.org/10.1142/S2345737615500049

Legambiente Osservatorio (2022). Rapporto CittàClima: "Il clima è già cambiato: gli impatti di siccità e caldo estremo sulle città, i territori e le persone".

Lehmann, E.L. (1975). Nonparametrics, Statistical Methods Based on Ranks. Holden-Day, San Francisco, USA.

Lehmann, J., Coumou, D., & Frieler, K. (2015). Increased record-breaking precipitation events under global warming. Climatic Change, 132, pp. 501-515. https://doi.org/10.1007/s10584-015-1434-y

Lewis, E., Fowler, H., Alexander, L., Dunn, R., McClean, F., Barbero, R., Guerreiro, S., Li, X.F., and Blenkinsop, S. (2019). GSDR: A Global Sub-Daily Rainfall Dataset. Journal of Climate, 32(15), pp. 4715-4729. https://doi.org/10.1175/JCLI-D-18-0143.1

Libertino, A., Allamano, P., Laio, F., and Claps, P. (2018a). Regional-scale analysis of extreme precipitation from short and fragmented records. Advances in Water Resources, 112, pp.147-159. https://doi.org/10.1016/j.advwatres.2017.12.015

Libertino, A., Ganora, D., and Claps, P. (2018b). Technical note: Space-time analysis of rainfall extremes in Italy: Clues from a reconciled dataset. Hydrology and Earth System Sciences, 22(5), pp. 2705-2715. https://doi.org/10.5194/hess-22-2705-2018

Libertino, A., Ganora, D., and Claps, P. (2019). Evidence for increasing rainfall extremes remains elusive at large spatial scales: The case of Italy. Geophysical Research Letters, 46, pp. 7437-7446. https://doi.org/10.1029/2019GL083371

Lionello, P., Congedi, L., Reale, M., Scarascia, L., and Tanzarella, A. (2014). Sensitivity of typical Mediterranean crops to past and future evolution of seasonal temperature and precipitation in Apulia. Regional Environmental Change, 14, pp. 2025-2038. https://doi.org/10.1007/s10113-013-0482-y

Liuzzo, L., Bono, E., Sammartano, V., and Freni, G., (2016). Analysis of spatial and temporal rainfall trends in Sicily during the 1921-2012 period. Theoretical and Applied Climatology, 126, pp. 113-129. https://doi.org/10.1007/s00704-015-1561-4

Loader, C. (1999). Local Regression and Likelihood. Statistics and Computing.

Longobardi, A., and Villani, P. (2010). Trend analysis of annual and seasonal rainfall time series in the Mediterranean area. International Journal of Climatology, 30, pp.1538-1546. https://doi.org/10.1002/joc.2001

Manfreda, S., Sole, A., and De Costanzo, G. (2015). Le precipitazioni estreme in Basilicata. Editrice Universo Sud.

Mann H.B. (1945). Nonparametric tests against trend. Econometrica, 13, pp. 245-259.

Mann, H.B., and Whitney, D.R., (1947). On a test of whether one of two random variables is stochastically larger than the other. The Annals of Mathematical Statistics, 18(1), pp. 50-60. https://doi.org/10.1214/aoms/1177730491

Mazzoglio, P., Butera, I., and Calps, P. (2020). I^2-RED: A Massive Update and Quality Control of the Italian Annual Extreme Rainfall Dataset. Water, 12(12), 3308. https://doi.org/10.3390/w12123308

Moberg, A., Jones, P.D., Lister, D., Walther, A., Brunet, M., Jacobeit, J., Alexander, L.V., Della-Marta, P.M., Luterbacher, J., Yiou, P., Chen, D., Klein Tank, A.M.G., Saladié, O., Sigró, J., Aguilar, E., Alexandersson, H., Almarza, C., Auer, I., Barriendos, M., Begert, M., Bergström, H., Böhm, R., Butler, C.J., Caesar, J., Drebs, A., Founda, D., Gerstengarbe, F.W., Micela, G., Maugeri, M., Österle, H., Pandzic, K., Petrakis, M., Srnec, L., Tolasz, R., Tuomenvirta, H., Werner, P.C., Linderholm, H., Philipp, A., Wanner, H., and Xoplaki, E. (2006). Indices for daily temperature and precipitation extremes in Europe analysed for the period 1901-2000. Journal of Geophysical Research: Atmospheres, 111, D22106. https://doi.org/10.1029/2006JD007103

Moral, F.J. (2010). Comparison of different geostatistical approaches to map climate variables: application to precipitation. International Journal of Climatology, 30, pp. 620-631. https://doi.org/10.1002/joc.1913

Morrison, A., Villarini, G., Zhang, W., and Scoccimarro, E. (2019). Projected changes in extreme precipitation at sub-daily and daily time scales. Global and Planetary Change, 182, 103004. https://doi.org/10.1016/j.gloplacha.2019.103004

Muschinski, T., and Katz, J. I. (2013). Trends in hourly rainfall statistics in the United States under a warming climate. Nature Climate Change, 3, pp. 577-580. https://doi.org/10.1038/nclimate1828

Nicholls, N., and Lavery, B. (1992). Australian rainfall trends during the twentieth century. International Journal of Climatology, 12(2), pp. 153-163. https://doi.org/10.1002/joc.3370120204

Noori, M.J., Hassan, H.H., and Mustafa, Y.T. (2014). Spatial Estimation of Rainfall Distribution and Its Classification in Duhok Governorate Using GIS. Journal of Water Resource and Protection, 6, pp. 75-82. http://dx.doi.org/10.4236/jwarp.2014.62012

O'Gorman, P.A. (2015). Precipitation Extremes Under Climate Change. Current Climate Change Reports, 1, pp. 49-59. https://doi.org/10.1007/s40641-015-0009-3

Odeh, I.O.A., Mcbratney, A.B., and Chittleborough, D.J. (1995) Further results on prediction of soil properties from terrain attributes: heterotopic cokriging and regression-kriging. Geoderma, 67(3), pp. 215-226. https://doi.org/10.1016/0016-7061(95)00007-B

Ohba, M., and Sugimoto, S. (2019). Differences in climate change impacts between weather patterns: possible effects on spatial heterogeneous changes in future extreme rainfall. Climate Dynamics, 52, pp. 4177-4191. https://doi.org/10.1007/s00382-018-4374-1

Page, C.M., Nicholls, N., Plummer, N., Trewin, B., Manton, M., Alexander, L., Chambers, L.E., Choi, Y., Collins, D.A., Gosai, A., Della-Marta, P., Haylock, M.R., Inape, K., Laurent, V., Maitrepierre, L., Makmur, E.E.P., Nakamigawa, H., Ouprasitwong, N., McGree, S., Pahalad, J., Salinger, M.J., Tibig, L., Tran, T.D., Vediapan, K., and Zhai, P. (2004). Data rescue in the southeast Asia and south Pacific regio - Challenges and opportunities. Bulletin of the American Meteorological Society, 85(10), pp. 1483-1489.

Papalexiou, S.M., Dialynas, Y.G., and Grimaldi S. (2016). Hershfield factor revisited: correcting annual maximum precipitation. Journal of Hydrology, 542, pp. 884-895. https://doi.org/10.1016/j.jhydrol.2016.09.058

Papalexiou, S.M., and Montanari, A. (2019). Global and regional increase of precipitation extremes under global warming. Water Resources Research, 55(6), pp. 4901-4914. https://doi.org/10.1029/2018WR024067

Pappas, C., Papalexiou, S.M., and Koutsoyiannis, D. (2014). A quick gap filling of missing hydrometeorological data. Journal of Geophysical Research: Atmospheres, 119(15), pp. 9290-9300. https://doi.org/10.1002/2014JD021633

Pellicone, G., Caloiero, T., Modica, G., and Guagliardi, I. (2018). Application of several spatial interpolation techniques to monthly rainfall data in the Calabria region (southern Italy). International Journal of Climatology, 38(9), pp. 3651-3666. https://doi.org/10.1002/joc.5525

Pelosi, A., and Furcolo, P. (2015). An Amplification Model for the Regional Estimation of Extreme Rainfall within Orographic Areas in Campania Region (Italy). Water, 7, pp. 6877-6891. https://doi.org/10.3390/w7126664

Pelosi, A., Furcolo, P., Rossi, F., and Villani, P. (2020). The characterization of extraordinary extreme events (EEEs) for the assessment of design rainfall depths with high return periods. Hydrological Processes, 34, pp. 2543-2559. https://doi.org/10.1002/hyp.13747

Pelosi, A., Chirico, G.B., Furcolo, P., and Villani, P. (2022). Regional Assessment of Sub-Hourly Annual Rainfall Maxima. Water, 14, 1179. https://doi.org/10.3390/w14071179

Pettitt, A.N. (1979). A non-parametric approach to the change-point problem. Journal of the Royal Statistical Society (Applied Statistics), 28(2), pp. 126-135.

Piccarreta, M., Capolongo, D., and Boenzi, F. (2004). Trend analysis of precipitation and drought in Basilicata from 1923 to 2000 within a Southern Italy context. International Journal of Climatology, 24, pp. 907-922. https://doi.org/10.1002/joc.1038

Piccarreta, M., Capolongo, D., Boenzi, F., and Bentivenga, M. (2006). Implications of decadal changes in precipitation and land use policy to soil erosion in Basilicata, Italy. Catena, 65(2), pp. 138-151. https://doi.org/10.1016/j.catena.2005.11.005

Piccarreta, M., Pasini, A., Capolongo, D., and Lazzari, M. (2013). Changes in daily precipitation extremes in the Mediterranean from 1951 to 2010: the Basilicata region, southern Italy. International Journal of Climatology, 33(15), pp. 3229-3248. https://doi.org/10.1002/joc.3670

Piervitali, E., Colacino, M., and Conte, M. (1998). Rainfall over the central-western Mediterranean basin in the period 1951-1995, Part I: Precipitation trends. Nuovo Cimento, C21, pp. 331-344. ISSN 1826-9885.

Polemio, M., and Lonigro, T. (2015). Trends in climate, short-duration rainfall, and damaging hydrogeological events (Apulia, Southern Italy). Natural Hazards, 75, pp. 515-540. https://doi.org/10.1007/s11069-014-1333-y

Scorzini, A.R., and Leopardi, M. (2019). Precipitation and temperature trends over central Italy (Abruzzo Region): 1951-2012. Theoretical and Applied Climatology, 135, pp. 959-977. https://doi.org/10.1007/s00704-018-2427-3

Sen, P.K. (1968). Estimates of the regression coefficient based on Kendall's tau. J Am Stat As, 63, pp. 1379-1389. https://doi.org/10.1080/01621459.1968.10480934

Sen, Z. (2012). Innovative Trend Analysis Methodology. Journal of Hydrologic Engineering, 17, pp. 1042-1046. https://doi.org/10.1061/(ASCE)HE.1943-5584.0000556

Sen, Z. (2017). Innovative trend significance test and applications. Theoretical and Applied Climatology, 127, pp. 939-947. https://doi.org/10.1007/s00704-015-1681-x

Shortridge, J. (2019). Observed trends in daily rainfall variability result in more severe climate change impacts to agriculture. Climatic Change, 157, pp. 429-444. https://doi.org/10.1007/s10584-019-02555-x

Simanton, J., and Osborn, H. (1980). Reciprocal Distance Estimate of Point Rainfall. Journal of the Hydraulics Division, 106(7), pp. 1242-246.

Skansi, M.d.l.M., Brunet, B., Sigró, J., Aguilar, E., Groening, J.A.A., Bentancur, O.J., Geier, Y.R.C., Amaya, R.L.C., Jácome, H., Ramos, A.M., Rojas, C.O., Pasten, A.M., Mitro, S.S., Jiménez, C.V., Martínez, R., Alexander, L.V., and Jones, P.D. (2013). Warming and wetting signals emerging from an analysis of changes in climate extreme indices over South America. Global and Planetary Change, 100, pp. 295307. https://doi.org/10.1016/j.gloplacha.2012.11.004

Sneyers, R. (1990). On the statistical analysis of series of observations. Technical Note 143, World Meteorological Organization (WMO).

Soldini, L., and Darvini, G. (2017). Extreme rainfall statistics in the Marche region, Italy. Hydrology Research, 48(3), pp. 686-700. https://doi.org/10.2166/nh.2017.091

Spearman, C. (1904). The proof and measurement of association between two things. American Journal of Psychology, 15, pp. 72-101.

Tangney, P. (2020). Understanding climate change as risk: a review of IPCC guidance for decision-making. Journal of Risk Research, 23(11), pp. 1424-1439. https://doi.org/10.1080/13669877.2019.1673801

Tanty, R., and Desmukh, T.S. (2015). Application of Artificial Neural Network in Hydrology - A Review. International Journal of Engineering Research & Technology, 4(6), pp. 184-188. ISSN: 2278-0181.

Tarquini, S., Vinci, S., Favalli, M., Doumaz, F., Fornaciai, A., and Nannipieri, L. (2012). Release of a 10-m-resolution DEM for the Italian territory: Comparison with global-coverage

DEMs and anaglyph-mode exploration via the web. Computers & Geosciences, 38, pp. 168-170. https://doi.org/10.1016/j.cageo.2011.04.018

Teegavarapu, R.S.V., and Chandramouli, V. (2005). Improved Weighting Methods, Deterministic and Stochastic Data-driven Models for Estimation of Missing Precipitation Records. Journal of Hydrology, 312, pp. 191-206. https://doi.org/10.1016/j.jhydrol.2005.02.015

Teegavarapu, R.S.V. (2009). Estimation of Missing Precipitation Records Integrating Surface Interpolation Techniques and Spatio-temporal Association Rules. Journal of Hydroinformatics, 11(2), pp. 133-146. https://doi.org/10.2166/hydro.2009.009

Teegavarapu, R. (2012). Ch-7: Floods in a changing climate. Extreme precipitation. Cambridge University Press, Cambridge. https://doi.org/10.1017/CBO9781139088442

Thiessen, A.H. (1911). Precipitation for large areas. Monthly Weather Review, 39, pp. 1082-1089. https://doi.org/10.1175/1520-0493(1911)39<1082b:PAFLA>2.0.CO;2

Trenberth, KE., Jones, PD., Ambenje, P., Bojariu, R., Easterling, D., Klein Tank, A., Parker, D., Rahimzadeh, F., Renwick, JA., Rusticucci, M., Soden, B., and Zhai, P. (2007). Observations: Surface and atmospheric climate change. In Solomon, S., Qin, D., Manning, M., Chen, Z., Marquis, M., Averyt, K.B., Tignor, M., and Miller H.L. (Eds.), Climate Change 2007: The Physical Science Basis. Contribution of Working Group 1 to the 4th Assessment Report of the Intergovernmental Panel on Climate Change Cambridge University Press.

Uboldi, F., and Lussana, C. (2018). Evidence of non-stationarity in a local climatology of rainfall extremes in northern Italy. International Journal of Climatology, 38(1), pp. 506-516. https://doi.org/10.1002/joc.5183

Van Belle, G., and Hughes, J.P. (1984). Nonparametric Tests for Trend in Water Quality. Water Resources Research, 20, pp. 127-136. http://dx.doi.org/10.1029/WR020i001p00127

van den Besselaar, E.J.M., Klein Tank, A.M.G., and Buishand, T.A. (2012). Trends in European precipitation extremes over 1951-2010. International Journal of Climatology, 33(12), pp. 2682-2689. https://doi.org/10.1002/joc.3619

Wang, F. (2006). Quantitative Methods and Applications in GIS.

Wang, X. L., Wan, H., Zwiers, F., Swail, V.R., Compo, G.P., Allan, R.P., Vose, R.S., Jourdian, S., and Yin, X. (2011). Trends and low-frequency variability of storminess over western Europe, 1878-2007. Climate Dynamics, 37, pp. 2355-2371. https://doi.org/10.1007/s00382-011-1107-0

Wardekker, A., and Lorenz, S. (2019). The visual framing of climate change impacts and adaptation in the IPCC assessment reports. Climatic Change, 156, pp. 273-292.

Webster, R. and Oliver, M.A. (2007). Geostatistics for Environmental Scientists, 2nd edition. West Sussex: John Wiley & Sons.

Westra, S., Alexander, L.V., and Zwiers, F.W. (2013). Global increasing trends in annual maximum daily precipitation. Journal of Climate, 26, pp. 3904-3918. https://doi.org/10.1175/JCLI-D-12-00502.1

Westra, S., Fowler, H.J., Evans, J.P., Alexander, L.V., Berg, P., Johnson, F., Kendon, E.J., Lenderink, G., and Roberts, N.M. (2014). Future changes to the intensity and frequency of short-duration extreme rainfall. Reviews of Geophysics, 52, pp. 522-555. https://doi.org/10.1002/2014RG000464

WMO, World Meteorological Organization (2014). Scientific Assessment of Ozone Depletion. Global Ozone Research and Monitoring Project - Report No. 55.

Xia, Y., Fabian, P., Stohl, A., and Winterhalter, M. (1999). Forest Climatology: Estimation of Missing Values for Bavaria, Germany. Agricultural and Forest Meteorology, 96(1-3), pp. 131-44.

Xu, W., Zou, Y., Zhang, G., and Linderman, M. (2015). A comparison among spatial interpolation techniques for daily rainfall data in Sichuan Province, China. International Journal of Climatology, 35, pp. 2898-2907. https://doi.org/10.1002/joc.4180

Yang, L., Villarini, G., Smith, J.A., Tian, F., and Hu, H. (2012). Changes in seasonal maximum daily precipitation in China over the period 1961-2006. International Journal of Climatology, 33(7), pp. 1646-1657. https://doi.org/10.1002/joc.3539

Yu, R., and Li, J. (2012). Hourly rainfall changes in response to surface air temperature over eastern contiguous China. Journal of Climate, 25, pp. 6851-6861. https://doi.org/10.1175/JCLI-D-11-00656.1

Zhang, C., and Zhang, S. (2002). Association Rule Mining: Models and Algorithms. Lecture Notes in Artificial Intelligence. Springer, New York.

Zolina, O., Simmer, C., Belyaev, K., Kapala, A., and Gulev, S. (2009). Improving Estimates of Heavy and Extreme Precipitation Using Daily Records from European Rain Gauges. Journal of Hydrometeorology, 10(3), pp. 701-716. https://doi.org/10.1175/2008JHM1055.1

Appendix

Appendix A: Additional results of the "Spatially-Constrained Ordinary Kriging (SC-OK)" methodology

This section reports the results of the calibration of the SC-OK method per region (Apulia, Basilicata, Calabria, Campania and Molise) and duration (1, 3, 6, 12, and 24 hours).

Table A. 1 *- Results of the optimization step for the Apulia region. In particular, for each value of ρ, the optimal value or R and N is reported.*

ρ	**1h**		**3h**		**6h**		**12h**		**24h**	
	R [km]	**N**	**R [km]**	**N**	**R [km]**	**N**	**R [km]**	**N**	**R [km]**	**N**
0.0005	94.41	14	50.46	4	50.46	4	50.46	4	50.46	4
0.0010	64.33	13	43.70	6	43.70	6	35.68	4	35.68	4
0.0015	29.13	4	32.57	5	32.57	5	52.52	13	43.70	9
0.0020	37.85	9	30.90	6	37.85	9	28.21	5	30.90	6
0.0025	42.22	14	40.68	13	29.85	7	29.85	7	29.85	7
0.0030	38.54	14	32.57	10	29.13	8	29.13	8	25.23	6
0.0035	23.36	6	28.61	9	30.16	10	30.16	10	26.97	8
0.0040	33.38	14	32.16	13	28.21	10	29.59	11	32.16	13
0.0045	18.81	5	20.60	6	16.82	4	16.82	4	32.57	15
0.0050	17.84	5	29.85	14	17.84	5	30.90	15	15.96	4
0.0055	29.46	15	20.13	7	20.13	7	15.22	4	15.22	4
0.0060	23.03	10	23.03	10	25.23	12	25.23	12	17.84	6
0.0065	23.21	11	25.23	13	25.23	13	25.23	13	15.65	5
0.0070	21.32	10	25.23	14	17.84	7	19.07	8	17.84	7
0.0075	20.60	10	24.38	14	22.57	12	25.23	15	15.96	6
0.0080	24.43	15	23.60	14	21.85	12	20.92	11	14.10	5
0.0085	23.70	15	23.70	15	23.70	15	13.68	5	13.68	5
0.0090	16.82	8	23.03	15	21.44	13	15.73	7	19.72	11
0.0095	12.94	5	20.05	12	12.94	5	20.05	12	14.18	6
0.0100	21.85	15	19.54	12	12.62	5	12.62	5	13.82	6

***Table A. 2** - Results of the optimization step for the Calabria region. In particular, for each value of ρ, the optimal value or R and N is reported.*

ρ	**1h**		**3h**		**6h**		**12h**		**24h**	
	R [km]	**N**	**R [km]**	**N**	**R [km]**	**N**	**R [km]**	**N**	**R [km]**	**N**
0.0005	66.76	7	66.76	7	66.76	7	75.69	9	66.76	7
0.0010	64.33	13	61.80	12	56.42	10	39.89	5	39.89	5
0.0015	54.51	14	54.51	14	29.13	4	29.13	4	35.68	6
0.0020	45.49	13	41.84	11	41.84	11	48.86	15	43.70	12
0.0025	22.57	4	35.68	10	35.68	10	35.68	10	43.70	15
0.0030	27.25	7	37.14	13	37.14	13	37.14	13	37.14	13
0.0035	28.61	9	28.61	9	21.32	5	25.23	7	26.97	8
0.0040	19.95	5	19.95	5	21.85	6	23.60	7	19.95	5
0.0045	16.82	4	16.82	4	18.81	5	16.82	4	18.81	5
0.0050	17.84	5	17.84	5	17.84	5	26.46	11	19.54	6
0.0055	27.43	13	17.01	5	18.63	6	18.63	6	18.63	6
0.0060	14.57	4	16.29	5	21.85	9	14.57	4	21.85	9
0.0065	15.65	5	20.99	9	20.99	9	15.65	5	20.99	9
0.0070	15.08	5	15.08	5	15.08	5	15.08	5	15.08	5
0.0075	14.57	5	14.57	5	15.96	6	15.96	6	15.96	6
0.0080	16.69	7	15.45	6	14.10	5	16.69	7	15.45	6
0.0085	18.36	9	16.19	7	17.31	8	16.19	7	17.31	8
0.0090	11.89	4	21.44	13	21.44	13	21.44	13	16.82	8
0.0095	11.58	4	20.05	12	21.66	14	20.05	12	17.37	9
0.0100	11.28	4	19.54	12	19.54	12	18.71	11	16.93	9

***Table A. 3** - Results of the optimization step for the Campania region. In particular, for each value of ρ, the optimal value or R and N is reported.*

ρ	**1h**		**3h**		**6h**		**12h**		**24h**	
	R [km]	**N**	**R [km]**	**N**	**R [km]**	**N**	**R [km]**	**N**	**R [km]**	**N**
0.0005	97.72	15	87.40	12	87.40	12	94.41	14	75.69	9
0.0010	61.80	12	64.33	13	35.68	4	66.76	14	69.10	15
0.0015	43.70	9	56.42	15	43.70	9	32.57	5	41.20	8

0.0020	25.23	4	47.20	14	41.84	11	25.23	4	41.84	11
0.0025	42.22	14	42.22	14	42.22	14	42.22	14	27.64	6
0.0030	39.89	15	39.89	15	30.90	9	37.14	13	23.03	5
0.0035	35.68	14	31.63	11	36.93	15	19.07	4	19.07	4
0.0040	30.90	12	26.76	9	26.76	9	17.84	4	17.84	4
0.0045	25.23	9	26.60	10	22.25	7	22.25	7	22.25	7
0.0050	22.57	8	21.11	7	17.84	5	15.96	4	19.54	6
0.0055	28.46	14	28.46	14	18.63	6	18.63	6	18.63	6
0.0060	16.29	5	14.57	4	14.57	4	14.57	4	14.57	4
0.0065	18.51	7	17.14	6	17.14	6	15.65	5	14.00	4
0.0070	17.84	7	15.08	5	15.08	5	16.52	6	13.49	4
0.0075	17.24	7	17.24	7	17.24	7	13.03	4	14.57	5
0.0080	16.69	7	14.10	5	14.10	5	14.10	5	14.10	5
0.0085	13.68	5	13.68	5	13.68	5	13.68	5	13.68	5
0.0090	15.73	7	13.30	5	13.30	5	13.30	5	14.57	6
0.0095	12.94	5	12.94	5	12.94	5	14.18	6	12.94	5
0.0100	11.28	4	11.28	4	11.28	4	11.28	4	13.82	6
0.0105	11.01	4	11.01	4	11.01	4	11.01	4	13.49	6
0.0110	10.76	4	10.76	4	10.76	4	10.76	4	10.76	4
0.0115	10.52	4	10.52	4	10.52	4	10.52	4	10.52	4
0.0120	10.30	4	10.30	4	10.30	4	12.62	6	12.62	6
0.0125	10.09	4	10.09	4	12.36	6	10.09	4	13.35	7
0.0130	9.90	4	9.90	4	9.90	4	9.90	4	14.00	8
0.0135	9.71	4	9.71	4	9.71	4	9.71	4	14.57	9
0.0140	9.54	4	9.54	4	9.54	4	11.68	6	14.30	9
0.0145	9.37	4	9.37	4	11.48	6	11.48	6	12.40	7
0.0150	9.21	4	9.21	4	9.21	4	9.21	4	12.19	7

Table A. 4 *- Results of the optimization step for the Molise region. In particular, for each value of ρ, the optimal value or R and N is reported.*

ρ	**1h**		**3h**		**6h**		**12h**		**24h**	
	R [km]	**N**	**R [km]**	**N**	**R [km]**	**N**	**R [km]**	**N**	**R [km]**	**N**
0.0005	56.42	5	50.46	4	50.46	4	50.46	4	50.46	4

0.0010	56.42	10	47.20	7	35.68	4	39.89	5	39.89	5
0.0015	52.52	13	52.52	13	35.68	6	35.68	6	54.51	14
0.0020	43.70	12	43.70	12	30.90	6	30.90	6	25.23	4
0.0025	42.22	14	29.85	7	29.85	7	27.64	6	25.23	5
0.0030	23.03	5	35.68	12	20.60	4	35.68	12	30.90	9
0.0035	35.68	14	33.04	12	30.16	10	30.16	10	19.07	4
0.0040	21.85	6	30.90	12	30.90	12	21.85	6	28.21	10
0.0045	23.79	8	26.60	10	31.47	14	31.47	14	31.47	14
0.0050	23.94	9	30.90	15	26.46	11	29.85	14	29.85	14
0.0055	28.46	14	28.46	14	27.43	13	20.13	7	20.13	7
0.0060	26.26	13	28.21	15	27.25	14	27.25	14	19.27	7
0.0065	23.21	11	14.00	4	20.99	9	19.79	8	17.14	6
0.0070	21.32	10	22.37	11	20.23	9	20.23	9	13.49	4
0.0075	25.23	15	13.03	4	13.03	4	13.03	4	25.23	15
0.0080	20.92	11	18.92	9	12.62	4	24.43	15	12.62	4
0.0085	13.68	5	22.06	13	23.70	15	12.24	4	12.24	4
0.0090	22.25	14	21.44	13	11.89	4	11.89	4	21.44	13
0.0095	12.94	5	11.58	4	11.58	4	11.58	4	11.58	4
0.0100	11.28	4	11.28	4	11.28	4	11.28	4	11.28	4

Table A. 5 *- Results of the calibration step for the Apulia region at 1-h duration, In particular, for each value of ρ, the number of observed (OD), reconstructed (RD) and total (TD) data and the percentage ratio between RD and OD is reported.*

ρ	**R [km]**	**N**	**Observed Data (OD)**	**Reconstructed Data (RD)**	**Total Data (TD)**	**Ratio RD/OD [%]**
0.0005	94.41	14	5209	2895	8104	55.58
0.0010	64.33	13	5209	2811	8020	53.96
0.0015	29.13	4	5209	2736	7945	52.52
0.0020	37.85	9	5209	2512	7721	48.22
0.0025	42.22	14	5209	2116	7325	40.62
0.0030	38.54	14	5209	1680	6889	32.25
0.0035	23.36	6	5209	1561	6770	29.97
0.0040	33.38	14	5209	1105	6314	21.21
0.0045	18.81	5	5209	1077	6286	20.68

0.0050	17.84	5	5209	892	6101	17.12
0.0055	29.46	15	5209	595	5804	11.42
0.0060	23.03	10	5209	551	5760	10.58
0.0065	23.21	11	5209	467	5676	8.97
0.0070	21.32	10	5209	350	5559	6.72
0.0075	20.60	10	5209	274	5483	5.26
0.0080	24.43	15	5209	206	5415	3.95
0.0085	23.70	15	5209	170	5379	3.26
0.0090	16.82	8	5209	140	5349	2.69
0.0095	12.94	5	5209	186	5395	3.57
0.0100	21.85	15	5209	38	5247	0.73

Table A. 6 *- Results of the calibration step for the Apulia region at 3-h duration, In particular, for each value of ρ, the number of observed (OD), reconstructed (RD) and total (TD) data and the percentage ratio between RD and OD is reported.*

ρ	**R [km]**	**N**	**Observed Data (OD)**	**Reconstructed Data (RD)**	**Total Data (TD)**	**Ratio RD/OD [%]**
0.0005	50.46	4	5255	2854	8109	54.31
0.0010	43.70	6	5255	2782	8037	52.94
0.0015	32.57	5	5255	2691	7946	51.21
0.0020	30.90	6	5255	2518	7773	47.92
0.0025	40.68	13	5255	2141	7396	40.74
0.0030	32.57	10	5255	1855	7110	35.30
0.0035	28.61	9	5255	1465	6720	27.88
0.0040	32.16	13	5255	1110	6365	21.12
0.0045	20.60	6	5255	1016	6271	19.33
0.0050	29.85	14	5255	717	5972	13.64
0.0055	20.13	7	5255	669	5924	12.73
0.0060	23.03	10	5255	552	5807	10.50
0.0065	25.23	13	5255	408	5663	7.76
0.0070	25.23	14	5255	325	5580	6.18
0.0075	24.38	14	5255	267	5522	5.08
0.0080	23.60	14	5255	228	5483	4.34
0.0085	23.70	15	5255	175	5430	3.33

0.0090	23.03	15	5255	135	5390	2.57
0.0095	20.05	12	5255	95	5350	1.81
0.0100	19.54	12	5255	75	5330	1.43

Table A. 7 *- Results of the calibration step for the Apulia region at 6-h duration, In particular, for each value of ρ, the number of observed (OD), reconstructed (RD) and total (TD) data and the percentage ratio between RD and OD is reported.*

ρ	**R [km]**	**N**	**Observed Data (OD)**	**Reconstructed Data (RD)**	**Total Data (TD)**	**Ratio RD/OD [%]**
0.0005	50.46	4	5287	2822	8109	53.38
0.0010	43.70	6	5287	2756	8043	52.13
0.0015	32.57	5	5287	2668	7955	50.46
0.0020	37.85	9	5287	2482	7769	46.95
0.0025	29.85	7	5287	2225	7512	42.08
0.0030	29.13	8	5287	1876	7163	35.48
0.0035	30.16	10	5287	1454	6741	27.50
0.0040	28.21	10	5287	1127	6414	21.32
0.0045	16.82	4	5287	1138	6425	21.52
0.0050	17.84	5	5287	911	6198	17.23
0.0055	20.13	7	5287	677	5964	12.80
0.0060	25.23	12	5287	529	5816	10.01
0.0065	25.23	13	5287	419	5706	7.93
0.0070	17.84	7	5287	376	5663	7.11
0.0075	22.57	12	5287	283	5570	5.35
0.0080	21.85	12	5287	222	5509	4.20
0.0085	23.70	15	5287	176	5463	3.33
0.0090	21.44	13	5287	117	5404	2.21
0.0095	12.94	5	5287	186	5473	3.52
0.0100	12.62	5	5287	144	5431	2.72

Table A. 8 *- Results of the calibration step for the Apulia region at 12-h duration, In particular, for each value of ρ, the number of observed (OD), reconstructed (RD) and total (TD) data and the percentage ratio between RD and OD is reported.*

ρ	**R [km]**	**N**	**Observed Data (OD)**	**Reconstructed Data (RD)**	**Total Data (TD)**	**Ratio RD/OD [%]**
0.0005	50.46	4	5318	2791	8109	52.48
0.0010	35.68	4	5318	2706	8024	50.88
0.0015	52.52	13	5318	2569	7887	48.31
0.0020	28.21	5	5318	2495	7813	46.92
0.0025	29.85	7	5318	2216	7534	41.67
0.0030	29.13	8	5318	1863	7181	35.03
0.0035	30.16	10	5318	1453	6771	27.32
0.0040	29.59	11	5318	1132	6450	21.29
0.0045	16.82	4	5318	1137	6455	21.38
0.0050	30.90	15	5318	721	6039	13.56
0.0055	15.22	4	5318	813	6131	15.29
0.0060	25.23	12	5318	538	5856	10.12
0.0065	25.23	13	5318	432	5750	8.12
0.0070	19.07	8	5318	379	5697	7.13
0.0075	25.23	15	5318	270	5588	5.08
0.0080	20.92	11	5318	214	5532	4.02
0.0085	13.68	5	5318	259	5577	4.87
0.0090	15.73	7	5318	150	5468	2.82
0.0095	20.05	12	5318	98	5416	1.84
0.0100	12.62	5	5318	139	5457	2.61

Table A. 9 *- Results of the calibration step for the Apulia region at 24-h duration, In particular, for each value of ρ, the number of observed (OD), reconstructed (RD) and total (TD) data and the percentage ratio between RD and OD is reported.*

ρ	**R [km]**	**N**	**Observed Data (OD)**	**Reconstructed Data (RD)**	**Total Data (TD)**	**Ratio RD/OD [%]**
0.0005	50.46	4	5345	2764	8109	51.71
0.0010	35.68	4	5345	2683	8028	50.20

0.0015	43.70	9	5345	2588	7933	48.42
0.0020	30.90	6	5345	2465	7810	46.12
0.0025	29.85	7	5345	2213	7558	41.40
0.0030	25.23	6	5345	1875	7220	35.08
0.0035	26.97	8	5345	1511	6856	28.27
0.0040	32.16	13	5345	1121	6466	20.97
0.0045	32.57	15	5345	875	6220	16.37
0.0050	15.96	4	5345	993	6338	18.58
0.0055	15.22	4	5345	819	6164	15.32
0.0060	17.84	6	5345	561	5906	10.50
0.0065	15.65	5	5345	501	5846	9.37
0.0070	17.84	7	5345	375	5720	7.02
0.0075	15.96	6	5345	349	5694	6.53
0.0080	14.10	5	5345	311	5656	5.82
0.0085	13.68	5	5345	261	5606	4.88
0.0090	19.72	11	5345	153	5498	2.86
0.0095	14.18	6	5345	157	5502	2.94
0.0100	13.82	6	5345	132	5477	2.47

Table A. 10 *- Results of the calibration step for the Basilicata region at 1-h duration, In particular, for each value of ρ, the number of observed (OD), reconstructed (RD) and total (TD) data and the percentage ratio between RD and OD is reported.*

ρ	**R [km]**	**N**	**Observed Data (OD)**	**Reconstructed Data (RD)**	**Total Data (TD)**	**Ratio RD/OD [%]**
0.0005	61.80	6	2267	4959	7226	218.75
0.0010	56.42	10	2267	4729	6996	208.60
0.0015	43.70	9	2267	3786	6053	167.00
0.0020	35.68	8	2267	3144	5411	138.69
0.0025	42.22	14	2267	2621	4888	115.62
0.0030	35.68	12	2267	2273	4540	100.26
0.0035	36.93	15	2267	1897	4164	83.68
0.0040	19.95	5	2267	1599	3866	70.53
0.0045	16.82	4	2267	1446	3713	63.78
0.0050	15.96	4	2267	1230	3497	54.26

0.0055	15.22	4	2267	1038	3305	45.79
0.0060	17.84	6	2267	860	3127	37.94
0.0065	15.65	5	2267	699	2966	30.83
0.0070	22.37	11	2267	423	2690	18.66
0.0075	15.96	6	2267	477	2744	21.04
0.0080	19.95	10	2267	293	2560	12.92
0.0085	14.99	6	2267	305	2572	13.45
0.0090	14.57	6	2267	269	2536	11.87
0.0095	14.18	6	2267	233	2500	10.28
0.0100	16.93	9	2267	108	2375	4.76

Table A. 11 *- Results of the calibration step for the Basilicata region at 3-h duration, In particular, for each value of ρ, the number of observed (OD), reconstructed (RD) and total (TD) data and the percentage ratio between RD and OD is reported.*

ρ	**R [km]**	**N**	**Observed Data (OD)**	**Reconstructed Data (RD)**	**Total Data (TD)**	**Ratio RD/OD [%]**
0.0005	50.46	4	2272	4919	7191	216.51
0.0010	35.68	4	2272	4380	6652	192.78
0.0015	35.68	6	2272	3708	5980	163.20
0.0020	37.85	9	2272	3179	5451	139.92
0.0025	35.68	10	2272	2722	4994	119.81
0.0030	35.68	12	2272	2282	4554	100.44
0.0035	33.04	12	2272	1899	4171	83.58
0.0040	25.23	8	2272	1609	3881	70.82
0.0045	26.60	10	2272	1306	3578	57.48
0.0050	26.46	11	2272	1097	3369	48.28
0.0055	20.13	7	2272	910	3182	40.05
0.0060	20.60	8	2272	718	2990	31.60
0.0065	15.65	5	2272	706	2978	31.07
0.0070	22.37	11	2272	422	2694	18.57
0.0075	14.57	5	2272	510	2782	22.45
0.0080	14.10	5	2272	422	2694	18.57
0.0085	14.99	6	2272	305	2577	13.42
0.0090	13.30	5	2272	313	2585	13.78

0.0095	14.18	6	2272	233	2505	10.26
0.0100	14.93	7	2272	128	2400	5.63

Table A. 12 *- Results of the calibration step for the Basilicata region at 6-h duration, In particular, for each value of ρ, the number of observed (OD), reconstructed (RD) and total (TD) data and the percentage ratio between RD and OD is reported.*

ρ	**R [km]**	**N**	**Observed Data (OD)**	**Reconstructed Data (RD)**	**Total Data (TD)**	**Ratio RD/OD [%]**
0.0005	94.41	14	2274	5006	7280	220.14
0.0010	35.68	4	2274	4379	6653	192.57
0.0015	41.20	8	2274	3789	6063	166.62
0.0020	37.85	9	2274	3189	5463	140.24
0.0025	42.22	14	2274	2643	4917	116.23
0.0030	35.68	12	2274	2281	4555	100.31
0.0035	31.63	11	2274	1903	4177	83.69
0.0040	29.59	11	2274	1565	3839	68.82
0.0045	26.60	10	2274	1312	3586	57.70
0.0050	26.46	11	2274	1101	3375	48.42
0.0055	20.13	7	2274	917	3191	40.33
0.0060	28.21	15	2274	644	2918	28.32
0.0065	14.00	4	2274	782	3056	34.39
0.0070	15.08	5	2274	595	2869	26.17
0.0075	21.61	11	2274	311	2585	13.68
0.0080	14.10	5	2274	428	2702	18.82
0.0085	12.24	4	2274	468	2742	20.58
0.0090	11.89	4	2274	414	2688	18.21
0.0095	15.31	7	2274	169	2443	7.43
0.0100	14.93	7	2274	128	2402	5.63

Table A. 13 *- Results of the calibration step for the Basilicata region at 12-h duration, In particular, for each value of ρ, the number of observed (OD), reconstructed (RD) and total (TD) data and the percentage ratio between RD and OD is reported.*

ρ	**R [km]**	**N**	**Observed Data (OD)**	**Reconstructed Data (RD)**	**Total Data (TD)**	**Ratio RD/OD [%]**
0.0005	50.46	4	2274	4925	7199	216.58
0.0010	39.89	5	2274	4495	6769	197.67
0.0015	41.20	8	2274	3790	6064	166.67
0.0020	41.84	11	2274	3163	5437	139.09
0.0025	40.68	13	2274	2658	4932	116.89
0.0030	35.68	12	2274	2284	4558	100.44
0.0035	19.07	4	2274	1967	4241	86.50
0.0040	19.95	5	2274	1612	3886	70.89
0.0045	30.32	13	2274	1321	3595	58.09
0.0050	26.46	11	2274	1102	3376	48.46
0.0055	20.13	7	2274	917	3191	40.33
0.0060	24.16	11	2274	751	3025	33.03
0.0065	26.18	14	2274	536	2810	23.57
0.0070	25.23	14	2274	424	2698	18.65
0.0075	21.61	11	2274	308	2582	13.54
0.0080	21.85	12	2274	238	2512	10.47
0.0085	14.99	6	2274	308	2582	13.54
0.0090	14.57	6	2274	274	2548	12.05
0.0095	15.31	7	2274	169	2443	7.43
0.0100	12.62	5	2274	260	2534	11.43

Table A. 14 *- Results of the calibration step for the Basilicata region at 24-h duration, In particular, for each value of ρ, the number of observed (OD), reconstructed (RD) and total (TD) data and the percentage ratio between RD and OD is reported.*

ρ	**R [km]**	**N**	**Observed Data (OD)**	**Reconstructed Data (RD)**	**Total Data (TD)**	**Ratio RD/OD [%]**
0.0005	50.46	4	2271	4929	7200	217.04
0.0010	39.89	5	2271	4497	6768	198.02

0.0015	41.20	8	2271	3803	6074	167.46
0.0020	41.84	11	2271	3170	5441	139.59
0.0025	42.22	14	2271	2642	4913	116.34
0.0030	39.89	15	2271	2219	4490	97.71
0.0035	33.04	12	2271	1897	4168	83.53
0.0040	25.23	8	2271	1603	3874	70.59
0.0045	27.89	11	2271	1326	3597	58.39
0.0050	22.57	8	2271	1122	3393	49.41
0.0055	25.23	11	2271	937	3208	41.26
0.0060	14.57	4	2271	905	3176	39.85
0.0065	26.18	14	2271	537	2808	23.65
0.0070	25.23	14	2271	426	2697	18.76
0.0075	21.61	11	2271	308	2579	13.56
0.0080	12.62	4	2271	567	2838	24.97
0.0085	22.90	14	2271	180	2451	7.93
0.0090	14.57	6	2271	275	2546	12.11
0.0095	15.31	7	2271	169	2440	7.44
0.0100	14.93	7	2271	128	2399	5.64

Table A. 15 *- Results of the calibration step for the Calabria region at 1-h duration, In particular, for each value of ρ, the number of observed (OD), reconstructed (RD) and total (TD) data and the percentage ratio between RD and OD is reported.*

ρ	**R [km]**	**N**	**Observed Data (OD)**	**Reconstructed Data (RD)**	**Total Data (TD)**	**Ratio RD/OD [%]**
0.0005	66.76	7	3163	6453	9616	204.02
0.0010	64.33	13	3163	5860	9023	185.27
0.0015	54.51	14	3163	5027	8190	158.93
0.0020	45.49	13	3163	4218	7381	133.35
0.0025	22.57	4	3163	3998	7161	126.40
0.0030	27.25	7	3163	3064	6227	96.87
0.0035	28.61	9	3163	2204	5367	69.68
0.0040	19.95	5	3163	2159	5322	68.26
0.0045	16.82	4	3163	1818	4981	57.48
0.0050	17.84	5	3163	1404	4567	44.39

0.0055	27.43	13	3163	567	3730	17.93
0.0060	14.57	4	3163	1092	4255	34.52
0.0065	15.65	5	3163	697	3860	22.04
0.0070	15.08	5	3163	586	3749	18.53
0.0075	14.57	5	3163	481	3644	15.21
0.0080	16.69	7	3163	304	3467	9.61
0.0085	18.36	9	3163	181	3344	5.72
0.0090	11.89	4	3163	414	3577	13.09
0.0095	11.58	4	3163	319	3482	10.09
0.0100	11.28	4	3163	260	3423	8.22

Table A. 16 - *Results of the calibration step for the Calabria region at 3-h duration, In particular, for each value of ρ, the number of observed (OD), reconstructed (RD) and total (TD) data and the percentage ratio between RD and OD is reported.*

ρ	**R [km]**	**N**	**Observed Data (OD)**	**Reconstructed Data (RD)**	**Total Data (TD)**	**Ratio RD/OD [%]**
0.0005	66.76	7	3161	6455	9616	204.21
0.0010	61.80	12	3161	5923	9084	187.38
0.0015	54.51	14	3161	5020	8181	158.81
0.0020	41.84	11	3161	4331	7492	137.01
0.0025	35.68	10	3161	3551	6712	112.34
0.0030	37.14	13	3161	2470	5631	78.14
0.0035	28.61	9	3161	2202	5363	69.66
0.0040	19.95	5	3161	2154	5315	68.14
0.0045	16.82	4	3161	1818	4979	57.51
0.0050	17.84	5	3161	1401	4562	44.32
0.0055	17.01	5	3161	1156	4317	36.57
0.0060	16.29	5	3161	910	4071	28.79
0.0065	20.99	9	3161	473	3634	14.96
0.0070	15.08	5	3161	586	3747	18.54
0.0075	14.57	5	3161	481	3642	15.22
0.0080	15.45	6	3161	309	3470	9.78
0.0085	16.19	7	3161	223	3384	7.05
0.0090	21.44	13	3161	84	3245	2.66

0.0095	20.05	12	3161	76	3237	2.40
0.0100	19.54	12	3161	59	3220	1.87

Table A. 17 *- Results of the calibration step for the Calabria region at 6-h duration, In particular, for each value of ρ, the number of observed (OD), reconstructed (RD) and total (TD) data and the percentage ratio between RD and OD is reported.*

ρ	**R [km]**	**N**	**Observed Data (OD)**	**Reconstructed Data (RD)**	**Total Data (TD)**	**Ratio RD/OD [%]**
0.0005	66.76	7	3162	6454	9616	204.11
0.0010	56.42	10	3162	6019	9181	190.35
0.0015	29.13	4	3162	5440	8602	172.04
0.0020	41.84	11	3162	4335	7497	137.10
0.0025	35.68	10	3162	3556	6718	112.46
0.0030	37.14	13	3162	2472	5634	78.18
0.0035	21.32	5	3162	2607	5769	82.45
0.0040	21.85	6	3162	2050	5212	64.83
0.0045	18.81	5	3162	1760	4922	55.66
0.0050	17.84	5	3162	1402	4564	44.34
0.0055	18.63	6	3162	1082	4244	34.22
0.0060	21.85	9	3162	601	3763	19.01
0.0065	20.99	9	3162	473	3635	14.96
0.0070	15.08	5	3162	585	3747	18.50
0.0075	15.96	6	3162	446	3608	14.10
0.0080	14.10	5	3162	398	3560	12.59
0.0085	17.31	8	3162	187	3349	5.91
0.0090	21.44	13	3162	84	3246	2.66
0.0095	21.66	14	3162	57	3219	1.80
0.0100	19.54	12	3162	59	3221	1.87

Table A. 18 *- Results of the calibration step for the Calabria region at 12-h duration, In particular, for each value of ρ, the number of observed (OD), reconstructed (RD) and total (TD) data and the percentage ratio between RD and OD is reported.*

ρ	R [km]	N	Observed Data (OD)	Reconstructed Data (RD)	Total Data (TD)	Ratio RD/OD [%]
0.0005	75.69	9	3162	6447	9609	203.89
0.0010	39.89	5	3162	6126	9288	193.74
0.0015	29.13	4	3162	5440	8602	172.04
0.0020	48.86	15	3162	4108	7270	129.92
0.0025	35.68	10	3162	3556	6718	112.46
0.0030	37.14	13	3162	2472	5634	78.18
0.0035	25.23	7	3162	2325	5487	73.53
0.0040	23.60	7	3162	1833	4995	57.97
0.0045	16.82	4	3162	1818	4980	57.50
0.0050	26.46	11	3162	818	3980	25.87
0.0055	18.63	6	3162	1082	4244	34.22
0.0060	14.57	4	3162	1091	4253	34.50
0.0065	15.65	5	3162	696	3858	22.01
0.0070	15.08	5	3162	585	3747	18.50
0.0075	15.96	6	3162	446	3608	14.10
0.0080	16.69	7	3162	304	3466	9.61
0.0085	16.19	7	3162	225	3387	7.12
0.0090	21.44	13	3162	84	3246	2.66
0.0095	20.05	12	3162	76	3238	2.40
0.0100	18.71	11	3162	74	3236	2.34

Table A. 19 *- Results of the calibration step for the Calabria region at 24-h duration, In particular, for each value of ρ, the number of observed (OD), reconstructed (RD) and total (TD) data and the percentage ratio between RD and OD is reported.*

ρ	R [km]	N	Observed Data (OD)	Reconstructed Data (RD)	Total Data (TD)	Ratio RD/OD [%]
0.0005	66.76	7	3161	6455	9616	204.21
0.0010	39.89	5	3161	6127	9288	193.83

0.0015	35.68	6	3161	5380	8541	170.20
0.0020	43.70	12	3161	4252	7413	134.51
0.0025	43.70	15	3161	3190	6351	100.92
0.0030	37.14	13	3161	2471	5632	78.17
0.0035	26.97	8	3161	2264	5425	71.62
0.0040	19.95	5	3161	2153	5314	68.11
0.0045	18.81	5	3161	1757	4918	55.58
0.0050	19.54	6	3161	1302	4463	41.19
0.0055	18.63	6	3161	1081	4242	34.20
0.0060	21.85	9	3161	601	3762	19.01
0.0065	20.99	9	3161	473	3634	14.96
0.0070	15.08	5	3161	584	3745	18.48
0.0075	15.96	6	3161	446	3607	14.11
0.0080	15.45	6	3161	309	3470	9.78
0.0085	17.31	8	3161	187	3348	5.92
0.0090	16.82	8	3161	134	3295	4.24
0.0095	17.37	9	3161	90	3251	2.85
0.0100	16.93	9	3161	72	3233	2.28

Table A. 20 *- Results of the calibration step for the Campania region at 1-h duration, In particular, for each value of ρ, the number of observed (OD), reconstructed (RD) and total (TD) data and the percentage ratio between RD and OD is reported.*

ρ	**R [km]**	**N**	**Observed Data (OD)**	**Reconstructed Data (RD)**	**Total Data (TD)**	**Ratio RD/OD [%]**
0.0005	97.72	15	5044	11936	16980	236.64
0.0010	61.80	12	5044	11635	16679	230.67
0.0015	43.70	9	5044	10947	15991	217.03
0.0020	25.23	4	5044	10352	15396	205.23
0.0025	42.22	14	5044	9546	14590	189.25
0.0030	39.89	15	5044	8766	13810	173.79
0.0035	35.68	14	5044	8109	13153	160.77
0.0040	30.90	12	5044	7502	12546	148.73
0.0045	25.23	9	5044	6910	11954	136.99
0.0050	22.57	8	5044	6348	11392	125.85

0.0055	28.46	14	5044	5100	10144	101.11
0.0060	16.29	5	5044	5379	10423	106.64
0.0065	18.51	7	5044	4549	9593	90.19
0.0070	17.84	7	5044	3939	8983	78.09
0.0075	17.24	7	5044	3463	8507	68.66
0.0080	16.69	7	5044	3095	8139	61.36
0.0085	13.68	5	5044	3186	8230	63.16
0.0090	15.73	7	5044	2467	7511	48.91
0.0095	12.94	5	5044	2656	7700	52.66
0.0100	11.28	4	5044	2738	7782	54.28
0.0105	11.01	4	5044	2552	7596	50.59
0.0110	10.76	4	5044	2313	7357	45.86
0.0115	10.52	4	5044	2130	7174	42.23
0.0120	10.30	4	5044	1967	7011	39.00
0.0125	10.09	4	5044	1864	6908	36.95
0.0130	9.90	4	5044	1766	6810	35.01
0.0135	9.71	4	5044	1638	6682	32.47
0.0140	9.54	4	5044	1551	6595	30.75
0.0145	9.37	4	5044	1454	6498	28.83
0.0150	9.21	4	5044	1436	6480	28.47

Table A. 21 *- Results of the calibration step for the Campania region at 3-h duration, In particular, for each value of ρ, the number of observed (OD), reconstructed (RD) and total (TD) data and the percentage ratio between RD and OD is reported.*

ρ	**R [km]**	**N**	**Observed Data (OD)**	**Reconstructed Data (RD)**	**Total Data (TD)**	**Ratio RD/OD [%]**
0.0005	87.40	12	5046	11930	16976	236.42
0.0010	64.33	13	5046	11648	16694	230.84
0.0015	56.42	15	5046	11066	16112	219.30
0.0020	47.20	14	5046	10308	15354	204.28
0.0025	42.22	14	5046	9541	14587	189.08
0.0030	39.89	15	5046	8761	13807	173.62
0.0035	31.63	11	5046	8206	13252	162.62
0.0040	26.76	9	5046	7558	12604	149.78

0.0045	26.60	10	5046	6850	11896	135.75
0.0050	21.11	7	5046	6342	11388	125.68
0.0055	28.46	14	5046	5097	10143	101.01
0.0060	14.57	4	5046	5426	10472	107.53
0.0065	17.14	6	5046	4660	9706	92.35
0.0070	15.08	5	5046	4309	9355	85.39
0.0075	17.24	7	5046	3468	8514	68.73
0.0080	14.10	5	5046	3484	8530	69.04
0.0085	13.68	5	5046	3186	8232	63.14
0.0090	13.30	5	5046	2936	7982	58.18
0.0095	12.94	5	5046	2659	7705	52.70
0.0100	11.28	4	5046	2732	7778	54.14
0.0105	11.01	4	5046	2549	7595	50.52
0.0110	10.76	4	5046	2313	7359	45.84
0.0115	10.52	4	5046	2129	7175	42.19
0.0120	10.30	4	5046	1966	7012	38.96
0.0125	10.09	4	5046	1862	6908	36.90
0.0130	9.90	4	5046	1763	6809	34.94
0.0135	9.71	4	5046	1634	6680	32.38
0.0140	9.54	4	5046	1548	6594	30.68
0.0145	9.37	4	5046	1454	6500	28.81
0.0150	9.21	4	5046	1436	6482	28.46

Table A. 22 *- Results of the calibration step for the Campania region at 6-h duration, In particular, for each value of ρ, the number of observed (OD), reconstructed (RD) and total (TD) data and the percentage ratio between RD and OD is reported.*

ρ	**R [km]**	**N**	**Observed Data (OD)**	**Reconstructed Data (RD)**	**Total Data (TD)**	**Ratio RD/OD [%]**
0.0005	87.40	12	5049	11927	16976	236.22
0.0010	35.68	4	5049	11481	16530	227.39
0.0015	43.70	9	5049	10943	15992	216.74
0.0020	41.84	11	5049	10317	15366	204.34
0.0025	42.22	14	5049	9514	14563	188.43
0.0030	30.90	9	5049	8995	14044	178.15

0.0035	36.93	15	5049	8038	13087	159.20
0.0040	26.76	9	5049	7543	12592	149.40
0.0045	22.25	7	5049	7067	12116	139.97
0.0050	17.84	5	5049	6557	11606	129.87
0.0055	18.63	6	5049	5837	10886	115.61
0.0060	14.57	4	5049	5428	10477	107.51
0.0065	17.14	6	5049	4668	9717	92.45
0.0070	15.08	5	5049	4320	9369	85.56
0.0075	17.24	7	5049	3484	8533	69.00
0.0080	14.10	5	5049	3493	8542	69.18
0.0085	13.68	5	5049	3196	8245	63.30
0.0090	13.30	5	5049	2944	7993	58.31
0.0095	12.94	5	5049	2668	7717	52.84
0.0100	11.28	4	5049	2737	7786	54.21
0.0105	11.01	4	5049	2554	7603	50.58
0.0110	10.76	4	5049	2316	7365	45.87
0.0115	10.52	4	5049	2129	7178	42.17
0.0120	10.30	4	5049	1966	7015	38.94
0.0125	12.36	6	5049	1366	6415	27.05
0.0130	9.90	4	5049	1765	6814	34.96
0.0135	9.71	4	5049	1636	6685	32.40
0.0140	9.54	4	5049	1549	6598	30.68
0.0145	11.48	6	5049	1040	6089	20.60
0.0150	9.21	4	5049	1436	6485	28.44

Table A. 23 *- Results of the calibration step for the Campania region at 12-h duration, In particular, for each value of ρ, the number of observed (OD), reconstructed (RD) and total (TD) data and the percentage ratio between RD and OD is reported.*

ρ	**R [km]**	**N**	**Observed Data (OD)**	**Reconstructed Data (RD)**	**Total Data (TD)**	**Ratio RD/OD [%]**
0.0005	94.41	14	5049	11932	16981	236.32
0.0010	66.76	14	5049	11654	16703	230.82
0.0015	32.57	5	5049	11000	16049	217.86
0.0020	25.23	4	5049	10344	15393	204.87

0.0025	42.22	14	5049	9526	14575	188.67
0.0030	37.14	13	5049	8828	13877	174.85
0.0035	19.07	4	5049	8507	13556	168.49
0.0040	17.84	4	5049	7857	12906	155.61
0.0045	22.25	7	5049	7066	12115	139.95
0.0050	15.96	4	5049	6615	11664	131.02
0.0055	18.63	6	5049	5834	10883	115.55
0.0060	14.57	4	5049	5426	10475	107.47
0.0065	15.65	5	5049	4804	9853	95.15
0.0070	16.52	6	5049	4196	9245	83.11
0.0075	13.03	4	5049	4182	9231	82.83
0.0080	14.10	5	5049	3492	8541	69.16
0.0085	13.68	5	5049	3195	8244	63.28
0.0090	13.30	5	5049	2941	7990	58.25
0.0095	14.18	6	5049	2413	7462	47.79
0.0100	11.28	4	5049	2740	7789	54.27
0.0105	11.01	4	5049	2558	7607	50.66
0.0110	10.76	4	5049	2320	7369	45.95
0.0115	10.52	4	5049	2131	7180	42.21
0.0120	12.62	6	5049	1496	6545	29.63
0.0125	10.09	4	5049	1866	6915	36.96
0.0130	9.90	4	5049	1767	6816	35.00
0.0135	9.71	4	5049	1637	6686	32.42
0.0140	11.68	6	5049	1099	6148	21.77
0.0145	11.48	6	5049	1041	6090	20.62
0.0150	9.21	4	5049	1437	6486	28.46

Table A. 24 *- Results of the calibration step for the Campania region at 24-h duration, In particular, for each value of ρ, the number of observed (OD), reconstructed (RD) and total (TD) data and the percentage ratio between RD and OD is reported.*

ρ	**R [km]**	**N**	**Observed Data (OD)**	**Reconstructed Data (RD)**	**Total Data (TD)**	**Ratio RD/OD [%]**
0.0005	75.69	9	5044	11916	16960	236.24
0.0010	69.10	15	5044	11666	16710	231.28

0.0015	41.20	8	5044	10964	16008	217.37
0.0020	41.84	11	5044	10332	15376	204.84
0.0025	27.64	6	5044	9720	14764	192.70
0.0030	23.03	5	5044	9080	14124	180.02
0.0035	19.07	4	5044	8505	13549	168.62
0.0040	17.84	4	5044	7857	12901	155.77
0.0045	22.25	7	5044	7068	12112	140.13
0.0050	19.54	6	5044	6490	11534	128.67
0.0055	18.63	6	5044	5841	10885	115.80
0.0060	14.57	4	5044	5426	10470	107.57
0.0065	14.00	4	5044	4906	9950	97.26
0.0070	13.49	4	5044	4535	9579	89.91
0.0075	14.57	5	5044	3921	8965	77.74
0.0080	14.10	5	5044	3500	8544	69.39
0.0085	13.68	5	5044	3204	8248	63.52
0.0090	14.57	6	5044	2698	7742	53.49
0.0095	12.94	5	5044	2674	7718	53.01
0.0100	13.82	6	5044	2170	7214	43.02
0.0105	13.49	6	5044	2037	7081	40.38
0.0110	10.76	4	5044	2322	7366	46.03
0.0115	10.52	4	5044	2132	7176	42.27
0.0120	12.62	6	5044	1500	6544	29.74
0.0125	13.35	7	5044	1288	6332	25.54
0.0130	14.00	8	5044	1104	6148	21.89
0.0135	14.57	9	5044	983	6027	19.49
0.0140	14.30	9	5044	940	5984	18.64
0.0145	12.40	7	5044	1000	6044	19.83
0.0150	12.19	7	5044	957	6001	18.97

Table A. 25 *- Results of the calibration step for the Molise region at 1-h duration, In particular, for each value of ρ, the number of observed (OD), reconstructed (RD) and total (TD) data and the percentage ratio between RD and OD is reported.*

ρ	**R [km]**	**N**	**Observed Data (OD)**	**Reconstructed Data (RD)**	**Total Data (TD)**	**Ratio RD/OD [%]**

0.0005	56.42	5	1343	2362	3705	175.87
0.0010	56.42	10	1343	2326	3669	173.19
0.0015	52.52	13	1343	2270	3613	169.02
0.0020	43.70	12	1343	2160	3503	160.83
0.0025	42.22	14	1343	1927	3270	143.48
0.0030	23.03	5	1343	1805	3148	134.40
0.0035	35.68	14	1343	1485	2828	110.57
0.0040	21.85	6	1343	1424	2767	106.03
0.0045	23.79	8	1343	1187	2530	88.38
0.0050	23.94	9	1343	1012	2355	75.35
0.0055	28.46	14	1343	791	2134	58.90
0.0060	26.26	13	1343	666	2009	49.59
0.0065	23.21	11	1343	585	1928	43.56
0.0070	21.32	10	1343	422	1765	31.42
0.0075	25.23	15	1343	241	1584	17.94
0.0080	20.92	11	1343	236	1579	17.57
0.0085	13.68	5	1343	324	1667	24.13
0.0090	22.25	14	1343	64	1407	4.77
0.0095	12.94	5	1343	263	1606	19.58
0.0100	11.28	4	1343	293	1636	21.82

Table A. 26 - *Results of the calibration step for the Molise region at 3-h duration, In particular, for each value of ρ, the number of observed (OD), reconstructed (RD) and total (TD) data and the percentage ratio between RD and OD is reported.*

ρ	**R [km]**	**N**	**Observed Data (OD)**	**Reconstructed Data (RD)**	**Total Data (TD)**	**Ratio RD/OD [%]**
0.0005	50.46	4	1343	2345	3688	174.61
0.0010	47.20	7	1343	2299	3642	171.18
0.0015	52.52	13	1343	2270	3613	169.02
0.0020	43.70	12	1343	2160	3503	160.83
0.0025	29.85	7	1343	1963	3306	146.17
0.0030	35.68	12	1343	1715	3058	127.70
0.0035	33.04	12	1343	1501	2844	111.76

0.0040	30.90	12	1343	1312	2655	97.69
0.0045	26.60	10	1343	1189	2532	88.53
0.0050	30.90	15	1343	931	2274	69.32
0.0055	28.46	14	1343	793	2136	59.05
0.0060	28.21	15	1343	619	1962	46.09
0.0065	14.00	4	1343	761	2104	56.66
0.0070	22.37	11	1343	409	1752	30.45
0.0075	13.03	4	1343	619	1962	46.09
0.0080	18.92	9	1343	291	1634	21.67
0.0085	22.06	13	1343	160	1503	11.91
0.0090	21.44	13	1343	115	1458	8.56
0.0095	11.58	4	1343	384	1727	28.59
0.0100	11.28	4	1343	293	1636	21.82

Table A. 27 - *Results of the calibration step for the Molise region at 6-h duration, In particular, for each value of ρ, the number of observed (OD), reconstructed (RD) and total (TD) data and the percentage ratio between RD and OD is reported.*

ρ	**R [km]**	**N**	**Observed Data (OD)**	**Reconstructed Data (RD)**	**Total Data (TD)**	**Ratio RD/OD [%]**
0.0005	50.46	4	1343	2345	3688	174.61
0.0010	35.68	4	1343	2276	3619	169.47
0.0015	35.68	6	1343	2214	3557	164.85
0.0020	30.90	6	1343	2095	3438	155.99
0.0025	29.85	7	1343	1963	3306	146.17
0.0030	20.60	4	1343	1799	3142	133.95
0.0035	30.16	10	1343	1549	2892	115.34
0.0040	30.90	12	1343	1313	2656	97.77
0.0045	31.47	14	1343	1124	2467	83.69
0.0050	26.46	11	1343	1019	2362	75.87
0.0055	27.43	13	1343	812	2155	60.46
0.0060	27.25	14	1343	629	1972	46.84
0.0065	20.99	9	1343	558	1901	41.55
0.0070	20.23	9	1343	472	1815	35.15
0.0075	13.03	4	1343	619	1962	46.09

0.0080	12.62	4	1343	546	1889	40.66
0.0085	23.70	15	1343	73	1416	5.44
0.0090	11.89	4	1343	444	1787	33.06
0.0095	11.58	4	1343	384	1727	28.59
0.0100	11.28	4	1343	293	1636	21.82

Table A. 28 *- Results of the calibration step for the Molise region at 12-h duration, In particular, for each value of ρ, the number of observed (OD), reconstructed (RD) and total (TD) data and the percentage ratio between RD and OD is reported.*

ρ	**R [km]**	**N**	**Observed Data (OD)**	**Reconstructed Data (RD)**	**Total Data (TD)**	**Ratio RD/OD [%]**
0.0005	50.46	4	1343	2345	3688	174.61
0.0010	39.89	5	1343	2285	3628	170.14
0.0015	35.68	6	1343	2214	3557	164.85
0.0020	30.90	6	1343	2095	3438	155.99
0.0025	27.64	6	1343	1987	3330	147.95
0.0030	35.68	12	1343	1717	3060	127.85
0.0035	30.16	10	1343	1549	2892	115.34
0.0040	21.85	6	1343	1425	2768	106.11
0.0045	31.47	14	1343	1125	2468	83.77
0.0050	29.85	14	1343	944	2287	70.29
0.0055	20.13	7	1343	829	2172	61.73
0.0060	27.25	14	1343	630	1973	46.91
0.0065	19.79	8	1343	568	1911	42.29
0.0070	20.23	9	1343	472	1815	35.15
0.0075	13.03	4	1343	619	1962	46.09
0.0080	24.43	15	1343	161	1504	11.99
0.0085	12.24	4	1343	514	1857	38.27
0.0090	11.89	4	1343	444	1787	33.06
0.0095	11.58	4	1343	384	1727	28.59
0.0100	11.28	4	1343	293	1636	21.82

Table A. 29 - *Results of the calibration step for the Molise region at 24-h duration, In particular, for each value of ρ, the number of observed (OD), reconstructed (RD) and total (TD) data and the percentage ratio between RD and OD is reported.*

ρ	**R [km]**	**N**	**Observed Data (OD)**	**Reconstructed Data (RD)**	**Total Data (TD)**	**Ratio RD/OD [%]**
0.0005	50.46	4	1343	2345	3688	174.61
0.0010	39.89	5	1343	2285	3628	170.14
0.0015	54.51	14	1343	2277	3620	169.55
0.0020	25.23	4	1343	2086	3429	155.32
0.0025	25.23	5	1343	1937	3280	144.23
0.0030	30.90	9	1343	1771	3114	131.87
0.0035	19.07	4	1343	1633	2976	121.59
0.0040	28.21	10	1343	1366	2709	101.71
0.0045	31.47	14	1343	1124	2467	83.69
0.0050	29.85	14	1343	944	2287	70.29
0.0055	20.13	7	1343	829	2172	61.73
0.0060	19.27	7	1343	737	2080	54.88
0.0065	17.14	6	1343	659	2002	49.07
0.0070	13.49	4	1343	681	2024	50.71
0.0075	25.23	15	1343	241	1584	17.94
0.0080	12.62	4	1343	546	1889	40.66
0.0085	12.24	4	1343	514	1857	38.27
0.0090	21.44	13	1343	115	1458	8.56
0.0095	11.58	4	1343	384	1727	28.59
0.0100	11.28	4	1343	293	1636	21.82

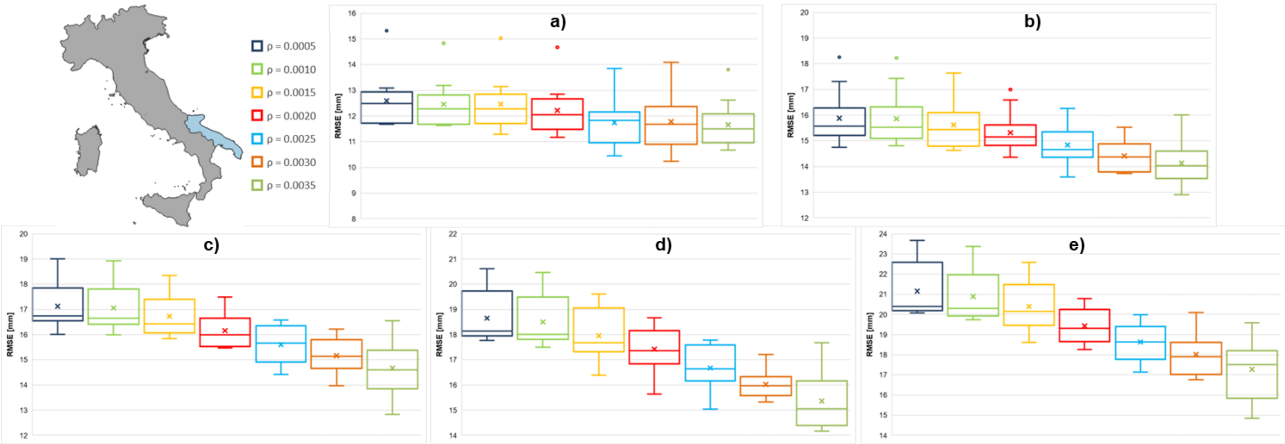

Figure A. 1 - *Box-plot of RMSE (root mean square error) values in relation to ρ (minimum density of rainfall stations required to perform the reconstruction) for the Apulia region and for each considered duration: a) 1h, b) 3h, c) 6h, d) 12h, e) 24h. The box-plot provides the representation of the following statistics: maximum and minimum (whiskers), 75th percentile and 25th percentile (rectangle edges), median or 50th percentile (horizontal line in the rectangle), mean (x symbol), outliers (o symbol).*

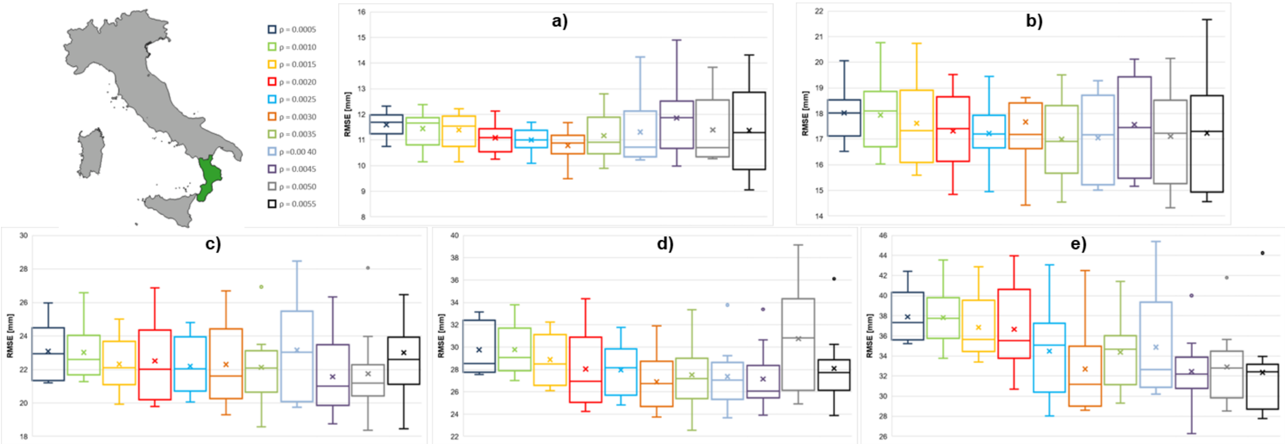

Figure A. 2 - *Box-plot of RMSE (root mean square error) values in relation to ρ (minimum density of rainfall stations required to perform the reconstruction) for the Calabria region and for each considered duration: a) 1h, b) 3h, c) 6h, d) 12h, e) 24h. The box-plot provides the representation of the following statistics: maximum and minimum (whiskers), 75th percentile and 25th percentile (rectangle edges), median or 50th percentile (horizontal line in the rectangle), mean (x symbol), outliers (o symbol).*

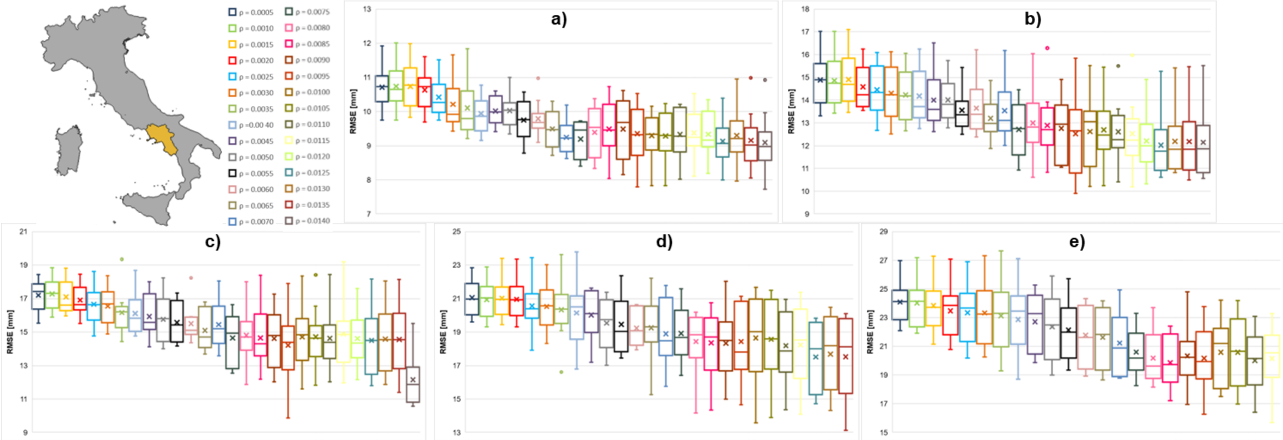

Figure A. 3 *- Box-plot of RMSE (root mean square error) values in relation to ρ (minimum density of rainfall stations required to perform the reconstruction) for the Campania region and for each considered duration: a) 1h, b) 3h, c) 6h, d) 12h, e) 24h. The box-plot provides the representation of the following statistics: maximum and minimum (whiskers), 75th percentile and 25th percentile (rectangle edges), median or 50th percentile (horizontal line in the rectangle), mean (x symbol), outliers (o symbol).*

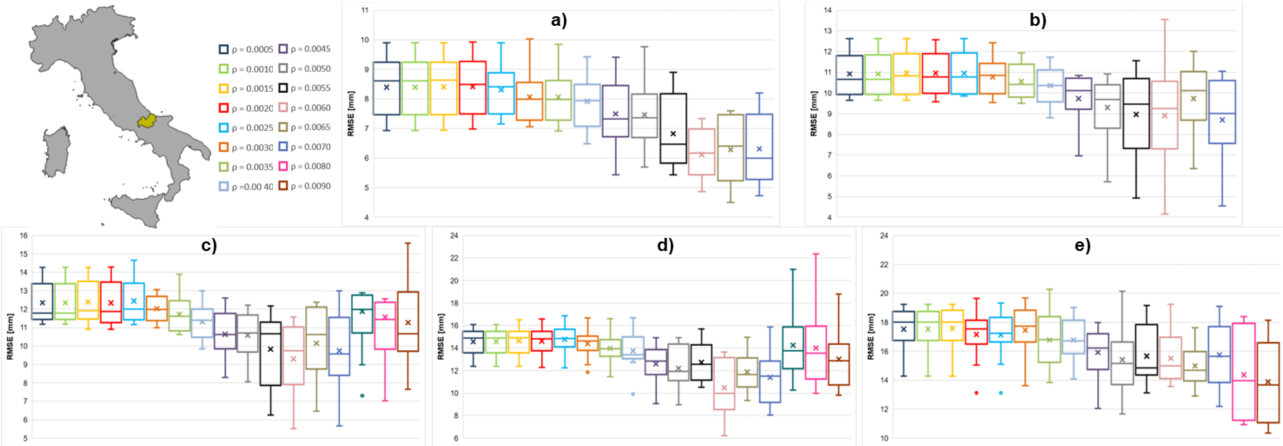

Figure A. 4 *- Box-plot of RMSE (root mean square error) values in relation to ρ (minimum density of rainfall stations required to perform the reconstruction) for the Molise region and for each considered duration: a) 1h, b) 3h, c) 6h, d) 12h, e) 24h. The box-plot provides the representation of the following statistics: maximum and minimum (whiskers), 75th percentile and 25th percentile (rectangle edges), median or 50th percentile (horizontal line in the rectangle), mean (x symbol), outliers (o symbol).*

Appendix B: The Hourly Rainfall Database for Southern Italy

In this section the detailed number of data (before and after the reconstruction with the SC-OK method) per year per duration is reported.

Table B. 1 *- Number of data per year for each duration before and after the reconstruction for Apulia region*

	Database before reconstruction					Database after reconstruction				
d [h]	1	3	6	12	24	1	3	6	12	24
1970	97	97	97	97	97	129	126	131	131	125
1971	96	96	96	96	96	128	123	126	126	124
1972	91	91	91	91	91	128	124	125	125	127
1973	89	89	89	89	89	121	120	120	120	119
1974	100	104	105	106	106	133	137	138	140	143
1975	95	98	100	106	106	128	133	133	135	135
1976	94	97	99	99	96	128	128	128	127	130
1977	107	107	107	107	108	135	136	135	137	136
1978	97	96	96	95	95	133	126	125	123	128
1979	105	106	107	106	106	141	140	139	138	138
1980	99	99	99	99	99	135	132	132	132	134
1981	106	106	106	106	106	135	133	135	135	136
1982	92	96	99	100	100	126	127	130	131	132
1983	91	92	93	95	96	124	119	119	122	124
1984	89	91	89	88	90	125	121	116	115	123
1985	82	83	89	91	93	120	117	126	126	128
1986	89	90	89	92	93	132	127	126	129	130
1987	85	88	89	92	93	116	111	113	118	122
1988	82	89	93	91	92	119	123	128	123	125
1989	93	94	91	91	94	124	127	121	122	125
1990	89	92	93	95	95	121	119	122	124	129
1991	93	96	97	96	96	127	124	123	123	125
1992	92	92	98	97	96	120	122	129	127	128
1993	86	88	90	91	92	114	117	117	120	123
1994	78	83	87	93	99	109	115	115	115	126
1995	80	79	81	84	86	109	104	107	113	117
1996	105	105	103	103	105	138	132	130	134	141

1997	91	94	96	102	107	130	125	124	129	135
1998	106	106	105	105	105	137	136	132	132	134
1999	106	106	107	108	109	141	139	136	138	140
2000	112	112	112	112	112	144	142	140	140	143
2001	108	109	109	109	109	140	141	141	141	142
2002	115	115	115	115	115	146	143	145	145	145
2003	107	107	107	107	107	142	138	139	139	141
2004	103	103	103	103	103	135	134	136	136	135
2005	94	94	94	94	94	129	123	123	123	124
2006	92	92	92	92	92	127	122	122	122	123
2007	91	91	91	91	91	123	119	119	119	120
2008	94	93	94	94	94	129	127	128	128	129
2009	91	92	92	92	94	124	127	128	128	128
2010	120	120	120	120	120	144	144	145	145	145
2011	123	123	123	123	123	145	147	146	146	147
2012	115	115	115	115	115	138	139	139	139	140
2013	115	115	115	116	116	137	140	141	142	143
2014	129	129	129	129	129	149	152	152	152	152
2015	130	130	130	130	130	149	152	151	151	152
2016	128	128	128	128	128	148	150	150	150	150
2017	135	135	135	135	135	153	155	155	155	155
2018	139	139	139	139	139	156	156	155	155	155
2019	135	135	135	135	135	154	154	154	154	153
2020	128	128	128	128	128	152	152	151	151	152

Table B. 2 *- Number of data per year for each duration before and after the reconstruction for Basilicata region*

	Database before reconstruction					**Database after reconstruction**				
d [h]	1	3	6	12	24	1	3	6	12	24
1970	44	44	44	44	44	56	86	54	54	52
1971	43	43	43	43	43	56	89	57	57	53
1972	40	40	40	40	40	50	79	51	51	48
1973	16	16	16	16	16	21	30	21	21	18
1974	22	22	23	23	23	28	35	30	30	29
1975	27	27	27	26	26	34	50	36	33	34

1976	21	21	22	22	22	23	45	30	30	30
1977	25	24	24	23	23	32	51	29	27	25
1978	30	30	30	30	30	39	54	37	37	41
1979	20	20	20	20	20	26	45	26	26	25
1980	18	18	18	18	18	23	32	23	23	21
1981	24	24	24	24	24	31	52	33	33	30
1982	27	27	27	27	28	34	58	35	36	41
1983	15	15	15	15	15	16	39	15	15	16
1984	18	19	18	16	14	24	41	25	19	14
1985	18	18	19	19	19	22	44	22	22	22
1986	26	26	25	25	24	34	50	34	34	29
1987	18	18	17	18	18	22	29	20	23	22
1988	21	23	25	25	25	23	35	33	33	30
1989	10	9	9	9	9	16	18	13	13	12
1990	13	13	13	13	13	20	26	20	20	20
1991	14	15	15	15	14	14	29	15	15	14
1992	20	21	21	21	21	24	32	26	26	27
1993	20	20	21	24	24	23	40	26	33	30
1994	23	23	23	23	23	26	40	28	28	28
1995	27	27	28	28	28	34	45	35	35	36
1996	27	28	26	26	26	37	48	34	34	33
1997	24	24	24	24	24	30	37	30	30	29
1998	29	30	30	30	30	39	51	38	38	42
1999	41	41	41	41	41	52	70	53	53	52
2000	39	39	39	39	39	47	68	49	49	47
2001	53	53	53	53	53	69	104	71	71	77
2002	60	60	60	60	60	83	121	85	85	87
2003	54	54	54	54	54	77	127	79	79	76
2004	66	66	66	66	66	97	139	100	100	99
2005	67	67	67	67	67	97	139	101	101	108
2006	76	76	76	76	76	109	132	111	111	114
2007	76	76	76	76	76	118	142	117	117	118
2008	66	66	66	66	66	99	135	106	106	101
2009	78	78	78	78	78	116	139	117	117	123
2010	80	80	80	80	80	113	143	120	120	123

2011	74	74	74	74	74	117	143	115	115	122
2012	81	81	81	81	81	120	143	123	123	125
2013	75	75	75	75	75	109	139	111	111	117
2014	77	77	77	77	77	108	137	112	112	117
2015	77	77	77	77	77	106	137	105	105	109
2016	90	90	90	90	90	130	141	132	132	131
2017	80	80	80	80	80	120	141	122	122	125
2018	92	92	92	92	92	124	139	125	125	127
2019	95	95	95	95	95	131	141	132	132	131
2020	90	90	90	90	90	128	141	129	129	128

Table B. 3 *- Number of data per year for each duration before and after the reconstruction for Calabria region*

	Database before reconstruction					**Database after reconstruction**				
d [h]	1	3	6	12	24	1	3	6	12	24
1970	72	72	72	72	72	167	152	121	103	156
1971	78	78	78	78	78	168	157	129	107	165
1972	67	67	67	67	67	151	125	107	92	133
1973	40	39	39	39	39	78	55	52	46	44
1974	41	41	41	41	41	87	66	65	53	65
1975	27	27	27	27	27	30	27	29	28	27
1976	1	1	1	1	1	1	1	1	1	1
1977	48	48	48	48	48	92	73	73	58	82
1978	60	60	60	60	60	140	117	105	81	121
1979	62	62	62	62	62	146	123	106	81	120
1980	67	67	67	67	67	158	122	107	91	128
1981	55	55	55	55	55	110	87	83	69	89
1982	58	58	58	58	58	124	103	88	75	107
1983	57	57	57	57	57	126	92	89	75	100
1984	51	51	51	51	51	99	74	73	66	81
1985	46	46	46	46	46	76	56	61	56	58
1986	52	52	52	52	51	97	76	70	67	64
1987	45	44	45	45	45	77	63	63	54	64
1988	53	53	53	53	53	105	80	83	69	92

1989	6	6	6	6	6	6	6	6	6	6
1990	35	35	35	35	35	55	40	43	43	37
1991	33	33	33	33	33	42	35	36	37	33
1992	45	45	45	45	45	85	75	73	56	79
1993	82	82	82	82	82	159	147	132	110	157
1994	82	82	82	82	82	165	147	131	110	154
1995	88	88	88	88	88	173	155	136	123	169
1996	84	84	84	84	84	163	144	131	114	156
1997	80	80	80	80	80	163	140	121	106	153
1998	63	63	63	63	63	130	104	91	77	109
1999	63	63	63	63	63	131	105	93	75	110
2000	66	66	66	66	66	141	111	98	82	122
2001	61	61	61	61	61	129	102	95	80	117
2002	80	80	80	80	80	172	158	138	113	165
2003	102	102	102	102	102	184	176	165	145	185
2004	104	104	104	104	104	189	184	171	144	188
2005	91	91	91	91	91	180	169	153	131	173
2006	69	69	69	69	69	143	122	116	99	135
2007	77	77	77	77	77	160	140	124	115	156
2008	79	79	79	79	79	156	144	130	113	150
2009	78	78	78	78	78	163	146	129	112	152
2010	79	79	79	79	79	160	144	128	114	149
2011	96	96	96	96	96	174	162	151	135	170
2012	94	94	94	94	94	172	157	150	134	168
2013	86	86	86	86	87	148	143	132	118	148
2014	82	82	82	82	82	137	132	121	113	138
2015	93	93	93	93	92	152	147	139	129	146
2016	64	64	64	64	64	137	122	118	93	125
2017	46	46	46	46	46	101	74	72	62	91
2018	31	31	31	31	31	59	33	38	36	39
2019	24	24	24	24	24	38	28	31	32	31
2020	20	20	20	20	20	28	22	25	24	24

Table B. 4 - *Number of data per year for each duration before and after the reconstruction for Campania region*

	Database before reconstruction					**Database after reconstruction**				
d [h]	1	3	6	12	24	1	3	6	12	24
1970	42	41	40	40	40	46	43	45	42	47
1971	63	63	63	63	63	112	80	98	80	104
1972	66	66	66	66	65	119	91	107	91	117
1973	76	76	76	76	75	141	107	122	107	129
1974	81	82	82	82	82	154	113	137	113	146
1975	93	93	93	92	92	184	129	153	128	170
1976	89	89	89	90	90	158	125	144	126	158
1977	101	101	101	101	100	194	151	178	151	187
1978	96	96	96	96	96	174	138	160	138	170
1979	95	96	96	96	96	178	141	163	141	173
1980	91	91	92	92	92	173	128	154	130	169
1981	75	75	75	75	75	121	92	106	92	120
1982	99	100	100	100	100	159	123	149	123	163
1983	98	98	98	98	98	172	124	150	124	164
1984	103	103	103	103	100	191	144	161	144	175
1985	95	95	96	97	97	169	122	136	125	157
1986	69	70	70	70	70	100	85	101	85	108
1987	41	42	41	42	42	50	43	47	43	51
1988	31	31	31	31	31	33	31	33	31	35
1989	29	29	29	29	29	34	32	32	32	34
1990	78	77	78	78	79	134	99	120	100	134
1991	54	54	53	52	52	75	57	63	55	69
1992	43	43	44	44	44	55	47	55	48	60
1993	82	82	84	84	84	119	93	109	95	125
1994	56	56	56	56	57	69	64	66	64	73
1995	64	64	64	64	64	78	69	75	69	81
1996	56	55	56	55	55	76	66	79	66	85
1997	66	66	65	65	65	114	88	101	89	114
1998	71	71	71	71	71	131	96	118	96	131
1999	63	63	63	63	64	136	89	117	89	131
2000	29	29	29	29	29	57	45	51	45	54

2001	75	75	75	75	75	156	127	136	127	144
2002	100	100	100	100	100	182	162	171	162	175
2003	108	108	108	108	108	186	164	172	164	180
2004	103	103	103	103	102	178	161	166	161	174
2005	104	104	104	104	103	181	161	167	161	172
2006	101	101	101	101	101	175	153	161	153	165
2007	109	109	109	109	109	183	165	172	165	176
2008	147	147	147	147	147	236	207	219	207	233
2009	153	153	153	153	153	249	215	231	215	245
2010	159	159	159	159	159	268	223	246	223	261
2011	158	158	158	158	158	269	222	245	222	261
2012	159	159	159	159	159	271	222	245	222	262
2013	158	158	158	158	158	271	222	246	222	262
2014	159	159	159	159	159	270	222	245	222	262
2015	168	168	168	168	168	277	225	247	225	262
2016	178	178	178	178	178	293	241	264	241	278
2017	177	177	177	177	177	289	240	264	240	276
2018	178	178	178	178	178	292	241	266	241	278
2019	176	176	176	176	176	289	239	261	239	274
2020	179	179	179	179	179	286	241	263	241	274

Table B. 5 - *Number of data per year for each duration before and after the reconstruction for Molise region*

	Database before reconstruction					**Database after reconstruction**				
d [h]	1	3	6	12	24	1	3	6	12	24
1970	18	18	18	18	18	18	18	18	18	20
1971	22	22	22	22	22	27	22	29	29	28
1972	19	19	19	19	19	22	23	22	22	24
1973	24	24	24	24	24	36	28	38	38	34
1974	31	31	31	31	31	54	45	53	53	48
1975	26	26	26	26	26	41	33	41	41	38
1976	22	22	22	22	22	28	24	28	28	27
1977	26	26	26	26	26	42	37	41	41	36
1978	16	16	16	16	16	17	18	17	17	21

1979	20	20	20	20	20	30	26	31	31	29
1980	35	35	35	35	35	55	52	57	57	52
1981	30	30	30	30	30	47	36	46	46	40
1982	23	23	23	23	23	37	32	38	38	30
1983	24	24	24	24	24	37	29	37	37	34
1984	26	26	26	26	26	38	32	41	41	35
1985	23	23	23	23	23	38	29	36	36	31
1986	26	26	26	26	26	37	29	37	38	33
1987	22	22	22	22	22	32	28	32	32	29
1988	22	22	22	22	22	28	23	25	25	26
1989	23	23	23	23	23	25	24	26	26	28
1990	27	27	27	27	27	39	31	37	37	35
1991	31	31	31	31	31	46	40	46	46	47
1992	30	30	30	30	30	47	40	47	47	44
1993	24	24	24	24	24	38	36	40	40	30
1994	30	30	30	30	30	44	38	45	45	44
1995	25	25	25	25	25	37	34	37	37	36
1996	28	28	28	28	28	43	38	43	43	37
1997	31	31	31	31	31	46	41	47	47	42
1998	33	33	33	33	33	53	44	49	49	48
1999	30	30	30	30	30	47	40	46	46	40
2000	29	29	29	29	29	41	38	40	40	39
2001	32	32	32	32	32	48	41	46	46	41
2002	39	39	39	39	39	60	56	58	58	55
2003	35	35	35	35	35	51	43	53	53	45
2004	19	19	19	19	19	21	19	20	20	22
2005	19	19	19	19	19	19	19	19	19	22
2006	24	24	24	24	24	24	25	24	24	31
2007	4	4	4	4	4	4	4	4	4	5
2008	5	5	5	5	5	5	5	5	5	6
2009	5	5	5	5	5	5	5	5	5	7
2010	37	37	37	37	37	59	53	57	57	55
2011	36	36	36	36	36	60	52	56	56	53
2012	36	36	36	36	36	60	52	56	56	53
2013	36	36	36	36	36	59	52	56	56	53

2014	36	36	36	36	36	60	52	56	56	53
2015	36	36	36	36	36	59	52	56	56	53
2016	36	36	36	36	36	60	52	56	56	53
2017	36	36	36	36	36	59	52	56	56	53
2018	36	36	36	36	36	61	53	58	58	53
2019	36	36	36	36	36	61	53	57	57	53
2020	4	4	4	4	4	4	4	4	4	6